

Západočeská univerzita v Plzni
Fakulta aplikovaných věd

GEOMETRICKÉ MODELOVÁNÍ V PRŮMYSLOVÝCH APLIKACÍCH

Ing. Kristýna Michálková

disertační práce
k získání akademického titulu doktor
v oboru Aplikovaná matematika

Vedoucí: Doc. Ing. Bohumír Bastl, Ph.D.
Katedra matematiky

Plzeň 2017

**University of West Bohemia
Faculty of Applied Sciences**

GEOMETRIC MODELLING IN INDUSTRIAL APPLICATIONS

Ing. Kristýna Michálková

**doctoral thesis
submitted in partial fulfillment
of the requirements for the degree of
Doctor of Philosophy (Applied Mathematics)**

**Supervisor: Doc. Ing. Bohumír Bastl, Ph.D.
Department of Mathematics**

Plzeň 2017

Anotace

Tato práce se zabývá geometrickým modelováním v průmyslových aplikacích. Hlavním cílem je popsat tvar vodních turbín s pomocí moderních geometrických metod. Proto byly použity B-spline/NURBS objekty pro definici hydraulických profilů vodních turbín a dále byly navrženy geometrické parametrizace, které jsou závislé na několika proměnných parametrech (délka, šířka, výška, úhly,...). Získáme tak dynamické modely, jež můžeme následně optimalizovat s pomocí isogeometrické analýzy (IGA). Díky tomu bude zlepšena nynější metodologie designu turbín, kdy analýza proudění je provedena pro jednu konkrétní turbínu a po obdržení výsledků z CFD systému je následně manuálně pozměněn CAD model turbíny na základě zkušeností konstruktéra a to tak aby došlo ke zlepšení vybraných vlastností (např. účinnosti nebo kavitace). Proces návrhu turbíny by tedy měl být více zautomatizován.

Práce je rozdělena do dvou částí. V první části se zaměříme na popis lopatek vodních turbín (koreček Peltonovy turbíny, lopatky Kaplanovy a Francisovy turbíny). Pro koreček Peltonovy turbíny je uveden nový algoritmus k sestrojení aproximační tečné plochy pro daný proměnný úhel. Lopatky Kaplanovy a Francisovy turbíny jsou sestrojeny za pomocí významných křivek: střednice a funkce tloušťky. V druhé části se zabýváme B-spline objemovou parametrizací Kaplanovy a Francisovy turbíny pro dané hraniční B-spline plochy. Tato parametrizace je následně použita jako vstup do IGA řešiče a může se tak analyzovat proudění turbínou. Zároveň jsou uvedeny různé možnosti parametrizací, které jsou poté porovnávány na základě vyhodnocení různých vlastností parametrizace.

Klíčová slova

B-spline/NURBS objekty, Isogeometrická analýza, Vodní turbíny, koreček Peltonovy turbíny, Kaplanova turbína, Francisova turbína

Annotation

This doctoral thesis deals with geometric modelling in industrial applications. The main goal is to describe the shape of water turbines with the help of modern geometric approaches. Therefore, we apply B-spline/NURBS objects to define hydraulic profiles of water turbines and we propose geometric parametrizations that depend on several parameters (length, width, height, angles, ...). Thus, we obtain dynamic models that could be further optimized with the help of isogeometric analysis (IGA). The usage of these dynamic models should improve the current methodology of turbine design. Nowadays, the result of the flow analysis (obtained with CFD solver) for one particular model is used for manually modified the turbine models in CAD systems with help of experience of designers to improve selected utility quantities (e.g. efficiency, cavitation). Thus, the design process should be more automatized.

The thesis is divided into two parts. In the first part of the thesis, we focus on the description of blades of water turbines (Pelton turbine bucket, blades of Kaplan and Francis turbines). The Pelton turbine bucket is described with the help of the new algorithm for obtaining the approximate tangent surface for given variable angle along its splitter or output from the bucket. Kaplan and Francis turbine blades are described with the help of important curves: camber line and the function of thickness. In the second part of the thesis, we deal with B-spline volumetric parameterization of Kaplan and Francis turbines for the given B-spline boundary surfaces. These parameterizations serve as input to flow analysis through the turbine based on isogeometric analysis. Moreover, the different approaches to the construction of these parameterizations are presented and the comparison of these approaches with respect to selected important properties of obtained parameterizations is given.

Keywords

B-spline/NURBS objects, Isogeometric analysis, Water turbines, Pelton bucket, Kaplan turbine, Francis turbine

Acknowledgements

The research presented in this doctoral thesis would not have been possible without the support of many people. My biggest thanks goes to my supervisor Doc. Ing. Bohumír Bastl, Ph.D., who is an excellent researcher, mentor, colleague and friend. I am grateful for his guidance and support over the years.

I would also like to thank my colleagues from TA03011157 project for pleasant cooperation during the past four years.

And last but not least, I would especially like to thank my amazing family for the love, support and constant encouragement.

I acknowledge the financial support of TAČR (Technologická Agentura České republiky) grant TA03011157.

I hereby declare, that to the best of my knowledge, this doctoral thesis includes my original research work and that any ideas, techniques, quotations, or any other materials from the work of other people included in my thesis are fully acknowledged with the standard referencing practices.

V Plzni dne

.....
Kristýna Michálková

Contents

Introduction	1
1 Preliminaries	5
1.1 B-spline/NURBS curves and surfaces	5
1.2 Water turbines	8
2 Geometric modelling of water turbine blades	14
2.1 Pelton turbine bucket	14
2.1.1 Inner surface	15
2.1.2 Outer surface	26
2.2 Kaplan turbine blade	28
2.2.1 Camber line	29
2.2.2 The function of thickness	31
2.2.3 Blade profile in 2D	33
2.2.4 3D profile of guide vanes/runner blades	35
2.2.5 Construction of the final blade from 3D profiles	41
2.3 Blades of Francis turbine	46
2.3.1 Stay vanes and guide vanes of FT	46
2.3.2 Runner blades of FT	48
3 B-spline volume parameterizations	51
3.1 Methods for determining B-spline/NURBS volumes	51
3.1.1 Polynomial approximation of a circle/circular arc	51
3.1.2 Approximate B-spline volume of revolution	52
3.1.3 Revision of algorithms for construction of planar and volume domains for given boundary	53
3.1.4 B-spline/NURBS volume for given boundary	60
3.2 Parts of water turbines as the boundaries for NURBS volumes	61
3.2.1 Spiral shaped pipe	62
3.2.2 Part with guide vanes and runner in KT	63
3.2.3 Part with guide vanes in FT	65
3.2.4 Hub and shroud of FT	66
3.2.5 Draft tube	67
3.3 Volume parameterizations in KT	70
3.3.1 3-patch model with guide vanes	70
3.3.2 Volume parameterizations surrounding the runner blade	71
3.4 Volume parameterizations in FT	73
3.4.1 FT volume parameterization between guide vanes	73
3.4.2 FT volume parameterizations around runner blade	73
Conclusion	74
Bibliography	76

Publications	82
Appendix A	85
Appendix B	87

List of Figures

1	Hydropower generation and forecast.	1
2	Scheme of optimization process.	4
1.1	B-spline basis functions	6
1.2	B-spline curve properties	7
1.3	NURBS surface	7
1.4	NURBS volume	8
1.5	Reaction and impulse turbines	9
1.6	The passage of flow through the runner	10
1.7	Turbine application chart	11
1.8	Design of turbine.	11
1.9	Velocity triangles for the blade.	12
1.10	The nomenclature of blade profile	13
2.1	A Pelton turbine	14
2.2	Three different views on the Pelton turbine bucket	15
2.3	Control net of Pelton bucket	16
2.4	Process of modelling the inner surface of Pelton bucket	17
2.5	Illustration for the proof of Theorem 1	23
2.6	The inner surface of a Pelton turbine bucket with different angle distributions along the outlet curve	25
2.7	The Pelton turbine bucket	26
2.8	Process of modelling the outer surface of Pelton bucket	27
2.9	Guide vanes and runner blades of KT.	28
2.10	The camber line with the basic parameters	29
2.11	Camber line represented as quadratic B-spline curve	29
2.12	Camber line represented as cubic B-spline curve	31
2.13	The function of thickness with parameters	32
2.14	The function of thickness represented as quadratic B-spline curve	33
2.15	The function of thickness represented as cubic B-spline curve	33
2.16	Process for the enveloped curve	34
2.17	Approximation of the enveloped curve	35
2.18	Mapping of blade profiles to cylinder surface.	40
2.19	Transformation of 2D profile for guide vanes	40
2.20	Mapping the the cone	41
2.21	Mapping to the cone.	42
2.22	Guide vane characteristic profiles.	43
2.23	The trailing edge	44
2.24	KT blade with important curves.	45
2.25	Guide vanes of KT.	45
2.26	Runner blades of KT.	47
2.27	The guide vanes of FT	48
2.28	The sections of the runner	49

2.29	The runner blades of FT	50
3.1	The control points of the approximation of the unit circle	52
3.2	B-spline volume of revolution	53
3.3	Planar parameterization methods.	56
3.4	Given boundary surfaces for volume parameterization.	57
3.5	Volume parameterization methods.	58
3.6	Steps for B-spline/NURBS volume for given boundary.	61
3.7	Kaplan turbine defined with B-spline parameterizations	62
3.8	Francis turbine defined with B-spline parameterizations	63
3.9	Spiral pipe	63
3.10	Housing of KT	64
3.11	New generatrices for the hub and turbine housing.	65
3.12	Part with guide vanes with parameters	65
3.13	Hub and shroud of FT	66
3.14	Segmentation of the draft tube.	67
3.15	3-patch model of guide vanes	69
3.16	5-patch model of KT runner	70
3.17	5-patch model of KT runner and 2-patch model of KT runner	71
3.18	FT blades	72

List of Tables

2.1	Errors and their improvements for Example 2	24
3.1	Functionals for the planar parameterization	55
3.2	Functionals for the volume parameterization	57
3.3	Functionals for the right patch	72
3.4	Functionals for the left patch	73

Introduction

This thesis mostly deals with the geometric shape of water turbines and their descriptions with the help of modern geometric methods. Moreover our aim is to change the proportions of water turbines to improve selected utility. The water turbines and hydropower play an important role in the industry of today. It is generally known that the use of renewable hydro-energy and construction of the hydropower plants protect nature against contamination which occurs during use of non-renewable resources such as oil and gas. Furthermore, we can list other advantages of hydropower usage, e.g. controlling floods (the amount of water going through the turbine is regulated), irrigation, costs to run and to maintain the hydroelectricity power plant are low, and so on. To stay objective, there are also the cons of hydropower. Some of them are high initial costs of building hydroelectricity power plant, dependence on water supply (droughts could cause several financial problems), life of fishes is affected due to intervention to their natural habitat. There are more information about pros and cons of hydropower in [25, 44, 46, 47]. Despite these disadvantages hydropower provides 16% of electricity generation worldwide and researchers have published several papers how to avoid problems connected with building hydroelectricity power plant, e.g. ruining aquatic life in the dams (see about fish-friendly turbines in [27, 28, 32, 72]). It is unavoidable to admit that hydropower is an important topic for the society and according to the forecast published in [45], the electric energy obtained by hydropower can be still increased in the next three years (see Fig. 1).

Current State

As we mentioned at the beginning, our aim is to describe the shape of water turbines with the help of modern geometric approaches. We mainly use B-spline or Non-uniform rational B-splines (NURBS) objects, which are standard objects used in current Computer Aided Design (CAD)/Computer Aided Manufacturing (CAM) systems (see more in [71]), to characterize silhouette of the water turbine. Looking to the history, uniform B-spline curves were introduced by I. Schoenberg in 1946 (see [75]). One

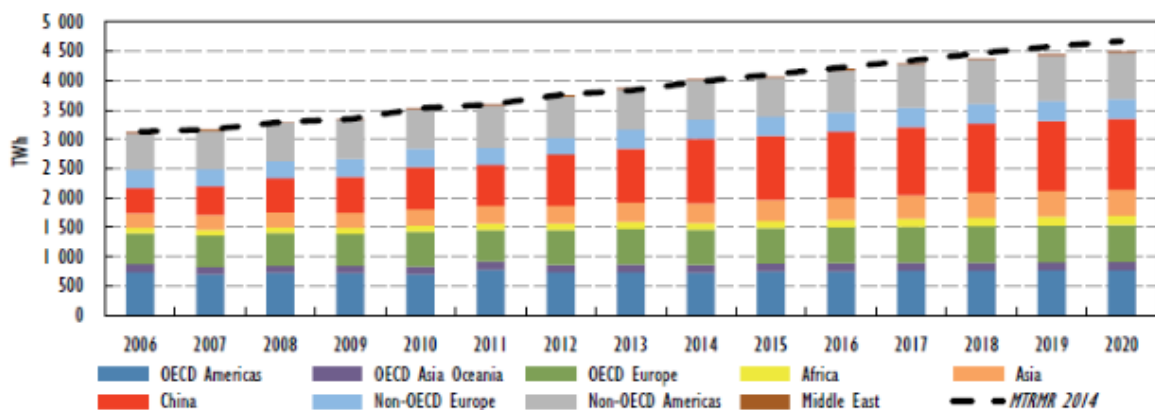


Figure 1: Hydropower generation and forecast by region. Source of graph is [45], MTRMR in graph is abbreviation for Medium-Term Renewable Energy Market Report.

year later they were generalized to non-uniform B-splines by H. Curry in [26]. The main research of these curves started after C. de Boor formulated a relatively fast and numerically stable algorithm for calculating points on splines (cf. [13]). Later, non-uniform rational B-splines were studied by S. Coons or A. R. Forrest but complete description of NURBS curves, as we know them nowadays, was done by K. Versprille (see [82] for more details). P. de Casteljau and P. Bézier are another well-known names connected with the history of geometric modelling. In 1960s, P. de Casteljau [19] described curves with the help of the so-called control polygon. Unfortunately, he was not allowed to publish the results of his research which were kept as an industrial secret of Citroën. Meanwhile, P. Bézier and his group reached similar results and he introduced the well-known Bézier curves (see [11, 12]) into Computer Aided Geometric Design (CAGD). It is obvious that B-splines or NURBS curves and surfaces are a reasonable tool for the modelling of water turbines, because of complicated shapes forming some parts of turbines.

The description of different parts of water turbines is closely related to the fluid dynamics computations (see [50, 64, 89] for more details), i.e., to the numerical experiments based on Finite Element Method (FEM), Finite Volume Method (FVM), or, in the last years, on isogeometric analysis (IGA). Since CAD and CAGD originated later than FEM, this is probably the reason why the connection between CAD/CAGD and FEM were not so strong. Nevertheless, Hughes et al. in [43] has proposed already mentioned IGA which bridges this gap and which strongly connects CAD and FEM or as it is written in [22]: “*IGA is a superb vehicle to promote the marriage of CAD and Finite Element Analysis (FEA).*”. A thorough analysis has followed, see e.g. [2, 6, 29, 40]. The overall strategy of IGA is similar to FEM in standard cases – the exact geometry in CAD system is used to construct a mesh of so-called NURBS elements and this mesh can be subsequently refined by h-, p- or k-refinements. Further, using the weak form of a boundary value problem we set a system of linear equations for control points of a new NURBS object representing the approximate solution of the original problem. One of the main advantages of the method is that we can avoid the generation of a triangular (quadrangular) mesh from CAD representation to be able to perform the finite element analysis and the necessity to create this mesh again and again after each change of the geometry because this task is very time-consuming. Another advantage is that the geometry is represented exactly, not only approximately. IGA is involved in several scientific areas nowadays, i.e. problems including structural vibrations [23, 79], electromagnetism [17, 61], biology [59, 78, 94] and others. There are numerous papers devoted to isogeometric analysis applied to flow problems (see [3, 4, 5, 8, 10, 14, 16, 63]). For example, in [63] the problem of Navier-Stokes flow in 2D is solved and the theoretical results are applied to a standard benchmark flow problem, namely the lid-driven cavity problem (see [6] for more details). IGA approach applied for turbulent modelling on single or multi-patch geometries is presented in [3, 4]. Another interesting problem of flows concerning rotating components (e.g. blades of water turbines, submarine and ship propellers) is studied in [9] and there is also an example that involves two propellers rotating inside a rectangular box. A lot of issues appeared with the development of IGA. We can divide the problems in several categories:

- Local refinement

During the analysis process in various problems (such as stress distribution along the machine components, flow through the turbine) we sometimes need to concentrate on individual parts of the analyzed environment, thus the meshes should be refined locally. Several generalizations of B-spline constructions were proposed to solve the local refinement problem: T-splines [7, 74], hierarchical splines [36, 83], LR B-splines [31, 49] or THB-splines [37, 38].

- Parameterization and usage of existing tetrahedral meshes

One of the key issues in IGA is finding of analysis-suitable parameterizations of computational domains. The quality of the parametrization can significantly affect the result of IGA simulations (see [22]). In [41] planar parameterizations are presented and several methods are shown (i.e. spring model, mean value coordinates, nonlinear methods). Planar parameterizations are also studied in [90], where generalization of discrete Coons method to B-spline volumes is shown in the Appendix. Another analysis and generalizations followed [91, 92, 93]. Further, methods for

construction of volumetric parameterizations are proposed in [53, 66]. Research is also devoted to the transformation of tetrahedral meshes to B-spline/NURBS solids because a lot of tetrahedral meshes were constructed for FEA. There are successful attempts to convert these meshes to the version suitable for IGA shown in [51, 84, 85].

- **Implementation**

The next crucial problem is the implementation of tensor-product, NURBS-based isogeometric analysis (for more information see [62] and the references therein). Luckily, the packages for commercial softwares (e.g. Matlab, Python) or open-source libraries that incorporate the paradigm of IGA have already been established (c.f. [39, 70, 81]), thus the researches could circumvent the implementation of basics of IGA.

It could be seen that researches are attracted to problems connected with parameterizations of complex geometries. However, there are not many papers concentrating only on geometric models of turbine parts, but there are several papers which focus on different techniques of geometric modelling of the blades because of their complicated shape and importance in the process of transferring energy. For example, the methods for interactive design of blades (mainly blades of gas turbines) are presented in [57]. The blades are represented with NURBS curves and blade sections are defined with respect to general surfaces of revolution. Another method for the modelling of turbine blades based on lofted B-splines is presented in [42], where the lofting process is extended to cylindrical and to conical isoparametric lines. A computer based process for blade modelling of horizontal axis turbines using B-spline surfaces is described in [68]. This method starts with the creation of a 3D set of offsets that constitute rotor blades based on a 2D definition of airfoils and there is an emphasis on the fitting of a blade's leading edge. Most of the methods for the modelling of turbine blades focus on using several profiles (sections) of blades and connecting them together to obtain geometric model, whereas M. Rossgatterer et al. (see [73]) use approach based on medial surface of a blade and profile curves attached to it and the construction of these curves depends on B-splines.

Summary and contribution of the work

If we look closely to the development in the field of water turbines, it is characteristic by blending conservative approaches and long-time experience on one hand and application of modern methods of fluid mechanics and numerical analysis, which uses powerful computational methods, on the other hand. Manufacturers of hydraulic turbines create models of turbines due to previous experiences and modernize only existing types of turbines. They form models in CAD systems and use CFD (Computational Fluid Dynamics) packages to analyze the flows. This is usually achieved thanks to the expert engineering solution when improvements are usually obtained due to the experience of a designer. The turbines are designed and built individually according to the specific requirements of the customer, generally based on the experience as well. These processes depend on each manufacturer and they are a part of their industrial secrets. Thus, publication of new methods is limited only to general principles.

Also the process of shape optimization based on the iterative modification of a hydraulic profile of a turbine in a CAD system using the results of a flow analysis obtained with the help of standard CFD packages could be very difficult (the process of optimization is shown in Fig. 2). One of the problems is the discretization of the area where the flow simulation based on FEM or FVM is solved. It is not possible to discretize complex shapes accurately. It introduces error in the next iteration of optimization and the error accumulates. Moreover, it is often necessary to fine-tune the discretization manually, which prevents any automatic process. The key to the formulation of such an automatic optimization process, which eliminates the above mentioned problems, is the creation of high quality dynamic geometric models of turbine components based on B-spline/NURBS objects, a successive discretization of a computational domain for flow simulation by finding its precise volumetric representation and numerical solution of flow equations based on the IGA. There are several papers devoted to shape optimization.

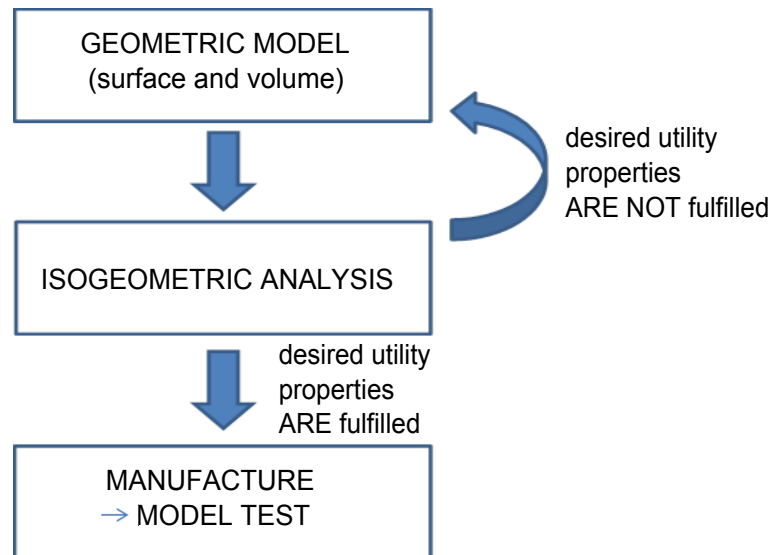


Figure 2: Scheme of optimization process.

The general framework of shape optimization solution problems by means of IGA is described in [60], whereas in [65] readers can find more specific problem of optimization in fluid mechanics.

In this thesis we create several dynamic geometric models of water turbines (Pelton turbine, Kaplan turbine and Francis turbine) so that the previously described processes are more automatized and less time-consuming. The proposed geometric models of chosen parts of water turbines depend on several shape parameters (length, width, angles, ...) to generalize the definition of the shape of the water turbine. It means that we are capable of describing different shapes of one type of water turbine or its selected part, e.g., blades. The main contributions of the dissertation thesis are also presented in the following papers:

- [1] P. Anděl, B. Bastl, K. Slabá: *Parameterizations of generalized NURBS volumes of revolution*. Engineering Mechanics, Vol. 19, pp. 293-306, 2012.
- [56] K. Micháľková, B. Bastl: *Imposing angle boundary conditions on B-spline/NURBS surfaces*. Computer-Aided Design, Vol. 62, pp. 1-9, 2015.

The remainder of the thesis is organized as follows. At the beginning of the first chapter (Section 1.1), we review basic facts and properties about B-spline/NURBS curves, surfaces and volumes. The first chapter (Section 1.2) is concluded with the basic nomenclature used in the rest of the thesis and the fundamentals of water turbines (in particular we focus on these three types: Kaplan turbine, Francis turbine and Pelton turbine). The second chapter is devoted to geometric models of water turbine blades. We start with presentation of the blades followed by particular examples: Pelton turbine bucket, Kaplan turbine guide vanes and runner blades and the last proposed models are stay vanes, guide vanes and runner blades of Francis turbine. The construction of each blade is based on describing the parameterization of important curves (e.g. boundary curves, camber line curve) and it is followed by the definition of the final surface of blade. In Chapter 3 we show the problem of finding NURBS volume parameterizations of computational domains from its boundary NURBS surfaces. At the beginning of the last chapter, we mention several methods used for the determination of NURBS volume parameterizations followed by the description of the boundary surfaces (entrance of the turbine, runner and draft tube). The main part of the third chapter is devoted to the NURBS volumes of Kaplan turbine segments and Francis turbine parts where we present several possible approaches. Finally, we conclude the work and we describe future goals.

1

Preliminaries

In this chapter we give a brief review of B-spline and NURBS curves, surfaces and volumes. We also mention some basics about hydraulic turbines, that are geometrically described in the following chapters.

1.1 B-spline/NURBS curves and surfaces

Current CAD/CAM systems mostly use the so-called B-spline and NURBS objects for representation of free-form curves and surfaces and they are considered to be de facto standard for shape representation of objects. In the following paragraphs we remind basic definitions and properties and show several examples of B-spline/NURBS curves, surfaces and volumes (see [69, 21] for more details).

Definition 1 A NURBS curve of degree p is determined by a control polygon of control points \mathbf{P}_i , their associated weights w_i , $i = 0, \dots, n$ and a knot vector $\mathbf{T} = (t_0, \dots, t_{n+p+1})$. Then its parameterization is of the form

$$\mathbf{c}(u) = \frac{\sum_{i=0}^n N_{i,p}(u)w_i\mathbf{P}_i}{\sum_{i=0}^n N_{i,p}(u)w_i}, \quad (1.1)$$

where $N_{i,p}(u)$ are B-spline basis functions of degree p corresponding to the knot vector \mathbf{T} .

For the given knot vector $\mathbf{T} = (t_0, \dots, t_{n+p+1})$, the B-spline basis functions are defined by a recursive formula

$$\begin{aligned} N_{i,0}(t) &= \begin{cases} 1, & t_i \leq t < t_{i+1}, \\ 0, & \text{otherwise,} \end{cases} \\ N_{i,k}(t) &= \frac{t - t_i}{t_{i+k} - t_i} N_{i,k-1}(t) + \frac{t_{i+k+1} - t}{t_{i+k+1} - t_{i+1}} N_{i+1,k-1}(t), \quad k = 1, \dots, p. \end{aligned}$$

The knot vector is a non-decreasing sequence of real numbers which determines the distribution of a parameter of the corresponding curve/surface/volume. In general, two different forms of the knot vector are commonly distinguished:

- *periodic* knot vector $\mathbf{T} = (t_0, \dots, t_{n+p+1})$ where we have to add the desired degree p of B-spline basis functions (see Fig. 1.1 (top row)),
- *non-periodic* knot vector $\mathbf{T} = (\underbrace{a, \dots, a}_{p+1}, t_{p+1}, \dots, t_n, \underbrace{b, \dots, b}_{p+1})$ where p is a degree of the associated B-spline basis functions (see Fig. 1.1 (bottom row)).

Further, we distinguish *uniform* (uniformly distributed knots) and *non-uniform* (non-uniformly distributed knots) knot vectors.

One of the main properties of B-spline basis functions is a relation between the multiplicity of knots in the knot vector and the continuity of the corresponding B-spline basis functions – the B-spline basis functions are of continuity C^{p-k} , where k is the maximal multiplicity of inner knots in the knot vector. Among their other properties belong non-negativity, partition of unity and local support.

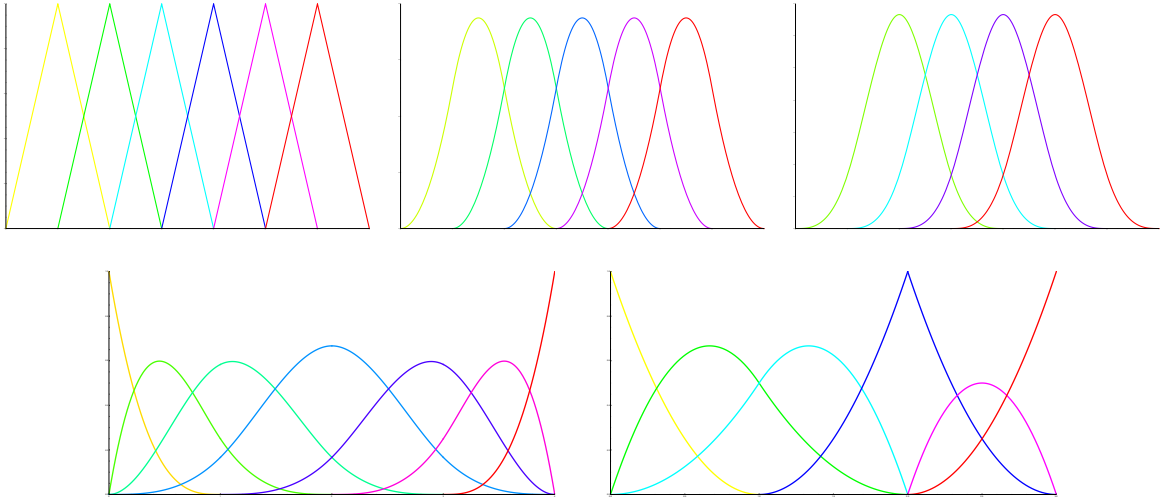


Figure 1.1: Top row: B-spline basis functions for the knot vector $\mathbf{T} = (0, 1, 2, 3, 4, 5, 6, 7)$ of degree p ($p = 1$ (left); $p = 2$ (middle); $p = 3$ (right)); Bottom row: B-spline basis functions for the knot vector $\mathbf{T} = (0, 0, 0, 0, 1, 2, 3, 4, 4, 4, 4)$ (left) and for the knot vector $\mathbf{T} = (0, 0, 0, 1, 2, 2, 3, 3, 3)$ (right).

Remark 1 *If all weights w_i of control points \mathbf{P}_i , $i = 0, \dots, n$, are equal, the denominator of (1.1) is a constant and a polynomial B-spline curve is obtained.*

B-spline/NURBS curves possess a lot of important practical properties which follow from their definition and from the properties of B-spline basis functions. Some of these are used later in NURBS volume modelling. The properties of B-spline curves are:

- Affine invariance

An affine transformation can be applied to the curve by applying it to the control points.

- Local modification

Changing the control point \mathbf{P}_i (or weight w_i) influences the curve on the interval $\langle u_i, u_{i+p+1} \rangle$. This property follows from the fact that the basis function $N_{i,p}(u)$ is non-zero on the interval $\langle u_i, u_{i+p+1} \rangle$.

- Convex hull property

The curve is in the convex hull of its control polygon. More precisely, if the part of the B-spline curve corresponding to $u \in \langle u_i, u_{i+1} \rangle$, $p \leq i < n$ is considered, then $c(u)$ is contained in the convex hull of the control points $\mathbf{P}_{i-p}, \dots, \mathbf{P}_i$.

- Variation diminishing property

This property holds for curve in plane or space and it means that the number of intersection points of any straight line (resp. plane) with the curve is less or equal to the number of intersections of this straight line (resp. plane) with the control polygon.

Several properties are shown in Fig. 1.2. Proofs and more information about B-spline/NURBS curve properties can be found in [69].

As a straightforward extension, we can define NURBS surfaces that share most of the properties with NURBS curves. Similarly to the curve case, if weights of all control points are the same, the definition covers also polynomial B-spline surfaces (see Fig. 1.3).

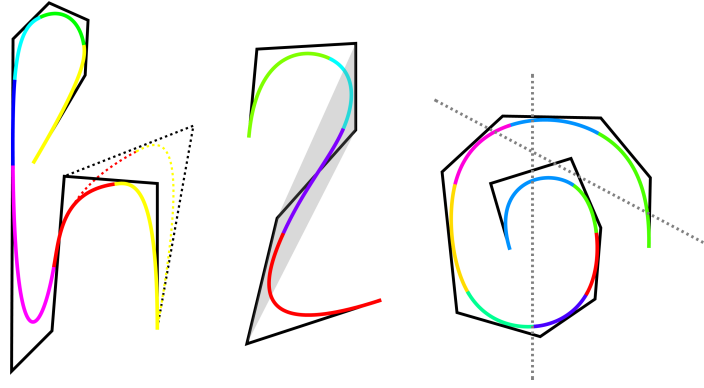


Figure 1.2: Left: Local modification property is shown. Changing the control polygon (dashed one) influences only the curve just in particular interval. Middle: Convex hull property is presented. The purple part of the curve lies in the convex hull (gray area) of corresponding control points. Right: Variation diminishing property is demonstrated.

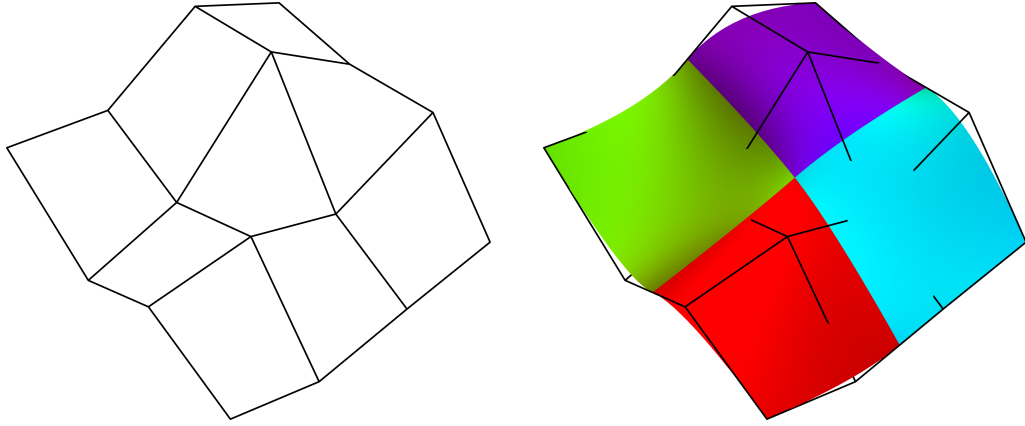


Figure 1.3: Left: Control net of a NURBS surface; Right: Control net and the corresponding NURBS surface composed of 4 patches.

Definition 2 A NURBS surface of degree (p, q) is determined by a control net of $(m + 1) \times (n + 1)$ control points \mathbf{P}_{ij} , their associated weights w_{ij} , $i = 0, \dots, m$, $j = 0, \dots, n$, and two knot vectors $\mathbf{U} = (u_0, \dots, u_{m+p+1})$, $\mathbf{V} = (v_0, \dots, v_{n+q+1})$. Then its parameterization is of the form

$$\mathbf{s}(u, v) = \frac{\sum_{i=0}^m \sum_{j=0}^n N_{i,p}(u) N_{j,q}(v) w_{ij} \mathbf{P}_{ij}}{\sum_{i=0}^m \sum_{j=0}^n N_{i,p}(u) N_{j,q}(v) w_{ij}}, \quad (1.2)$$

where $N_{i,p}(u)$ and $N_{j,q}(v)$ are B-spline basis functions of degrees p and q corresponding to the knot vectors \mathbf{U} and \mathbf{V} , respectively.

Finally, we would like to remind the B-spline/NURBS volumes (see [21, 1]).

Definition 3 A NURBS volume of degree (p, q, r) is determined by a control net $(m+1) \times (n+1) \times (l+1)$ of control points \mathbf{P}_{ijk} , with weights w_{ijk} , $i = 0, \dots, m$, $j = 0, \dots, n$, $k = 0, \dots, l$ and three knot vectors $\mathbf{U} = (u_0, \dots, u_{m+p+1})$, $\mathbf{V} = (v_0, \dots, v_{n+q+1})$, $\mathbf{W} = (w_0, \dots, w_{l+r+1})$. Parameterization is then

$$\mathbf{v}(u, v, w) = \frac{\sum_{i=0}^m \sum_{j=0}^n \sum_{k=0}^l N_{i,p}(u) N_{j,q}(v) N_{k,r}(w) w_{ijk} \mathbf{P}_{ijk}}{\sum_{i=0}^m \sum_{j=0}^n \sum_{k=0}^l N_{i,p}(u) N_{j,q}(v) N_{k,r}(w) w_{ijk}},$$

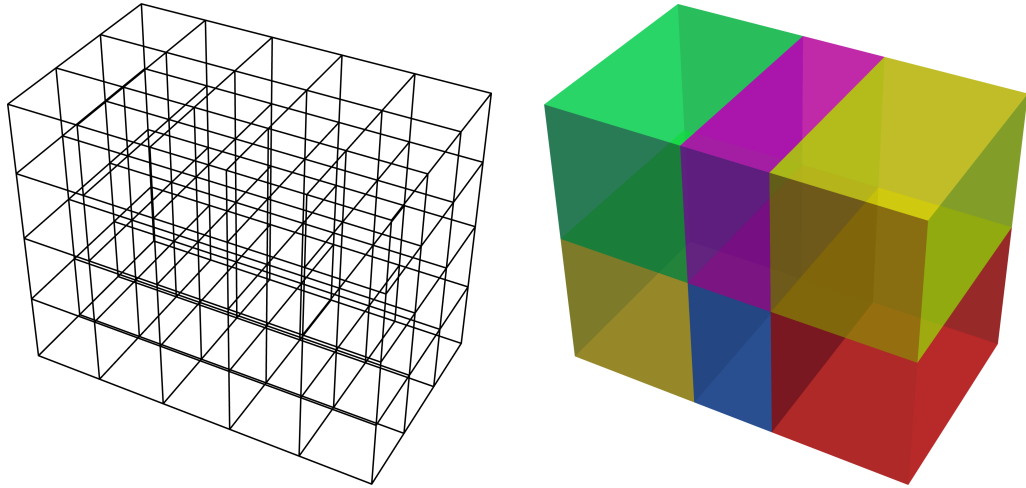


Figure 1.4: Left: Control net of a NURBS volume; Right: Corresponding NURBS volume composed of 6 parts.

where $N_{i,p}(u)$, $N_{j,q}(v)$ and $N_{k,r}(w)$ are B-spline basis functions of degrees p , q and r corresponding to the knot vectors \mathbf{U} , \mathbf{V} and \mathbf{W} , respectively.

In the case of B-spline volumes all weights w_{ijk} of control points \mathbf{P}_{ijk} are equal. In Fig. 1.4 the example of NURBS volume and its control net is shown. NURBS volumes are generalization of NURBS surfaces and therefore they possess analogous properties as NURBS surfaces, i.e., it is fast and numerically stable to generate points on NURBS volumes, and computation of these points is invariant with respect to projective transformations (for more information see [69]).

1.2 Water turbines

In this section we mention some basic facts about hydraulic turbines (see [80] for more details).

The main principle of water turbine is based on a conversion of potential energy of water to kinetic energy of a water machine. The predecessor of hydraulic turbine is a water wheel invented by Ancient Greeks (cf. [52, 87]), especially used for water-lifting during irrigation or later utilized as a part of a water mill.

The first water turbine based on theoretical foundations (dynamics of frictionless liquid by L. Euler and D. Bernoulli) was constructed by B. Fourneyron, who built the first centrifugal turbine in St. Blasien in 1835. Further, it is important to mention the most famous turbines that are still in use: Francis turbine (1848), Pelton turbine (1870s) and Kaplan turbine (1912). While water power stations with Francis or Pelton turbine are built in places with medium or high head, Kaplan turbine is used for low heads (see [52] for more information about efficiency of water turbines). Other examples of turbines are in [86, 95]. The runners of mentioned turbines are shown in Fig. 1.5 (left column).

We distinguish several types of turbines which are classified in the following categories:

- The manner of transferring energy

The main category, that divides turbines in two types, depends on the manner in which the water causes a turbine runner to rotate. The first type are *reaction turbines* where a piece of the energy is transferred in the diffusion ring and the rest of energy is changed in the runner. Further, the blades are fully flooded during the process of transferring energy. On the contrary, in the *impulse turbines* whole pressure energy changes to kinetic in the nozzle and at the beginning and at the end of the runner the same values of pressure can be measured. Moreover, impulse turbines operate with their

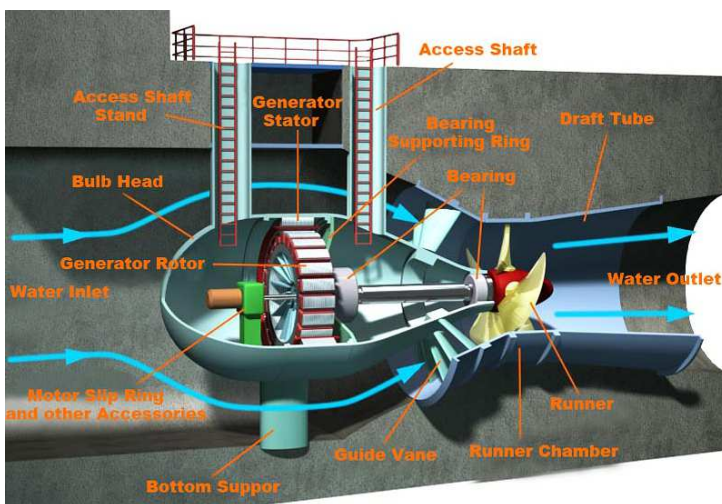
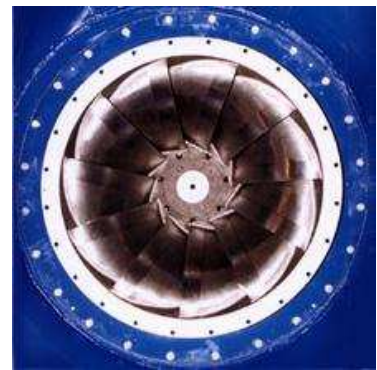
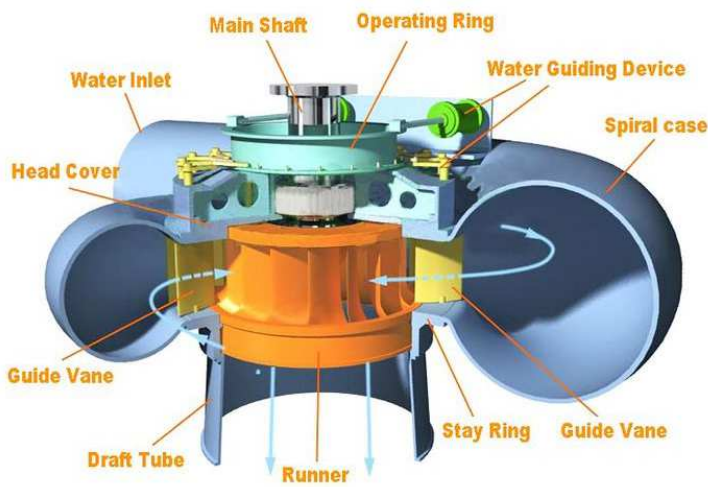
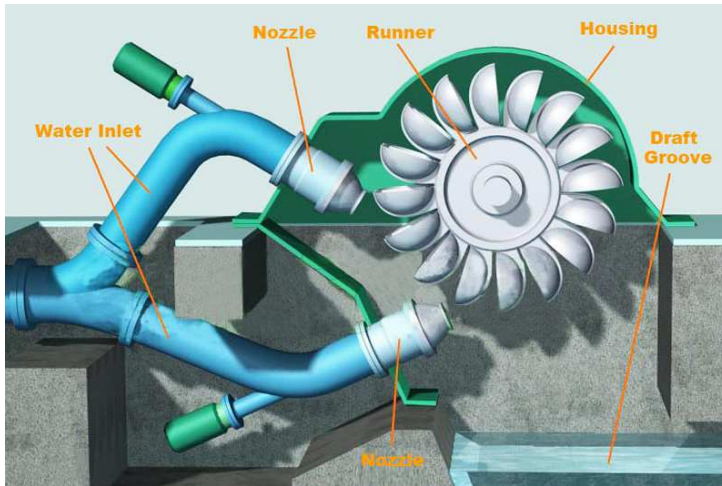


Figure 1.5: Description of reaction and impulse turbines (left) with corresponding runners (right). Top: Pelton turbine. Middle: Francis turbine. Bottom: Kaplan turbine. (Source: [33, 54])

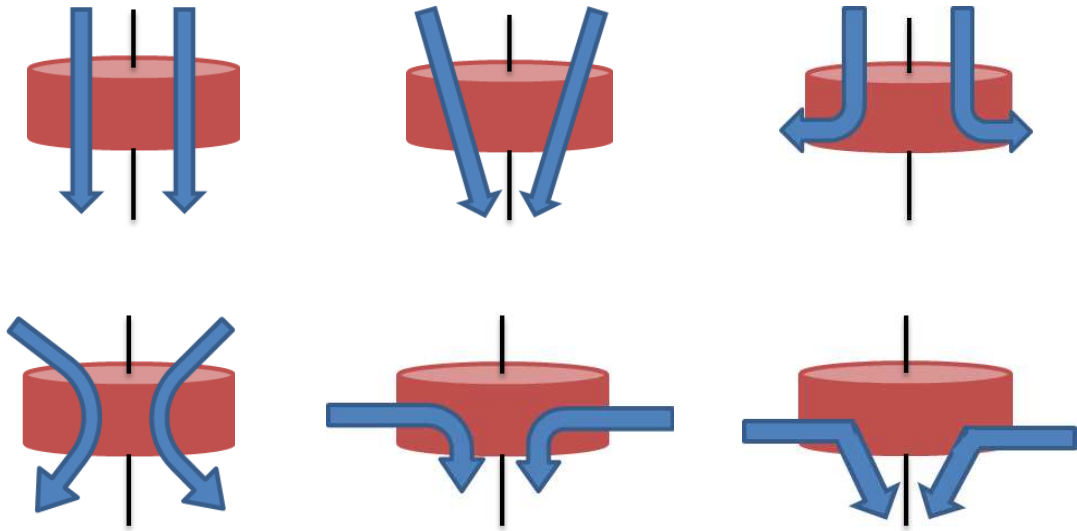


Figure 1.6: The passage of flow through the runner. Top: axial, diagonal, radial centrifugal; Bottom: Tangential, radial axial, radial centripetal

blades also in the air. The examples of reaction turbines are Kaplan turbines and Francis turbines, whereas the Pelton turbine is an example of an impulse turbine. The description of individual parts of reaction and impulse turbines is shown in Fig. 1.5 (left column).

- The passage of flow through the runner

This category depends on the direction of flow at the beginning and at the end of the runner. The possibilities are the following: *radial centrifugal*, *radial centripetal*, *radial-axial*, *diagonal*, *axial* and *tangential*. For example, Pelton turbine is an example of tangential turbine, Francis turbine is typically radial-axial and Kaplan turbine is usually of axial type. See illustrative Fig. 1.6.

- The position of the runner

The type of turbine depends on the placement of the runner towards the flow. There are two eventualities: *horizontal* (Kaplan/Pelton turbine) or *vertical* (Francis/Kaplan turbine).

The more detailed description of the chosen turbines (the one that are presented in the Chapters 2 and 3) is shown in the following paragraphs. We start with the *Pelton turbine* (see Fig. 1.5 (top)). This turbine is the only one mentioned here which has multiphase flow. It means that blades operates not only under the water but they go through a phase that are completely in the air. The runner is composed of the buckets and it is moved by the flow that is brought by nozzle. The number of nozzles can be different for each turbine and depends on the given *head* H (the approximate vertical distance through which water falls) and *flow rate/discharge* Q (the volume flow rate of the water that passes through plant), but the maximum number is 6 nozzles. The first part of the design of runner is dependant on chosen width of the bucket and the computed diameter of the runner. These are also dependant on the given flow rate, head and velocity of the water that is brought to the runner. Water leaves the runner to the draft groove. The Pelton turbine operates on the high heads and low flow rates (see Fig. 1.7). Pelton turbine efficiency is about 91%.

The next type of turbine that also operates on high heads but for a larger range of flow rates is *vertical Francis turbine* (see Fig. 1.5 (middle)). The water is brought to the guide vanes by the spiral shaped pipe (there could be included stay vanes that are not moveable). Then the water is prepared by guide vanes to the runner which has non-moveable blades. The water leaves the runner through a draft tube (device for water drainage) that has the elbow shape. The only moveable blades are the guide vanes. The Francis turbine can reach the highest efficiency almost 94%.

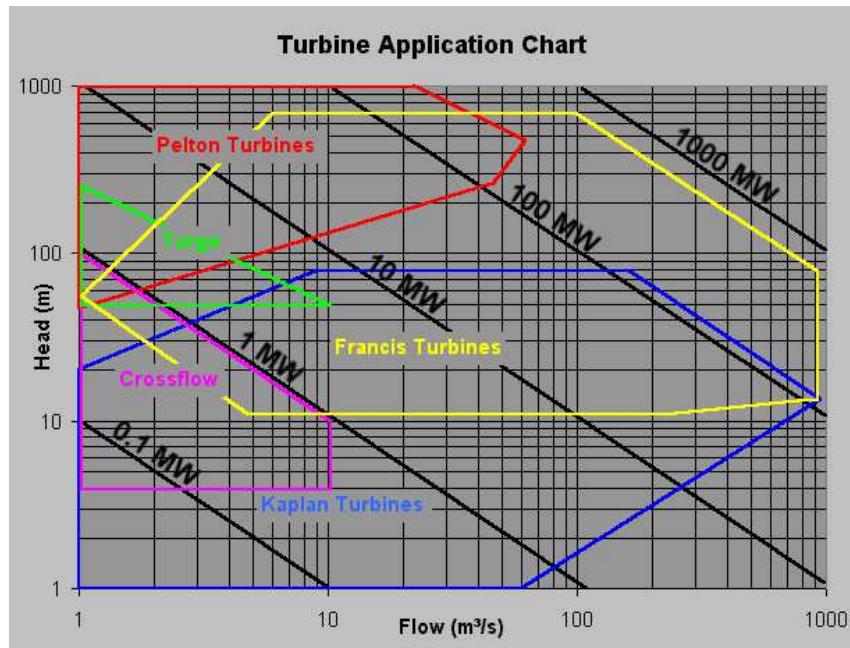


Figure 1.7: Turbine application chart, the dependency on the flow rate. (Source: [88])

The similar process happens in the last type of turbine presented in this thesis – *tubular Kaplan turbine* (see Fig. 1.5 (bottom)). This turbine is optimal for the low heads compared to the previous ones. Water is immediately brought to the guide vanes and continues to the runner. A straight draft tube is also at the end of the turbine. The main difference between the Francis and the Kaplan turbine is that runner blades in Kaplan turbine are moveable. Efficiency of Kaplan turbine is about 93%.

The steps of water turbine design process are shown in the next text (see [80, 76]). First, the designer determines the most suitable type of a turbine for the given site. Each turbine operates on different flows (see Fig. 1.7). As it was mentioned Kaplan turbine is more suitable for low heads whereas Pelton and Francis turbine operate on higher heads. Assume that the suitable type is Kaplan turbine (the process is analogous for the Francis turbine). The basic parameters for determining the water turbine design are

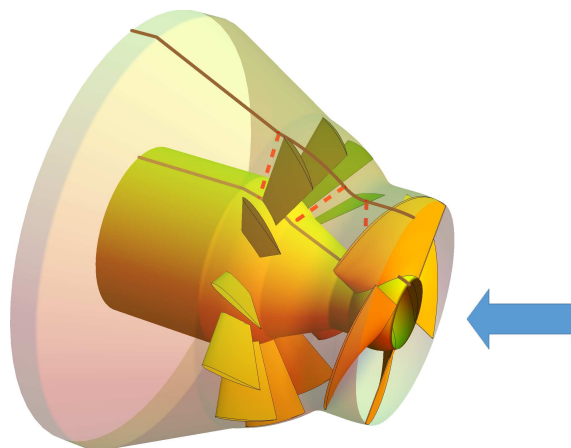


Figure 1.8: The parts of turbine and the arrow shows the “direction” of design.

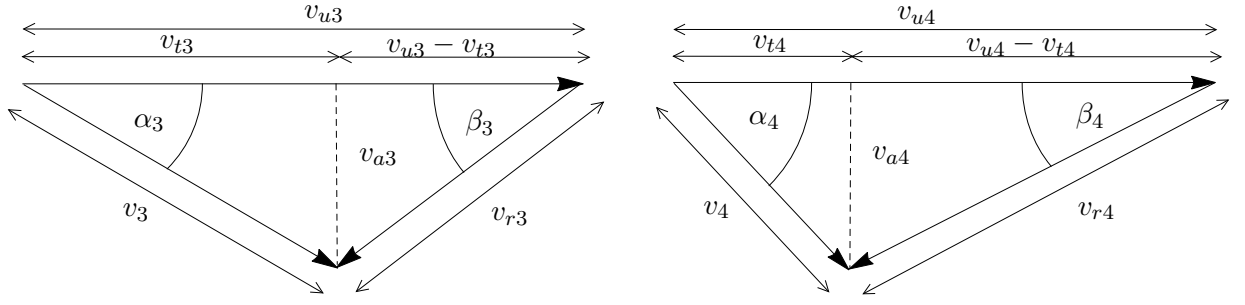


Figure 1.9: Left: Inlet velocity triangle for the runner blade; Right: Outlet velocity triangle for the runner blade. The components of velocity are: v_u is the velocity of the blade, v_t is the tangential velocity, v is the absolute velocity of the water, v_r is the relative velocity of the water and v_a is the axial velocity.

head H and flow rate/discharge Q . The specific discharge Q_{11} and unit speed n_{11} are determined by

$$Q_{11} = \frac{Q}{\sqrt{H}D^2},$$

$$n_{11} = \frac{nD}{\sqrt{H}},$$

where D is the diameter of the runner. The design starts “against the flow” (see Fig. 1.8) and the velocity of flow is the most important element in the design process. Indexes 1, 2 are input and output components for guide vanes and 3, 4 are input and output components for runner blades respectively (see Fig. 1.9) in the following text. If index is not mentioned it means that the definition holds also for every index $1, \dots, 4$.

The output velocity of the runner blade has influence on the draft tube efficiency. One of the component is *axial velocity* v_a

$$v_a = \frac{4Q}{\pi(D^2 - d^2)},$$

where d is the diameter of the hub. The next component is *velocity of the blade* v_u and it is generally (not just for the runner blades) computed as

$$v_u = r\omega, \quad (1.3)$$

where ω is angular velocity of the runner and r is the radius of the cylindrical surface (definition follows in the next paragraph). The next component is *tangential velocity* v_{t4} given by

$$v_{t4} = f(r, v_{u4}),$$

where function f depends on the type of turbine and v_{u4} is defined for the runner blades analogically as in (1.3). The further step is to compute output angle of the flow α_4 and the output angle of the blade β_4

$$\tan \alpha_4 = \frac{v_{a4}}{v_{t4}}, \quad (1.4)$$

$$\tan \beta_4 = \frac{v_{a4}}{v_{u4} - v_{t4}}. \quad (1.5)$$

As the Euler equation is satisfied, the tangential velocity v_{t3} for the input is computed

$$v_{t3} = \frac{gH_n + v_{u4}v_{t4}}{v_{u3}},$$

where v_{u3} is generally defined in (1.3) and H_n is ideal increase of total head (increase of head when all losses are ignored), see [20]. Then, the input angle of the flow α_3 and the input angle of the blade β_3 are defined analogically to (1.4) and (1.5).

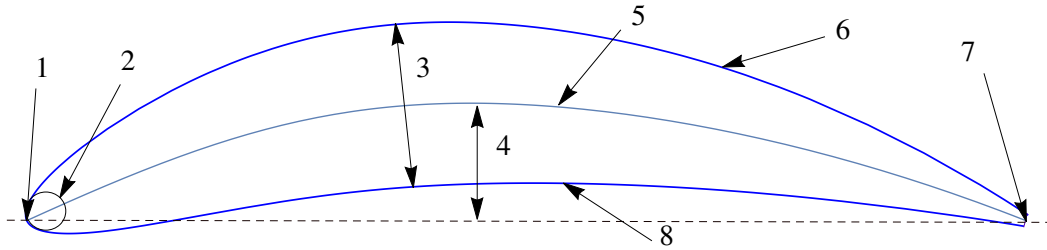


Figure 1.10: The nomenclature of blade profile. 1 – leading edge; 2 – nose circle; 3 – thickness; 4 – camber; 5 – main camber line; 6 – suction side; 7 – trailing edge; 8 – pressure side.

Now, we define the geometry of runner blades from β_3 and β_4 . It is composed of several profiles. Each profile lies on a cylindrical surface with radius r (see (1.3)). The blade profile is composed of pressure and suction sides and water attacks the blade on the leading edge and leaves it on trailing edge (see Fig. 1.10). The construction of the profile was inspired by the airfoil NACA profiles (cf. [18, 48]). It means that the profile is determined by the camber line and the function of thickness. There are several characteristic parameters for the profile (see more in Chapter 2). Leading edge angle β_3 and trailing edge angle β_4 . This determines the camber of the profile. Further, the guide vanes are constructed. The only difference from the previous description of runner blades is that guide vane is determined with just one profile on a conical surface (see Chapter 2). The angles β_1 and β_2 are computed as β_3 and β_4 using (1.5). We define the components of velocities for guide vanes from the inlet velocity triangle of the runner blade

$$\begin{aligned} v_{u2} &= g(v_{u3}), \\ v_{a2} &= k(v_{a3}), \end{aligned}$$

where functions g and k depends on the type of turbine. The design of water turbine blades from geometric point of view is more described in Chapter 2.

2

Geometric modelling of water turbine blades

In this chapter we present several types of water turbines blades and we focus on their geometric description in the class of B-spline/NURBS objects. Moreover, design parameters (e.g. length, width, depth, ... of blade) are included in the geometric descriptions. In the following sections we specify four types of blades: Pelton turbine bucket, Kaplan and Francis turbine guide vanes, runner blades of Kaplan turbine and runner blades of Francis turbine. The construction of blades is based on several algorithms and geometric approaches that are also presented in the next paragraphs. The results of this chapter are used as the input for computation of B-spline volumes important for analysing the flow through the whole turbine. The chapter is organized as follows. We start with the description of a parametric model of Pelton turbine bucket where we focus mainly on preserving the angle along the outlet curve. Then we show Kaplan turbine guide vanes and runner blades and the chapter is concluded with the Francis turbine stay vanes/guide vanes and runner blades.

2.1 Pelton turbine bucket

The Pelton turbine bucket (see Fig. 2.1) can be described by several parameters (e.g. lengths, widths, angles, ...). Our goal is to propose a method which returns a B-spline model of the bucket satisfying given shape parameters, i.e., to create what we will call “parametric geometric model” or “dynamic geometric model” in the following text. We divide the task to two parts. At first, the inner surface of the bucket is described and then the outer surface is presented. Moreover, the bucket is symmetrical with respect to the splitter, i.e., we focus on half of the bucket.



Figure 2.1: A Pelton turbine with the runner. (Source: [67])

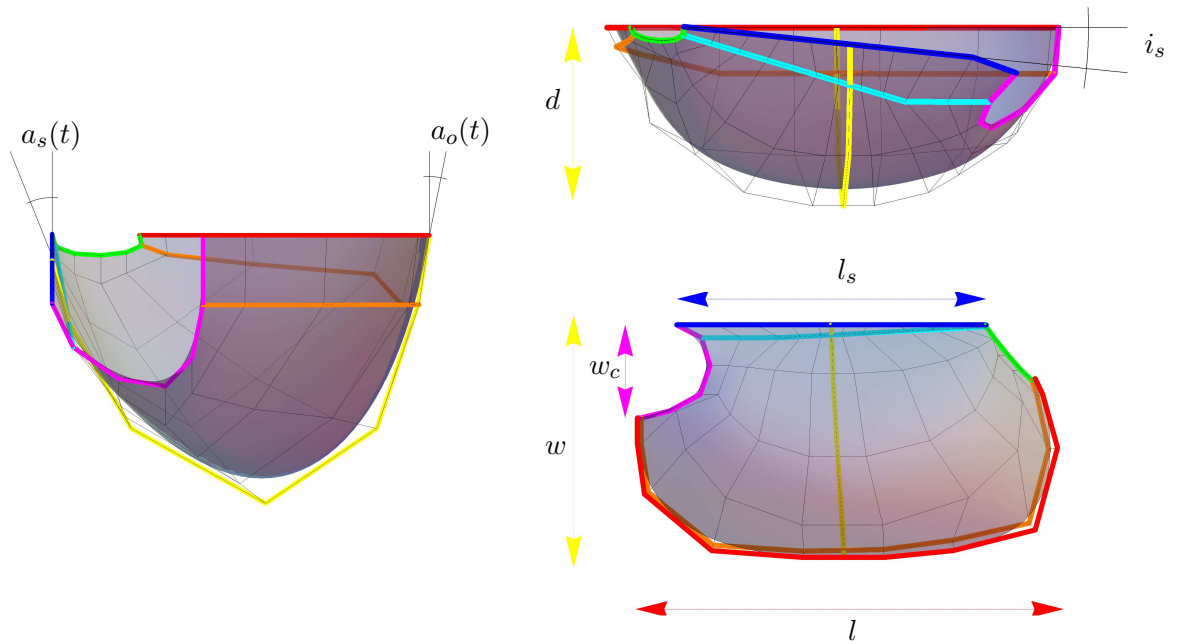


Figure 2.2: Three different views on the Pelton turbine bucket (splitter (blue), outlet curve (red), cutout (magenta)) with the prescribed parameters.

2.1.1 Inner surface

The one part of inner surface of the Pelton turbine bucket is usually given by several angles and distances (see Fig.2.2):

- l ... length,
- w ... width,
- d ... depth,
- l_s ... length of a splitter,
- w_c ... width of a cutout in a bucket,
- i_s ... inclination of a splitter,
- $a_s(t)$... angle distribution along a splitter,
- $a_o(t)$... outlet angle distribution from the bucket.

The geometric model of the inner surface of a Pelton turbine bucket can be based on uniform bicubic B-spline surfaces. Now, we mention how to prescribe some of the parameters determining the shape of the bucket. One way is to start with the boundary of a B-spline surface describing a bucket, i.e., we describe the control points of the boundary curves. With the help of standard algorithms for knot insertion and knot removal (cf. [69]) it is possible to satisfy given parameters.

Firstly, the splitter is constructed (Fig. 2.4 (top row, left)) as the cubic B-spline curve and its control points are defined. This ensures that the prescribed parameters l_s (length of a splitter) and i_s (inclination of a splitter) are preserved. The next step is to satisfy the l (length), w (width) and w_c (width of a cutout in a bucket) thus the outlet curve is prescribed also as the cubic B-spline curve (Fig. 2.4 (top row, right)). It is followed by the preserving of angle distributions $a_s(t)$ (along a splitter) and $a_o(t)$ along the outlet curve which generates neighbouring control points to splitter and outlet curve (see Fig. 2.4 second, row).

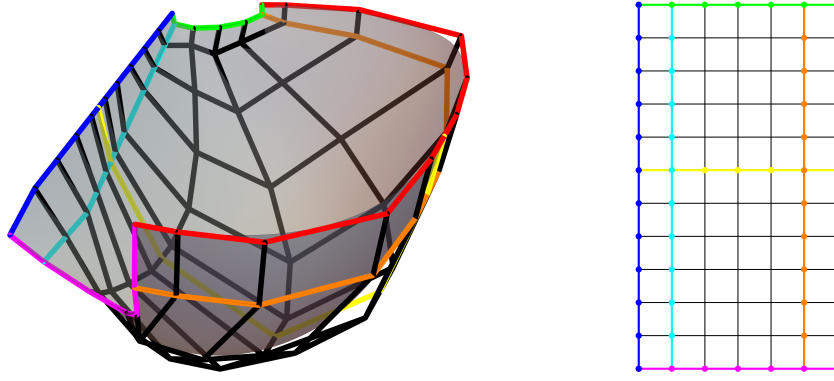


Figure 2.3: Left: The Pelton bucket is shown with the control net and important curves. Right: The schematic control net with marked control polygons of important curves.

These steps of preserving angle distributions are more complicated, therefore this problem is discussed in more detail in Section 2.1.1.1. The next step is to define the cutout of the bucket (the cutout curve is shown in Fig. 2.4 third row, left). This curve is already partially determined by preserving of the angle distributions $a_s(t)$ and $a_o(t)$ (the second and the last but one control points are defined) and the rest of the control points is computed from the minimization of second differences i.e. we establish objective function

$$F = \sum_{i=0}^n (\mathbf{P}_i - 2\mathbf{P}_{i+1} + \mathbf{P}_{i+2})^2, \quad (2.1)$$

where \mathbf{P}_i are the control points of the curve, $i = 0, \dots, n$ and $n + 1$ is the number of control points. Derivatives of F with respect to unknown variables lead to a system of linear equations for these unknown variables. The minimization of second differences can be understood as minimization of curvature of the control polygon. Further, it is necessary to preserve the given depth d of the bucket. Suitably chosen inner curve is included into the model via determining its control points (see Fig. 2.4 third row, right). The last curve is the curve that connects the bucket to the runner. This curve is constructed in the same way as the cutout of the bucket (Fig. 2.4 last row, left). Finally, remaining control points are obtained from minimization of second differences (Fig. 2.4 last row, right). The control net (see Fig. 2.3) has dimension 12×7 and the knot vectors of B-spline surface are

$$\begin{aligned} \mathbf{U} &= (0, 0, 0, 0, 1/7, 2/7, 3/7, 4/7, 4/7, 4/7, 5/7, 6/7, 1, 1, 1, 1), \\ \mathbf{V} &= (0, 0, 0, 0, 1/4, 1/2, 3/4, 1, 1, 1, 1). \end{aligned}$$

Intermediate steps of the construction of a B-spline surface representing the inner surface are shown in Fig. 2.4.

2.1.1.1 Imposing angle distribution along the given curve

We study the following problem (see more in [56]): Let

$$\mathbf{c}(t) = (c_x(t), c_y(t), 0)^\top, t \in [0, 1]$$

be a polynomial/rational parameterization of a given curve, e.g. B-spline/NURBS curve being a boundary curve of a general NURBS surface $\mathbf{s}(s, t)$, let $\mathbf{u} = (0, 0, 1)^\top$ be a given vector and let $f(t)$ be a function describing desired angle distribution which we need to prescribe on $\mathbf{s}(s, t)$ along $\mathbf{c}(t)$ with respect to \mathbf{u} , i.e., it holds that

$$\cos f(t) = (0, 0, 1)^\top \cdot \frac{(c'_x(t), c'_y(t), 0)^\top \times \mathbf{n}(0, t)}{\|(c'_x(t), c'_y(t), 0)^\top \times \mathbf{n}(0, t)\|} \quad (2.2)$$

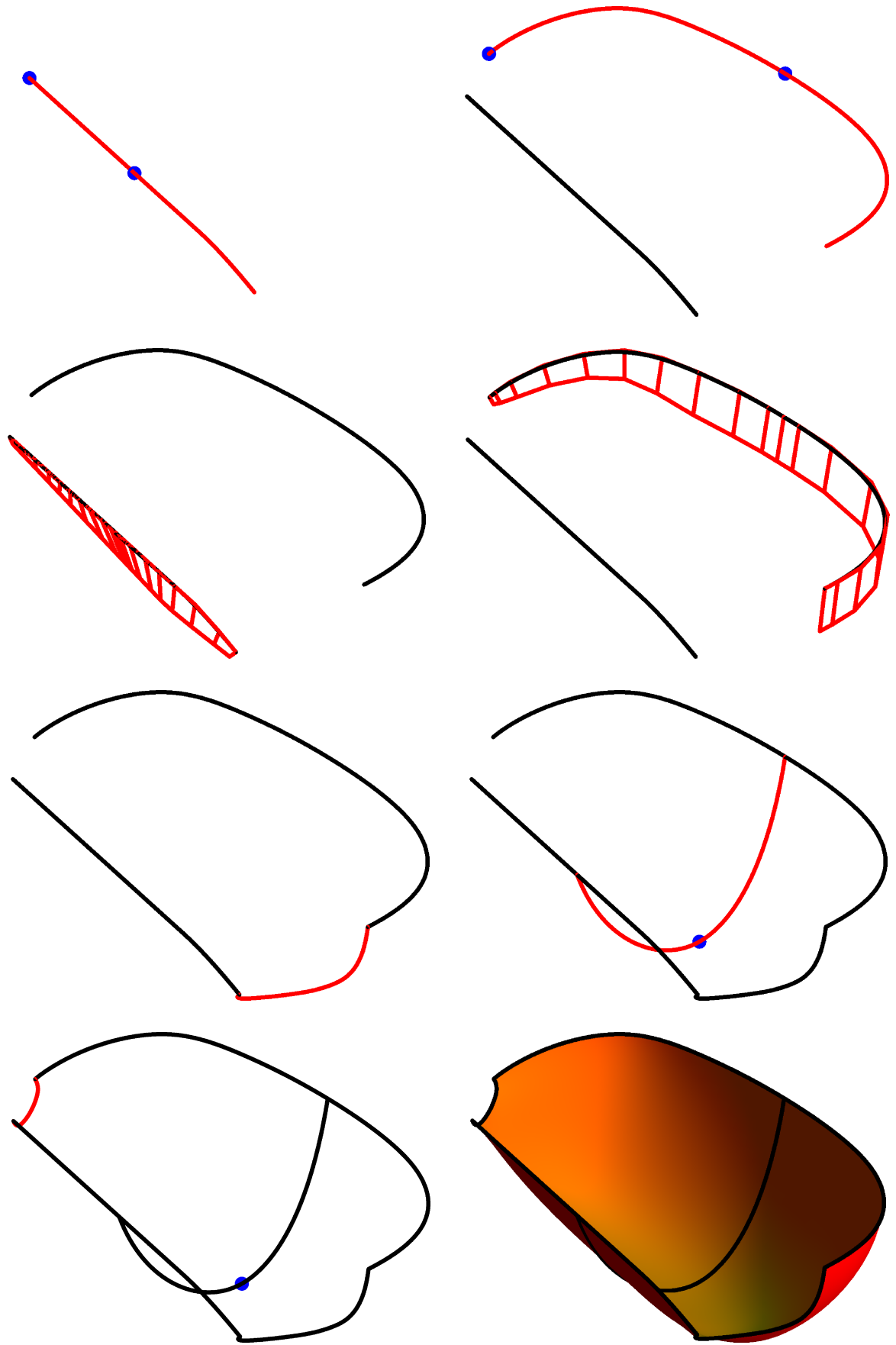


Figure 2.4: Process of modelling the inner surface of Pelton bucket with the help of B-spline curves and surfaces. Blue points are important to preserve prescribed parameters (length, width, depth, length of splitter).

where

$$\mathbf{n}(s, t) = \frac{\mathbf{r}_s(s, t) \times \mathbf{r}_t(s, t)}{\|\mathbf{r}_s(s, t) \times \mathbf{r}_t(s, t)\|}$$

is a normalized normal vector field of a ruled surface

$$\mathbf{r}(s, t) = (1 - s)\mathbf{c}(t) + s\mathbf{d}(t), (s, t) \in \mathbb{R} \times [0, 1] \quad (2.3)$$

determined by the curves $\mathbf{c}(t)$ and $\mathbf{d}(t) = (d_x(t), d_y(t), d_z(t))^\top, t \in [0, 1]$. Is it possible to find polynomial/rational curve $\mathbf{d}(t)$ such that the ruled surface (2.3) (and also $s(s, t)$) satisfies the prescribed angle distribution $f(t)$ along $\mathbf{c}(t)$?

The ruled surface $\mathbf{r}(s, t)$ represents the tangent surface to the desired surface $s(s, t)$ with $\mathbf{c}(t)$ being the boundary curve of $s(s, t)$ and $f(t)$ the prescribed angle distribution along $\mathbf{c}(t)$. In the context of B-spline/NURBS surfaces, whereas the control polygon of $\mathbf{c}(t)$ determines the boundary column (row) of the control net of $s(s, t)$, the control polygon of $\mathbf{d}(t)$ (defined for the same knot vector) represents the neighbouring column (row) of this control net. Altogether, control polygons of $\mathbf{c}(t)$ and $\mathbf{d}(t)$ determine the control net of the ruled surface (2.3) representing the tangent surface to the B-spline/NURBS surface $s(s, t)$ and also the first and second columns (rows) of the control net for the NURBS surface $s(s, t)$.

Remark 2 *Let us emphasize that the angle distribution defined in (2.2) is independent of directions of the rulings of $\mathbf{r}(s, t)$, as it is related to the normal vector of $\mathbf{r}(s, t)$ along $\mathbf{c}(t)$.*

Remark 3 *We study this case for the simplicity of the presented results, but exactly the same approach, presented in the following paragraphs, can be used for a general case, where $\mathbf{c}(t) = (c_x(t), c_y(t), c_z(t))^\top, t \in [0, 1]$ and $\mathbf{u} = (u_x, u_y, u_z)^\top$, only the results are too long to be included into the thesis.*

For the modelling of an inner surface of a Pelton turbine bucket. The curve $\mathbf{c}(t)$ could be the splitter or the outlet curve and the corresponding angle distributions are $a_s(t)$ along the splitter and outlet angle distribution from the bucket $a_o(t)$ (shown in Fig. 2.2 (right)).

Is there an exact solution? In this section, we will study the existence of an exact solution of the above mentioned problem. Let $\mathbf{c}(t)$ and \mathbf{u} be defined as in the beginning of Section 2.1.1.1 and let $f(t)$ be a given function defined for $t \in [0, 1]$. We want to determine if there *always* exists another polynomial/rational curve $\mathbf{d}(t) = (d_x(t), d_y(t), d_z(t))^\top, t \in [0, 1]$ such that the ruled surface $\mathbf{r}(s, t)$ (cf. (2.3)) fulfils (2.2), or if such a curve $\mathbf{d}(t)$ exists *only in special cases*.

Thus, in the first step we need to compute $\mathbf{d}(t)$ for given $\mathbf{c}(t)$, \mathbf{u} and $f(t)$. Normal vectors of $\mathbf{r}(s, t)$ along $\mathbf{c}(t)$ can be written in the form (for brevity we mention not normalized form)

$$\mathbf{n}(s, t) \Big|_{s=0} = \begin{pmatrix} -d_z(t)c'_y(t) \\ d_z(t)c'_x(t) \\ c'_x(t)(c_y(t) - d_y(t)) + (d_x(t) - c_x(t))c'_y(t) \end{pmatrix}.$$

Substituting to (2.2) we obtain

$$\cos f(t) = \frac{d_z(t)\sqrt{c'_x(t)^2 + c'_y(t)^2}}{\sqrt{(c'_x(t)(c_y(t) - d_y(t)) + (d_x(t) - c_x(t))c'_y(t))^2 + d_z(t)^2(c'_x(t)^2 + c'_y(t)^2)}}. \quad (2.4)$$

If we denote $g(t) = \cos f(t)$, then we compare $g^2(t)$ with the square of the right-hand side of (2.4), i.e.,

$$g^2(t) = \frac{d_z^2(t)(c'_x(t)^2 + c'_y(t)^2)}{(c'_x(t)(c_y(t) - d_y(t)) + (d_x(t) - c_x(t))c'_y(t))^2 + d_z(t)^2(c'_x(t)^2 + c'_y(t)^2)}, \quad (2.5)$$

and we can solve this equation with respect to $d_x(t)$. We arrive at

$$d_x(t) = c_x(t) + \frac{c'_x(t)(d_y(t) - c_y(t))}{c'_y(t)} \pm d_z(t) \frac{\sqrt{1-g^2(t)}}{g(t)} \frac{\sqrt{c'_x(t)^2 + c'_y(t)^2}}{c'_y(t)}. \quad (2.6)$$

Similarly, we can solve (2.5) with respect to $d_y(t)$ to obtain

$$d_y(t) = c_y(t) + \frac{c'_y(t)(d_x(t) - c_x(t))}{c'_x(t)} \pm d_z(t) \frac{\sqrt{1-g^2(t)}}{g(t)} \frac{\sqrt{c'_x(t)^2 + c'_y(t)^2}}{c'_x(t)} \quad (2.7)$$

or with respect to $d_z(t)$ to obtain

$$d_z(t) = \frac{g}{\sqrt{1-g^2(t)}} \frac{c'_x(t)(c_y(t) - d_y(t)) + c'_y(t)(d_x(t) - c_x(t))}{\sqrt{c'_x(t)^2 + c'_y(t)^2}}. \quad (2.8)$$

Thus, (2.6) obtained for an arbitrary $d_y(t)$, $d_z(t)$ (or (2.7) obtained for an arbitrary $d_x(t)$, $d_z(t)$, or (2.8) obtained for an arbitrary $d_x(t)$, $d_y(t)$) completes the parameterization of the curve $\mathbf{d}(t)$ such that the ruled surface $\mathbf{r}(s, t)$ given in (2.3) satisfies the given angle distribution $f(t)$ along $\mathbf{c}(t)$ (cf. (2.2)).

Further, we focus on an analysis of polynomiality/rationality of $\mathbf{d}(t)$. Firstly, if a given curve $\mathbf{c}(t)$ is a rationally parameterized curve, when is also the curve $\mathbf{d}(t)$ rational? In other words, if $\mathbf{c}(t)$ is a NURBS curve, when is also $\mathbf{d}(t)$ a NURBS curve? We can distinguish two cases:

1. $\mathbf{c}(t)$ is a *Pythagorean hodograph (PH) curve*: the defining property of planar PH curves (for more details see [35] and references cited therein) is that square of the norm of its hodograph is a square of some rational function. This implies that the square root $\sqrt{c'_x(t)^2 + c'_y(t)^2}$ in (2.6) cancels. Thus, $d_x(t)$ is rational if and only if $d_y(t)$ and $d_z(t)$ are rational and

$$\frac{\sqrt{1-g^2(t)}}{g(t)} = q(t)$$

for some rational function $q(t)$. Thus, $g^2(t)$ must be of the form

$$g^2(t) = \frac{1}{1+q^2(t)}, \quad q(t) \in \mathbb{R}(t). \quad (2.9)$$

It is obvious that expressions (2.7) and (2.8) lead to exactly the same condition.

2. $\mathbf{c}(t)$ is not a *Pythagorean hodograph curve*: $d_x(t)$ is rational if and only if $d_y(t)$ and $d_z(t)$ are rational and

$$\frac{\sqrt{1-g^2(t)}}{g(t)} \sqrt{c'_x(t)^2 + c'_y(t)^2} = q(t)$$

for some rational function $q(t)$. Thus, $g^2(t)$ must be of the form

$$g^2(t) = \frac{c'_x(t)^2 + c'_y(t)^2}{c'_x(t)^2 + c'_y(t)^2 + q^2(t)}, \quad q(t) \in \mathbb{R}(t). \quad (2.10)$$

It is again obvious that expressions (2.7) and (2.8) lead to exactly the same condition.

We can summarize this part in the following proposition.

Proposition 1 *Let $\mathbf{c}(t)$ be a given NURBS curve, representing boundary curve of a NURBS surface. Then there exists another NURBS curve $\mathbf{d}(t)$ such that the ruled surface (2.3) fulfils angle distribution (2.2) for given $f(t)$ along $\mathbf{c}(t)$ if and only if either $\mathbf{c}(t)$ is a Pythagorean hodograph curve and $g^2(t) = \cos^2 f(t)$ is of the form (2.9) for some $q(t) \in \mathbb{R}(t)$, or $g^2(t) = \cos^2 f(t)$ is of the form (2.10) for some $q(t) \in \mathbb{R}(t)$.*

Secondly, we can ask, whether there exists a polynomial parameterization $\mathbf{d}(t)$, if the given curve $\mathbf{c}(t)$ is polynomial. We can use the similar approach as above but we have to distinguish between the cases represented by (2.6), (2.7) and (2.8) now:

1. $d_x(t)$ is polynomial if and only if $d_y(t)$ and $d_z(t)$ are polynomial and

$$\frac{c'_x(t)(d_y(t) - c_y(t))}{c'_y(t)} \pm d_z(t) \frac{\sqrt{1 - g^2(t)}}{g(t)} \frac{\sqrt{c'_x(t)^2 + c'_y(t)^2}}{c'_y(t)} = q(t)$$

for some polynomial function $q(t)$. Thus, $g^2(t)$ must be of the form

$$g^2(t) = \frac{d_z(t)^2(c'_x(t)^2 + c'_y(t)^2)}{(c_y(t)c'_x(t) - d_y(t)c'_x(t) + q(t)c'_y(t))^2 + d_z(t)^2(c'_x(t)^2 + c'_y(t)^2)}, \quad q(t) \in \mathbb{R}[t]; \quad (2.11)$$

2. $d_y(t)$ is polynomial if and only if $d_x(t)$ and $d_z(t)$ are polynomial and

$$\frac{c'_y(t)(d_x(t) - c_x(t))}{c'_x(t)} \pm d_z(t) \frac{\sqrt{1 - g^2(t)}}{g(t)} \frac{\sqrt{c'_x(t)^2 + c'_y(t)^2}}{c'_x(t)} = q(t)$$

for some polynomial function $q(t)$. Thus, $g^2(t)$ must be of the form

$$g^2(t) = \frac{d_z(t)^2(c'_x(t)^2 + c'_y(t)^2)}{(c_x(t)c'_y(t) - d_x(t)c'_y(t) + q(t)c'_x(t))^2 + d_z(t)^2(c'_x(t)^2 + c'_y(t)^2)}, \quad q(t) \in \mathbb{R}[t]; \quad (2.12)$$

3. $d_z(t)$ is polynomial if and only if $d_x(t)$ and $d_y(t)$ are polynomial and

$$\frac{g}{\sqrt{1 - g^2(t)}} \frac{c'_x(t)(c_y(t) - d_y(t)) + c'_y(t)(d_x(t) - c_x(t))}{\sqrt{c'_x(t)^2 + c'_y(t)^2}} = q(t)$$

for some polynomial function $q(t)$. Thus, $g^2(t)$ must be of the form

$$g^2(t) = \frac{q^2(t)(c'_x(t)^2 + c'_y(t)^2)}{(c_y(t)c'_x(t) - d_y(t)c'_x(t) - c_x(t)c'_y(t) + d_x(t)c'_y(t))^2 + q^2(t)(c'_x(t)^2 + c'_y(t)^2)}, \quad q(t) \in \mathbb{R}[t]. \quad (2.13)$$

Proposition 2 Let $\mathbf{c}(t)$ be a given B-spline curve, representing a boundary curve of a B-spline surface. Then there exists another B-spline curve $\mathbf{d}(t)$ such that the ruled surface (2.3) fulfils angle distribution (2.2) for given $f(t)$ along $\mathbf{c}(t)$ if and only if $g^2(t) = \cos^2 f(t)$ is of the form (2.11), (2.12) or (2.13) for some $q(t) \in \mathbb{R}[t]$.

Example 1 Let $\mathbf{c}(t)$ be a Bézier curve given by control points $\mathbf{P}_0 = (0, 0, 0)^\top$, $\mathbf{P}_1 = (1, 2, 0)^\top$, $\mathbf{P}_2 = (4, 1, 0)^\top$, $\mathbf{P}_3 = (5, -1, 0)^\top$, i.e.,

$$\mathbf{c}(t) = (t(3 + 6t - 4t^2), t(6 - 9t + 2t^2), 0)^\top, \quad t \in [0, 1],$$

and let

$$\begin{aligned} \cos f(t) &= \\ &= \frac{2(2+3t-6t^2+3t^3)\sqrt{5-16t+52t^2-56t^3+20t^4}}{\sqrt{84-52t-51t^2+1648t^3-2518t^4-3604t^5+15641t^6-22072t^7+16108t^8-6016t^9+916t^{10}}}. \end{aligned}$$

We want to know if there exists a polynomial $\mathbf{d}(t)$ (as $\mathbf{c}(t)$ is polynomial) such that $\mathbf{r}(s, t)$ defined in (2.3) fulfils given $f(t)$. Thus, we need to check if $\cos f(t)$ is of the form (2.11). Let us arbitrarily choose $d_y(t)$, $d_z(t)$, e.g.

$$d_y(t) = \frac{1}{2}t(9 - 18t + 5t^2), \quad d_z(t) = -2 - 3t + 6t^2 - 3t^3.$$

Then, the necessary and sufficient condition for the existence of a polynomial $d_x(t)$ is that there exists a polynomial $q(t)$ such that (2.11) holds. Thus, we can substitute components of $\mathbf{c}(t)$, $d_y(t)$, $d_z(t)$ and $f(t)$ into (2.11) and solve for $q(t)$. We obtain

$$q(t) = \frac{1}{2}(1 - 3t - 3t^2 + 5t^3).$$

Thus, the exact solution exists! Then, with the help of (2.6) we arrive at

$$d_x(t) = \frac{1}{2}(1 + 3t + 9t^2 - 3t^3).$$

It is obvious that this example is artificial. For general function $f(t)$, there is no polynomial $q(t)$ and $\mathbf{d}(t)$ (see below). In this particular case, we just wanted to show that if we start from the solution (we basically started with $\mathbf{d}(t)$ and computed the corresponding $f(t)$ in this example), we can reconstruct the exact solution.

On the other hand, if we choose another angle function, e.g.

$$\cos f(t) = t^2,$$

then we can test if there exists at least some rational curve $\mathbf{d}(t)$ such that $\mathbf{r}(s, t)$ defined in (2.3) fulfils given $f(t)$ with the help of expression (2.10). Substituting components of $\mathbf{c}(t)$ and $f(t)$ to (2.10) and solving with respect to $q(t)$ we obtain

$$q(t) = \pm \frac{\sqrt{-20t^8 + 56t^7 - 52t^6 + 16t^5 + 15t^4 - 56t^3 + 52t^2 - 16t + 5}}{2t^2(t^2 - 3t + 1)}$$

which is not rational. According to Proposition 1 we can conclude that there exists no exact solution of the above mentioned problem for this choice of the angle function $f(t)$.

Remark 4 Propositions 1 and 2 imply that an exact solution, represented by a B-spline/NURBS curve $\mathbf{d}(t)$, for a given B-spline/NURBS curve $\mathbf{c}(t)$ exists only for a very special form of the given function $f(t)$ representing an angle distribution along $\mathbf{c}(t)$, i.e., only in very rare cases. In practice, $f(t)$ is usually given as a polynomial function which is clearly not of the form mentioned in Propositions 1 and 2. Thus, this problem does not have an exact solution in most cases. This motivates us to formulate an algorithm for finding an approximate solution which is demonstrated and studied in the next paragraph.

Approximate solution In this part, we formulate an algorithm for finding an approximate solution to the problem stated in the previous paragraph, derive an upper bound for the error of approximate angle distribution and study an approximation order of the method.

Algorithm starts with a given regular B-spline curve $\mathbf{c}(t) = (x(t), y(t), 0)$, $t \in [0, 1]$, which is described by its control polygon $\{\mathbf{P}_i\}_{i=0}^n$ and knot vector U , and with a function $f(t)$ describing the desired angle distribution along $\mathbf{c}(t)$.

In the first step, we determine the exact solution $\mathbf{r}(s, t) = \mathbf{c}(t) + s\mathbf{v}(t)$, $(s, t) \in \mathbb{R} \times [0, 1]$, where $\mathbf{v}(t)$ is a vector field along $\mathbf{c}(t)$ such that

$$(0, 0, 1)^\top \cdot \frac{\mathbf{v}(t)}{\|\mathbf{v}(t)\|} = \cos f(t).$$

Thus, $\mathbf{v}(t)$ is of the form

$$\mathbf{v}(t) = \mathbf{R}(f(t)) \cdot (0, 0, 1)^\top,$$

where $\mathbf{R}(f(t))$ is the rotation matrix describing the counterclockwise rotation around the unit tangent vector

$$\mathbf{w}(t) = \frac{1}{\sqrt{x'(t)^2 + y'(t)^2}} (x'(t), y'(t), 0)^\top,$$

Algorithm 1 Finds an approximate tangent ruled surface along a boundary curve of a B-spline surface with the prescribed angle distribution

Input: Control points $\{\mathbf{P}_i\}$, $i = 0, \dots, n$ of a boundary curve $\mathbf{c}(t)$, $t \in [0, 1]$, knot vector U , vector $\mathbf{z} = (z_i)$, angle function $f(t)$

Output: Control points $\{\bar{\mathbf{P}}_i\}$, $i = 0, \dots, n$ of $\bar{\mathbf{c}}(t)$

1: Compute the exact tangent surface parameterization:

$$\mathbf{r}(s, t) = \mathbf{c}(t) + s \left(\frac{\sin(f(t))y'(t)}{\sqrt{x'(t)^2 + y'(t)^2}}, -\frac{\sin(f(t))x'(t)}{\sqrt{x'(t)^2 + y'(t)^2}}, \cos(f(t)) \right), \quad (s, t) \in \mathbb{R} \times [0, 1]$$

2: Determine the initial control polygon of $\hat{\mathbf{c}}(t)$:

$$\hat{\mathbf{P}}_i = (P_{i,x}, P_{i,y}, z_i), \quad i = 0, \dots, n, \quad \hat{\mathbf{c}}(t) = \text{bsplinecurve}(\{\hat{\mathbf{P}}_i\}, U, t)$$

3: Set the control points of $\bar{\mathbf{c}}(t)$ with unknown shifts:

$$\bar{\mathbf{P}}_i = \hat{\mathbf{P}}_i + (X_i, Y_i, Z_i), \quad i = 0, \dots, n, \quad \bar{\mathbf{c}}(t) = \text{bsplinecurve}(\{\bar{\mathbf{P}}_i\}, U, t)$$

4: Initialization of an objective function:

$$F = 0$$

5: Form the objective function for the follow-up minimization:

6: **for** $k = 0 \rightarrow N$ **do**

7: $T = k/N$

▷ Select the parameter in the interval $[0, 1]$

8: $\mathbf{Q} \in \mathbf{r}(s, T) \cap (z = \hat{c}_z(T))$

▷ Compute an intersection point of the ruling $\mathbf{r}(s, T)$

9:

with the plane parallel with xy -plane

10: $F = F + \|\bar{\mathbf{c}}(T) - \mathbf{Q}\|^2$

▷ F is a function of unknowns X_i, Y_i, Z_i

11: **end for**

12: Minimize the objective function by solving a linear system of equations:

$$\{(\bar{X}_i, \bar{Y}_i, \bar{Z}_i)\} = \text{solve} \left(\frac{\partial F}{\partial X_i} = 0 \wedge \frac{\partial F}{\partial Y_i} = 0 \wedge \frac{\partial F}{\partial Z_i} = 0 \right)$$

13: **return** $\bar{\mathbf{P}}_i = \hat{\mathbf{P}}_i + (\bar{X}_i, \bar{Y}_i, \bar{Z}_i)$, $i = 0, \dots, n$

i.e.,

$$\begin{aligned} \mathbf{R}(f(t)) &= \mathbf{w}(t)\mathbf{w}(t)^\top + \cos f(t)(\mathbf{I} - \mathbf{w}(t)\mathbf{w}(t)^\top) + \\ &+ \sin f(t) \begin{pmatrix} 0 & -w_z(t) & w_y(t) \\ w_z(t) & 0 & -w_x(t) \\ -w_y(t) & w_x(t) & 0 \end{pmatrix}. \end{aligned}$$

We obtain

$$\mathbf{v}(t) = \left(\frac{\sin(f(t))y'(t)}{\sqrt{x'(t)^2 + y'(t)^2}}, -\frac{\sin(f(t))x'(t)}{\sqrt{x'(t)^2 + y'(t)^2}}, \cos(f(t)) \right)^\top. \quad (2.14)$$

Thus, we found a non-rational parameterization of a ruled surface $\mathbf{r}(s, t)$ such that the angle between its ruling $\mathbf{r}(s, T)$ and the vector $(0, 0, 1)^\top$ is $f(T)$, for any $T \in [0, 1]$.

Then, the approximation starts with selecting a suitable initial control polygon of a B-spline curve $\hat{\mathbf{c}}(t)$ which will be refined to the final approximation curve $\bar{\mathbf{c}}(t)$ in the follow-up minimization procedure. Let us emphasize that the number of control points and the knot vector of $\hat{\mathbf{c}}(t)$ and $\bar{\mathbf{c}}(t)$ (i.e., also the degree) are not arbitrary, they must be the same as for $\mathbf{c}(t)$ because $\mathbf{c}(t)$ and $\bar{\mathbf{c}}(t)$ must fit into the same

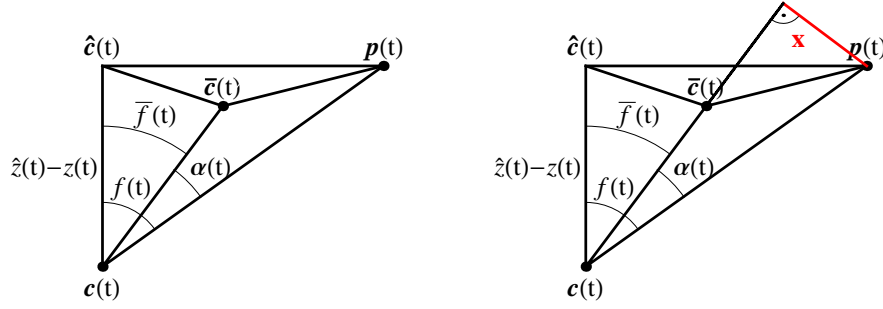


Figure 2.5: Illustration for the proof of Theorem 1: For an arbitrary $t \in [0, 1]$, the points $\mathbf{c}(t)$, $\hat{\mathbf{c}}(t)$, $\bar{\mathbf{c}}(t)$, $\mathbf{p}(t)$ represent the points on a given curve, initial approximation curve, final approximation curve and exact curve on ruled surface $\mathbf{r}(s, t)$, respectively, and generally form a tetrahedron (left) and illustration for x (right).

control net of a final B-spline/NURBS surface and we do not want to change the number of control points and knot vector of $\mathbf{c}(t)$.

Because of our consideration the given curve $\mathbf{c}(t)$ being a planar curve in xy -plane (which is motivated by the practical example of modelling an inner surface of a Pelton turbine bucket) we choose control points $\{\hat{\mathbf{P}}_i\}_{i=0}^n$ of $\hat{\mathbf{c}}(t)$ to have x - and y -coordinates the same as $\{\mathbf{P}_i\}_{i=0}^n$, only z -coordinates are changed. The choice of z -coordinate z_i of the point $\hat{\mathbf{P}}_i$ is arbitrary with one exception: $z_i \neq 0$ must hold. Thus, vector of z -coordinates $\mathbf{z} = (z_i)_{i=0}^n$ of control points $\{\hat{\mathbf{P}}_i\}_{i=0}^n$ is another input to the algorithm.

Since we need to refine the control points $\{\hat{\mathbf{P}}_i\}_{i=0}^n$ such that the corresponding B-spline curve is the best approximation of the selected points on $\mathbf{r}(s, t)$, we introduce new control points

$$\bar{\mathbf{P}}_i = \hat{\mathbf{P}}_i + (X_i, Y_i, Z_i), \quad i = 0, \dots, n \quad (2.15)$$

of the final approximation B-spline curve $\bar{\mathbf{c}}(t)$ with unknown shifts (X_i, Y_i, Z_i) , $i = 0, \dots, n$. Then we sample the B-spline curve $\hat{\mathbf{c}}(t)$ and for each selected point $\hat{\mathbf{c}}(T)$ on the curve we find the corresponding point $\mathbf{Q}(T)$ on the ruling $\mathbf{r}(s, T)$, obtained for the same parameter value T , lying in the plane parallel to xy -plane and going through the point $\hat{\mathbf{c}}(T)$. Then the differences of such points $\mathbf{Q}(T)$ and the corresponding points $\bar{\mathbf{c}}(T)$ give us an objective function

$$F = \sum_{i=0}^N \|\bar{\mathbf{c}}(i/N) - \mathbf{Q}(i/N)\|^2, \quad i = 0, \dots, N$$

which we need to minimize. Therefore, we solve the system of linear equations

$$\frac{\partial F}{\partial X_i} = 0 \wedge \frac{\partial F}{\partial Y_i} = 0 \wedge \frac{\partial F}{\partial Z_i} = 0, \quad i = 0, \dots, n$$

and the solution is substituted back to (2.15). This gives us the control points $\{\bar{\mathbf{P}}_i\}_{i=0}^n$ of the approximation curve $\bar{\mathbf{c}}(t)$. Consequently, we obtain the approximate ruled surface

$$\bar{\mathbf{r}}(s, t) = (1 - s)\mathbf{c}(t) + s\bar{\mathbf{c}}(t)$$

which approximately determines the tangent surface along $\mathbf{c}(t)$ and which gives approximate angle distribution along $\mathbf{c}(t)$. The obtained control points $\{\bar{\mathbf{P}}_i\}_{i=0}^n$ are then used as the neighbouring row/column of boundary control points $\{\mathbf{P}_i\}_{i=0}^n$ in the control net describing a B-spline/NURBS surface and the same angle distribution along $\mathbf{c}(t)$ is guaranteed also for the B-spline surface. The whole algorithm is summarized in Algorithm 1.

Parts	$f_1(t)$		$f_2(t)$	
	Error	Ratio	Error	Ratio
1	0.102455	/	0.052222	/
2	0.002531	40.4773	0.00301	17.3495
4	0.000062	39.4252	0.00017	28.226
8	$1.586 \cdot 10^{-6}$	26.5405	$6.142 \cdot 10^{-6}$	22.2259
16	$5.976 \cdot 10^{-8}$	20.9415	$2.766 \cdot 10^{-7}$	19.017
32	$2.854 \cdot 10^{-9}$	18.4016	$1.454 \cdot 10^{-8}$	17.4878
64	$1.551 \cdot 10^{-10}$	17.1868	$8.317 \cdot 10^{-10}$	16.7394
128	$9.024 \cdot 10^{-12}$	16.5895	$4.969 \cdot 10^{-11}$	16.3687
256	$5.43 \cdot 10^{-13}$	16.2939	$3.0355 \cdot 10^{-12}$	16.1841
512	$3.338 \cdot 10^{-14}$	16.1468	$1.875 \cdot 10^{-13}$	16.0920
1024	$2.068 \cdot 10^{-15}$	16.0733	$1.165 \cdot 10^{-14}$	16.045
2048	$1.286 \cdot 10^{-16}$	16.037	$7.263 \cdot 10^{-16}$	16.023

Table 2.1: Errors and their improvements (ratios of two consecutive errors) for Example 2

Remark 5 In the previous, we chose for simplicity (and because of the motivation by the practical example of a Pelton turbine bucket) a planar input curve $\mathbf{c}(t)$ and an angle was determined with respect to the unit normal vector \mathbf{u} of a plane containing the curve $\mathbf{c}(t)$, i.e., $\mathbf{u} = (0, 0, 1)^\top$.

Nevertheless, it is possible to generalize the algorithm also for an arbitrary regular curve $\mathbf{c}(t) = (x(t), y(t), z(t))^\top$, $t \in [0, 1]$ and vector $\mathbf{u} = (u_x, u_y, u_z)^\top$ which fulfil that $\mathbf{c}'(t)$ is not co-linear with \mathbf{u} for all $t \in [0, 1]$. Then, $\mathbf{w}(t)$ is a perpendicular projection of $\mathbf{c}'(t)$ to the plane perpendicular to \mathbf{u} and $\mathbf{v}(t)$ is computed analogously. This gives us the exact tangent surface $\mathbf{r}(s, t)$. Further, the control points $\{\widehat{\mathbf{P}}_i\}_{i=0}^n$ of $\widehat{\mathbf{c}}(t)$ are chosen as translated control points $\{\mathbf{P}_i\}_{i=0}^n$ in direction of \mathbf{u} and the rest of the algorithm is exactly the same.

In the following we will show that the error of angle distribution approximation is bounded by the approximation error resulting from Algorithm 1.

Theorem 1 Let $\widehat{\mathbf{c}}(t) = (\widehat{x}(t), \widehat{y}(t), \widehat{z}(t))$ be the B-spline curve defined in Step 2 of Algorithm 1, $\mathbf{p}(t) = (p_x(t), p_y(t), p_z(t))$ be the curve on the ruled surface $\mathbf{r}(s, t)$ defined in Step 1 of Algorithm 1 such that $p_z(t) = \widehat{z}(t)$ and $\bar{\mathbf{c}}(t) = (\bar{x}(t), \bar{y}(t), \bar{z}(t))$ be its B-spline approximation computed using Algorithm 1. Let $f(t)$ and $\bar{f}(t)$ be functions describing the exact and approximate angle distributions along $\mathbf{c}(t)$, respectively. Then it holds

$$\sin |f(t) - \bar{f}(t)| \leq \delta \max_{t \in [0, 1]} \|\mathbf{p}(t) - \bar{\mathbf{c}}(t)\|,$$

$$\text{where } \delta = \max_{t \in [0, 1]} \frac{1}{|\widehat{z}(t) - z(t)|}.$$

PROOF: For arbitrary t , with the help of the triangle inequality (see Fig. 2.5 (left)) we obtain

$$\|\mathbf{p}(t) - \mathbf{c}(t)\| \geq |\widehat{z}(t) - z(t)|.$$

Further, $|f(t) - \bar{f}(t)| \leq \alpha(t)$, $\alpha(t) \in \langle 0, \frac{\pi}{2} \rangle$ and it holds that

$$\sin \alpha(t) = \frac{x}{\|\mathbf{p}(t) - \mathbf{c}(t)\|}.$$

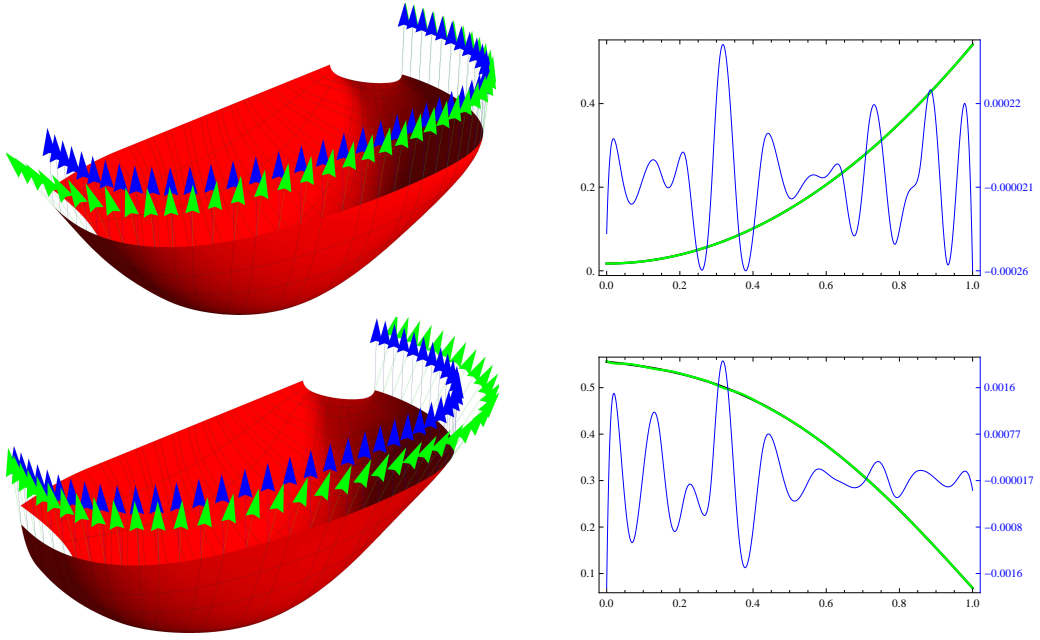


Figure 2.6: The inner surface of a Pelton turbine bucket (red) with quadratic (top row) and quartic (bottom row) distribution of angle along an outlet curve (green) measured with respect to the reference vector (blue) and the comparison of the exact (black) and the approximate (green) angle distributions, together with an error plot (thin blue, the corresponding scale is on the right) (right column).

Moreover, as $x \leq \|\mathbf{p}(t) - \bar{\mathbf{c}}(t)\|$ (see Fig. 2.5 (right)) we can write

$$\sin \alpha(t) \leq \frac{\|\mathbf{p}(t) - \bar{\mathbf{c}}(t)\|}{\|\mathbf{p}(t) - \mathbf{c}(t)\|}.$$

Thus, we obtain

$$\sin |f(t) - \bar{f}(t)| \leq \sin \alpha(t) \leq \frac{\|\mathbf{p}(t) - \bar{\mathbf{c}}(t)\|}{\|\mathbf{p}(t) - \mathbf{c}(t)\|} \leq \frac{1}{|\hat{z}(t) - z(t)|} \|\mathbf{p}(t) - \bar{\mathbf{c}}(t)\|.$$

Finally, by denoting $\delta = \max_{t \in [0,1]} \frac{1}{|\hat{z}(t) - z(t)|}$, the statement follows. \square

Apart from deriving a bound for the error of an approximate angle distribution obtained with the help of Algorithm 1, we also analyze the approximation order of our above mentioned algorithm. We apply Algorithm 1 on a given B-spline curve $\mathbf{c}(t)$ and a given angle function $f(t)$ and we obtain a surface which approximately satisfies the given angle distribution $f(t)$. Further, we analyze the obtained angle distribution on the resulting surface – the approximation error corresponds to the Hausdorff distance between the exact and approximate angle distributions. Then, we insert a new knot into each knot span (with the help of knot insertion algorithm – see [69]) and the process repeats for new data. We examine the ratio of two consecutive errors and we find out that the approximation order of the mentioned algorithm is 4, see Example 2.

Example 2 Let us consider the functions $f_1(t) = \frac{\pi}{6}t^2 + \frac{\pi}{180}$ and $f_2(t) = \frac{4}{13}t^4 - \frac{3}{5}t^3 - \frac{1}{9}t^2 - \frac{1}{12}t + \frac{5}{9}$ and the B-spline curve on the interval $t \in [0, 1]$ with the control points $\{(0, 0, 0)^\top, (1, 2, 0)^\top, (2, 2, 0)^\top, (4, 0, 0)^\top\}$ and the knot vector $(0, 0, 0, 0, 1, 1, 1, 1)$. Table 2.1 summarizes the approximation error and its improvement (ratio of two consecutive errors). The error was obtained by measuring the Hausdorff distance. The improvement ratio tends to $16 = 2^4$ in both cases which indicates that the approximation order of the above mentioned procedure is 4.

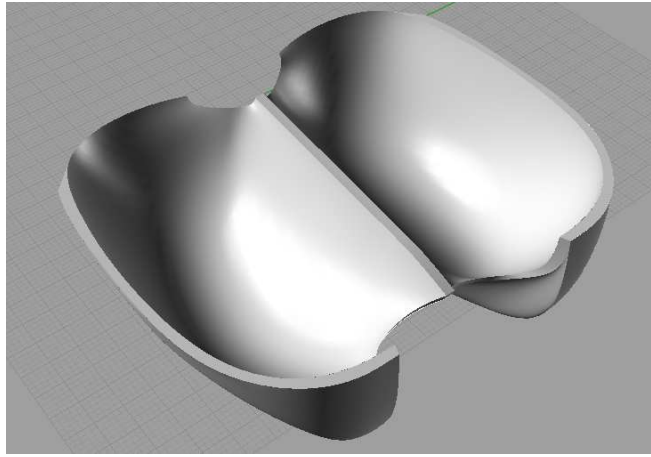


Figure 2.7: The Pelton turbine bucket.

Remark 6 *Let us emphasize that refining a boundary curve $\mathbf{c}(t)$, i.e., increasing the number of knot spans in order to decrease the approximation error obtained in Algorithm 1, is not always appropriate because B-spline description (i.e., control net and knot vectors) of the corresponding B-spline surface becomes more complex.*

In the following example, we applied Algorithm 1 to the particular case of the model of a Pelton turbine bucket and its outlet curve and we show results for different functions describing the angle distribution along the outlet curve.

Example 3 *In this example, we show the results obtained for the Pelton turbine bucket model and its outlet curve with the help of Algorithm 1 for two functions, in particular;*

1. $f_1(t) = \frac{\pi}{6}t^2 + \frac{\pi}{180}$, $t \in [0, 1]$, see Fig. 2.6 (top row), based on the analysis of the existing and used bucket,
2. $f_2(t) = \frac{4}{13}t^4 - \frac{3}{5}t^3 - \frac{1}{9}t^2 - \frac{1}{12}t + \frac{5}{9}$, $t \in [0, 1]$, see Fig. 2.6 (bottom row), based on the recommendations presented in [77].

Let us point out that an outlet curve on the model is composed of fourteen parts. Fig. 2.6 (right column) shows the difference in comparison of the exact and approximate angle distributions. Refining the B-spline model of an inner surface of the Pelton turbine bucket would lead to the better angle function approximation (as demonstrated in Example 2), but also to the more complex B-spline model.

2.1.2 Outer surface

We use another approach for a model of the Pelton turbine bucket outer surface. The boundary curves are derived from boundary curves of the inner surface with the help of approximation of variable offsets by B-spline curves. Thus the parameters for the outer surface are

- $d_s(t)$... function of distance along the splitter,
- $d_o(t)$... function of distance along the outlet curve,
- $d_d(t)$... function of distance along the curve determining the depth of inner surface,
- $d_c(t)$... function of distance along the cutout curve.

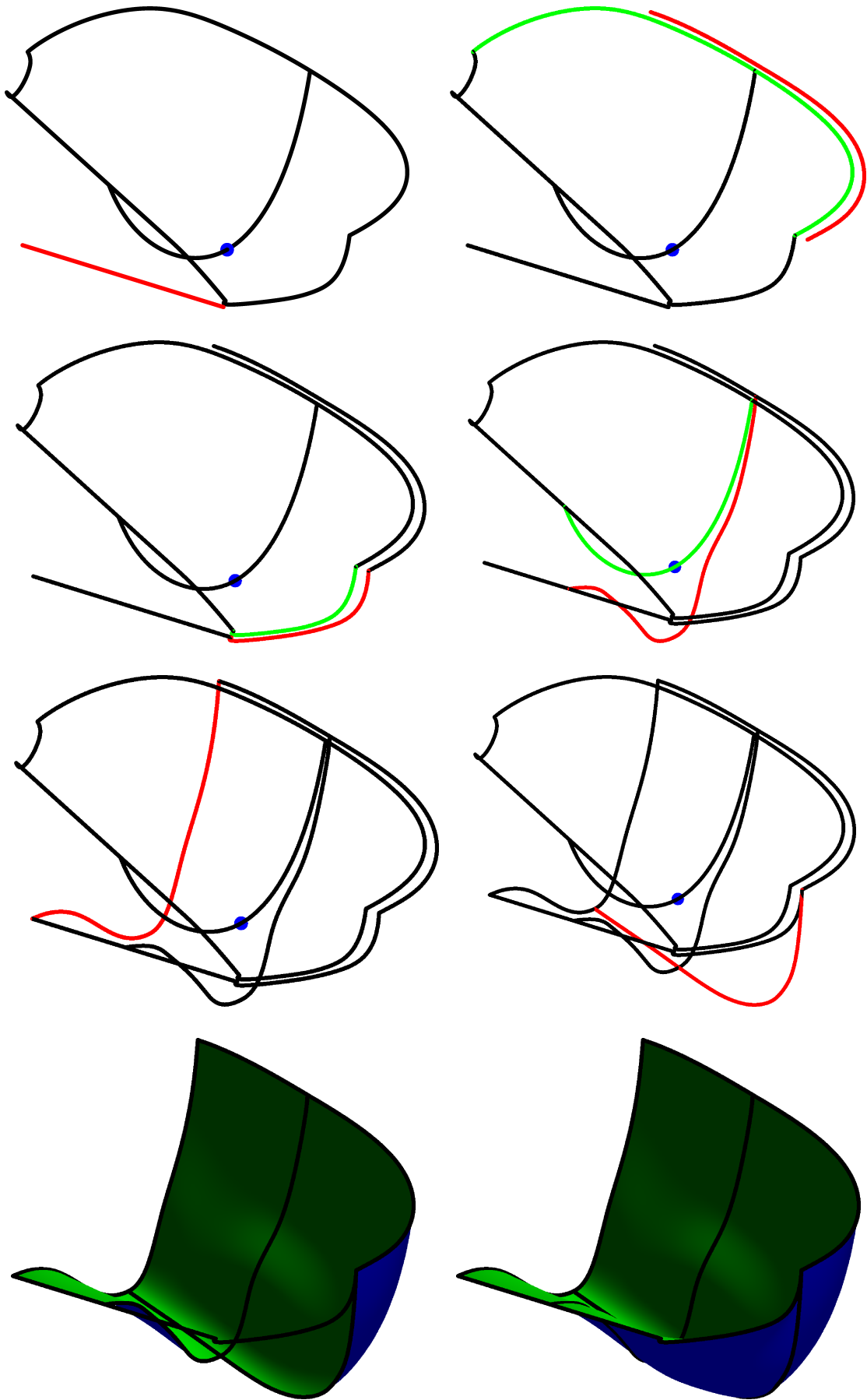


Figure 2.8: Creating B-spline surface representing the outer surface.

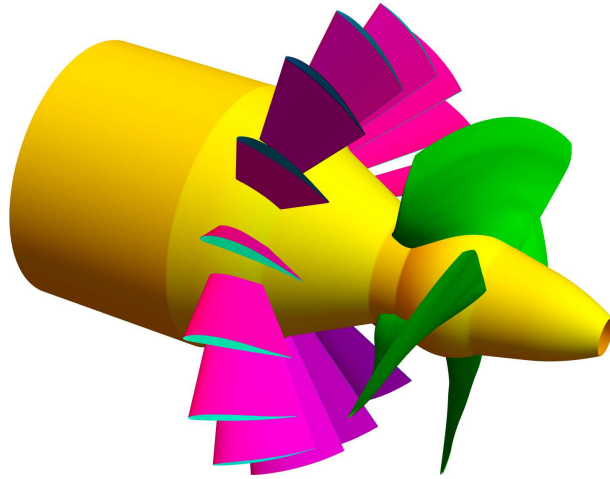


Figure 2.9: Guide vanes (purple) and runner blades (green) of KT.

We start with the curve derived from splitter (see Fig. 2.8 (top row, left)) and the curve derived from outlet curve (see Fig. 2.8 (top row, right)) and we use the $d_s(t)$ and $d_o(t)$ to determine the B-spline curve that approximates variable offset of the splitter or outlet curve. The cutout curve (preserving $d_c(t)$) is computed analogically to the previous curves (see Fig. 2.8 (second row, right)). In the Fig. 2.8 (second row, right) is shown the curve that is derived as the variable offset of the depth curve and we satisfy the parameter $d_d(t)$. The specific shape of the curve is determined by the different pressure on the bucket. Moreover, the curve that forms the back side of the bucket is added (Fig. 2.8 (third row, left)) the curve is similar to the curve that defines the depth of the outer surface. The last curve is the one that forms the front side of the bucket (Fig. 2.8 (third row, right)).

Further, the outer surface is divided into four parts, their edges are specific parts of the boundary curves. The three of them are derived as bicubic Coons patches (cf. [24]) for given boundary. Coons patches are subsequently transformed to B-spline surfaces by finding their corresponding control nets and knot vectors (see Fig. 2.8 (last row, left)). This process is based mainly on the conversion of the polynomial functions to the B-spline basis functions it also means to use the knot insertion and knot deletion algorithms (see more in [69]). Now, when the control points of three parts are defined, we correct some control points to obtain the result surface with C^2 continuity, i.e., the control points around the common curves are corrected such that the C^2 continuity conditions are fulfilled (see more in Section 2.2.1). The front piece patch with the part of a splitter and a cut-out is obtained as a B-spline surface (see Fig. 2.8 (last row, right)). Because this part includes sharp passage we enforce only G^1 continuity conditions around the corresponding part of the boundary. In Fig. 2.7 the final Pelton bucket is shown exported to the Rhinoceros software. There can be seen that there is added surface along the splitter. This is just for technical reasons because it is not possible to construct the bucket with zero thickness along the the splitter.

2.2 Kaplan turbine blade

In the following sections we describe the creation of Kaplan turbine (KT) blades with B-spline/NURBS curves and surfaces. There are two types of blades in KT: guide vanes and runner blades. The guide vanes serve to streamline the flow of water before it reaches the runner blades. On the other hand, the runner blades transform the energy of the flow. From the geometric point of view we start with the description of 2D profile of the blade and its geometric parameterization. The construction of 2D profile is composed of several steps, we start with the camber line which is subsequently “enveloped” by the function describing the thickness of the blade. This principle of the 2D blade profile construction is

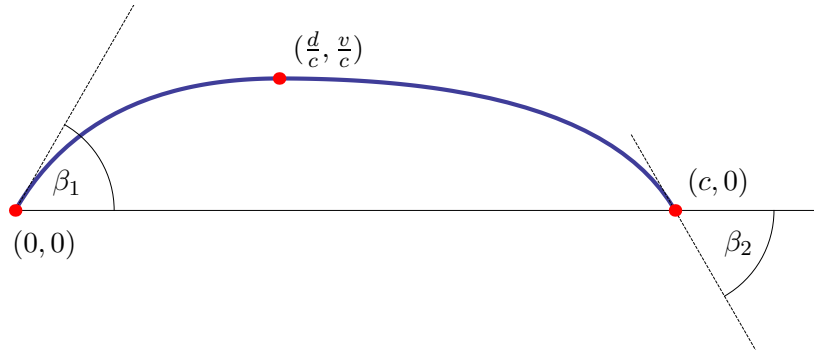


Figure 2.10: Illustrative figure of the camber line with the basic parameters.

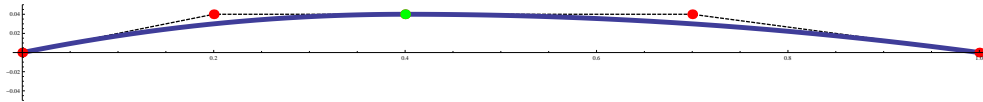


Figure 2.11: Camber line represented as quadratic B-spline curve. Control points are marked red and the joint point is green.

motivated by NACA profiles (cf. [18, 48, 58]). We present several options to describe the camber line parameterization and the function of thickness (e.g. choice of different degrees of the final curve), thus it is possible to obtain an optimal shape of the blade in the future with respect to the flow in turbine. The 2D blade profile is mapped to the cylindrical surface (in case of the runner blades) or transformed and mapped to the conical surface (in case of the guide vanes). The final blade surface is created from several different blade profiles, as it is described in the second part of this section. Both profiles (planar and spatial) are modified so that the continuity of curves is C^{p-1} , where p is the degree of the approximation B-spline curve everywhere, except the leading edge where it is G^2 . The guide vanes and runner blades are shown in Fig. 2.9.

2.2.1 Camber line

Firstly, the description of the camber line which is subsequently enveloped by the function of thickness is presented. In order to obtain the camber line, two options are proposed, depending on the degree and the number of curves that are used for modelling of the camber line. The following parameters are common in all demonstrated cases. If they are not sufficient for the determination of the curve, we mention other parameters in the relevant sections. The basic parameters are:

- length of the reference chord c ,
- maximum relative camber $\frac{v}{c}$,
- position of maximal camber $\frac{d}{c}$,
- angle of attack β_1 (between the chord and the tangent of the camber line),
- trailing-edge angle β_2 (between the chord and the tangent of the camber line).

In the following cases, we consider $c = 1$ and we also maintain the global maximum of the camber line in the point (d, v) . The angles are without orientation, i.e. only the size of the angle is given. The camber line is positioned such that the beginning is in the origin of the Cartesian coordinate system and the end of the camber line lies on the x -axis. The basic parameters are shown in Fig. 2.10.

Parabolic case - 2 curves

At first the camber line is described such that two parabolic curves are connected in the point (d, v) . The continuity of the camber line is G^1 , i.e. the adjacent control points to the connecting point and the point (d, v) are collinear¹. The fulfilment of C^0 conditions, i.e., the curves have the same point of continuity, is clear from the construction of the knot vector which is in the form

$$U = (0, 0, 0, \frac{1}{2}, \frac{1}{2}, 1, 1, 1).$$

The point (d, v) is the global maximum of the final parametrization of the curve and the tangent vector in this point is collinear with the x -axis. Control points (with the included continuity conditions G^1) are the following:

$$\mathbf{P} = \{(0, 0), (v \cot \alpha_1, v), (d, v), (1 - v \cot \beta_2, v), (1, 0)\}.$$

Unfortunately, it is not possible to increase the given continuity to C^1 in this case, because there are not enough degrees of freedom².

In Fig. 2.11, the camber line constructed as quadratic B-spline curve is illustrated, relevant parameters were chosen so that the camber line corresponds to the profile NACA 4412: $v = 0.04$, $d = 0.4$, $\beta_1 = 0.19739555984988075$, $\beta_2 = 0.13255153229667402$.

Cubic case - 2 curves

Other possibility of modelling the camber line is to use higher degree curves. If we use only one cubic curve we do not have the required number of degrees of freedom to fulfil the condition that the point (d, v) is the maximum of the curve. Therefore, B-spline curve composed of two cubic segments is chosen similarly to the previous case. The joint point has the coordinates (d, v) and the continuity of the curve is C^2 . The conditions for the control points are derived from the relations for derivatives of the B-spline curve. Control points of the s -th derivative of the B-spline curve given by the control polygon $\{\mathbf{P}_i\}_{i=0}^n$, where $n + 1$ is the number of control points, are given by the recurrent relation (see more in [69])

$$\mathbf{P}_i^k = \frac{p - k + 1}{u_{i+p+1} - u_{i+k}} (\mathbf{P}_{i+1}^{k-1} - \mathbf{P}_i^{k-1}), \quad k = 1, \dots, s, \quad i = 0, \dots, n - s, \quad (2.16)$$

where $\mathbf{P}_i^0 = \mathbf{P}_i$ and relevant values of knots can be found from the knot vector which is

$$U = (\underbrace{0, \dots, 0}_{p+1}, u_{p+1}, \dots, u_{m-p-1}, \underbrace{1, \dots, 1}_{p+1})$$

and m is the size of the knot vector. For a higher derivatives, it is necessary to change of the knot vector to

$$U' = (\underbrace{0, \dots, 0}_{p-k}, u_{p-k}, \dots, u_{m-p-k}, \underbrace{1, \dots, 1}_{p-k}).$$

From (2.16) for our case ($n = 6$ and $U = (0, 0, 0, 0, \frac{1}{2}, \frac{1}{2}, \frac{1}{2}, 1, 1, 1, 1)$), it is clear that the following conditions must be fulfilled

$$\mathbf{P}_3 - \mathbf{P}_2 = \mathbf{P}_4 - \mathbf{P}_3, \quad (2.17)$$

$$\mathbf{P}_1 - 2\mathbf{P}_2 + \mathbf{P}_3 = \mathbf{P}_5 - 2\mathbf{P}_4 + \mathbf{P}_3. \quad (2.18)$$

Then the continuity in the point \mathbf{P}_3 is C^2 because the equation (2.17) stands for the conditions for the continuity of the first derivative and equation (2.18) for the continuity of the second derivative. The continuity C^0 arise from the choice of the knot vector which is in the form

$$U = (0, 0, 0, 0, \frac{1}{2}, \frac{1}{2}, \frac{1}{2}, 1, 1, 1, 1).$$

¹Continuity G^1 is the continuity of tangents, i.e., it does not depend on the size of the given vectors.

²Continuity C^1 is the continuity of tangent vectors.

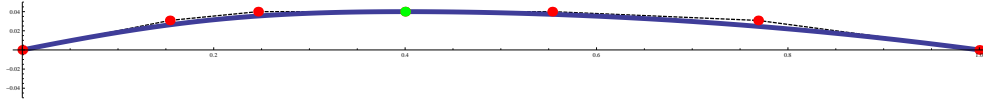


Figure 2.12: Camber line represented as cubic B-spline curve. Control points are marked red, joint point is marked green.

By direct computations, it could be shown that control points that satisfy the conditions (2.17), (2.18) and also maintain the basic parameters are the following:

$$\mathbf{P} = \left\{ (0, 0), \left(-\frac{(4d - 4P_{2x} - 1) \cos \beta_1 \sin \beta_2}{\cos \beta_2 \sin \beta_1 + \cos \beta_1 \sin \beta_2}, -\frac{(4d - 4P_{2x} - 1) \sin \beta_1 \sin \beta_2}{\cos \beta_2 \sin \beta_1 + \cos \beta_1 \sin \beta_2} \right), (P_{2x}, v), (d, v), \right. \\ \left. (2d - P_{2x}, v), \left(\frac{(4d - 4P_{2x} - 1) \cos \beta_2 \sin \beta_1}{\cos \beta_2 \sin \beta_1 + \cos \beta_1 \sin \beta_2} + 1, -\frac{(4d - 4P_{2x} - 1) \sin \beta_1 \sin \beta_2}{\cos \beta_2 \sin \beta_1 + \cos \beta_1 \sin \beta_2} \right), (1, 0) \right\}.$$

As it is seen from the coordinates of control points, the curve is not unambiguously determined by the given parameters and the coordinate P_{2x} still needs to be determined, e.g. by minimization of second differences, i.e. we establish objective function

$$F = \sum_{i=0}^4 (\mathbf{P}_i - 2\mathbf{P}_{i+1} + \mathbf{P}_{i+2})^2.$$

Through the derivation of F according to unknown variables (in our case according to P_{2x}) we get a linear equation for P_{2x} , and its solution gives us the remaining variable so that coordinates of all control points are determined. The minimization of second differences can be understood as minimization of curvature of the control polygon.

Fig. 2.12 shows the control points obtained with the help of cubic B-spline curve, the relevant parameters are chosen so that the result curve corresponds to the NACA profile 4412: $v = 0.04$, $d = 0.4$, $\beta_1 = 0.19739555984988075$, $\beta_2 = 0.13255153229667402$.

2.2.2 The function of thickness

The function of thickness is defined with the following parameters:

- the length of the reference chord c ,
- maximum relative thickness $\frac{v_t}{c}$,
- position of maximal thickness $\frac{d_t}{c}$,
- ending offset k_t ,
- output angle γ .

If the given process of the description of the function of thickness enables it, the radius of osculating circle r will be prescribed in the beginning (i.e. parameter, which amends the curvature at the beginning). Similarly as in the case of the camber line, we consider $c = 1$ and furthermore in the point (d_t, v_t) , it is necessary to have the global maximum. The output angle is taken without orientation, i.e. only the size of the angle is given. The curve describing the function of thickness is set in a manner so that the beginning is located in the origin of the Cartesian coordinate system. With regard to the tangent in the beginning point, we assume that it is collinear with the direction of the y -axis because the tangent of the final profile in the leading edge must be orthogonal to the camber line. The basic parameters are illustrated in Fig. 2.13.

Parabolic case - 2 curves

At first we introduce the possibility, when the function of the thickness is described with the help of B-spline curve with two quadratic segments. Two parabolic curves are connected in point (d_t, v_t) and the continuity of thickness function is G^1 . The continuity C^0 is implied directly from the knot vector, which is

$$U = (0, 0, 0, \frac{1}{2}, \frac{1}{2}, 1, 1, 1).$$

Point (d_t, v_t) is the point of global maximum of the final B-spline curve. Control points (described already with the G^1 continuity conditions) are the following:

$$\mathbf{P} = \{(0, 0), (0, v_t), (d_t, v_t), (1 + (k_t - v_t) \cot \gamma, v_t), (1, k_t)\}.$$

In this case, there is not enough degrees of freedom to include the parameter of radius of curvature in the beginning. The radius can be retrospectively computed from the parameterization of the curve with the help of the first curvature that is in the form

$$({}^1\kappa)^2 = \frac{(\mathbf{K}'(t) \times \mathbf{K}''(t))^2}{(\mathbf{K}'(t) \cdot \mathbf{K}'(t))^3}, \quad (2.19)$$

where $\mathbf{K}(t)$ is parameterization of given curve and then radius r is

$$r = \frac{1}{{}^1\kappa}.$$

Fig. 2.14 shows the function of thickness defined by quadratic B-spline curve. Relevant parameters (except for the radius r) are set such that the thickness corresponds to the chosen NACA profile 4412: $v_t = 0.06$, $d_t = 0.3$, $\gamma = 0.13939996933185556$, $k_t = 0.0012599999999999777$. Calculated radius is $r = 0.024$.

Cubic case - 2 curves

Now, we describe the thickness function with B-spline curve composed of two cubic segments. Advantage is that there are more degrees of freedom to include the radius r . Analogically to the case of camber line with two cubics, we obtain the coordinates of points not only from prescribing the parameters but also with the help of the continuity conditions of the first and second derivatives (equation (2.17) and (2.18)). Control points are in the form

$$\mathbf{P} = \left\{ (0, 0), (0, P_{1y}), \left(\frac{-1 + 4d_t - k_t \cot \gamma + P_{1y} \cot \gamma}{4}, v_t \right), (d_t, v_t), \right. \\ \left. \left(2d_t + \frac{1}{4}(1 - 4d_t + k_t \cot \gamma - P_{1y} \cot \gamma), v_t \right), (1 + (k_t - P_{1y}) \cot \gamma, P_{1y}), (1, k_t) \right\}. \quad (2.20)$$

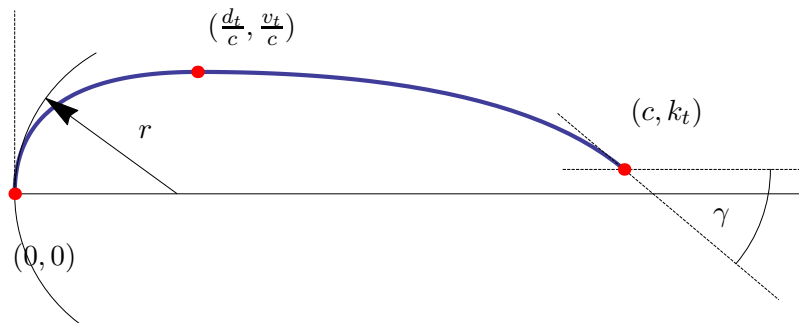


Figure 2.13: Illustrative figure of thickness function with basic parameters.

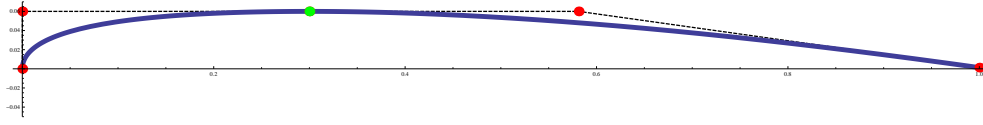


Figure 2.14: The function of thickness represented as quadratic B-spline curve. Control points are marked red and the joint point is green.

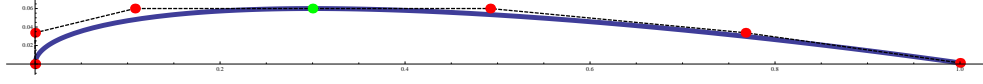


Figure 2.15: The function of thickness represented as cubic B-spline curve. Control points are marked red and the joint point is green.

As it is shown in the expression for control points, there is still one degree of freedom which can be used for the radius of the curvature in the beginning. If we know r , we can calculate the coordinate P_{1y} from the equation (2.19) where $\mathbf{K}(t)$ is the general parameterization depending on control points (2.20) and the knot vector

$$U = (0, 0, 0, 0, \frac{1}{2}, \frac{1}{2}, \frac{1}{2}, 1, 1, 1, 1).$$

After solving this equation, the curve is determined unambiguously. The continuity of the curve of thickness is C^2 .

Fig. 2.15 shows the function of thickness described by cubic B-spline curve. The relevant parameters were again chosen so that the curve corresponds to NACA profile 4412: $v_t = 0.06$, $d_t = 0.3$, $\gamma = 0.13939996933185556$, $k_t = 0.0012599999999999777$, $r = 0.0158674$.

2.2.3 Blade profile in 2D

In order to get the final 2D profile of the blade, it is necessary to use several steps. At first, it is crucial to map the function of thickness on the camber line as it is described in the following paragraphs. To map the thickness on the camber line, the relevant values of thickness function are applied on the normals of the camber line to obtain point-wise description of the blade profile. Consequently, these points are approximated by suitably chosen B-spline curve. The final polygon is modified such that the surrounding of the leading edge is G^2 . The whole process can be divided into three steps:

1. Applying the thickness to the normals of the camber line

Firstly, the corresponding function of thickness is applied on the normal of camber line. We sample the camber line and compute the normal vectors in the sample points. Normals are shown in Fig. 2.16 (top). Then we sample also the function of thickness. Let us assume that the function of thickness and the camber line have the same length of chord c . For each point on the camber line we look for the point on the thickness function such that it has the same coordinate x . Searching for points is done approximately, i.e. we find the *first point* among sampled points on the thickness function such that its x -coordinate x_t fulfills $x_t > x_s$, where x_s x -coordinate of the point on camber line. Further, y -coordinate of this point on the thickness function is mapped on the normal at the given point of the camber line in both directions. Output of this operation is a set of points of the resulting 2D profile. Applying the function of thickness to the camber line is shown in Fig. 2.16 (bottom). The last step is to sort the points, for example from the trailing edge along the suction side to the leading edge, analogously on the pressure side.

2. Approximation with a B-spline curve

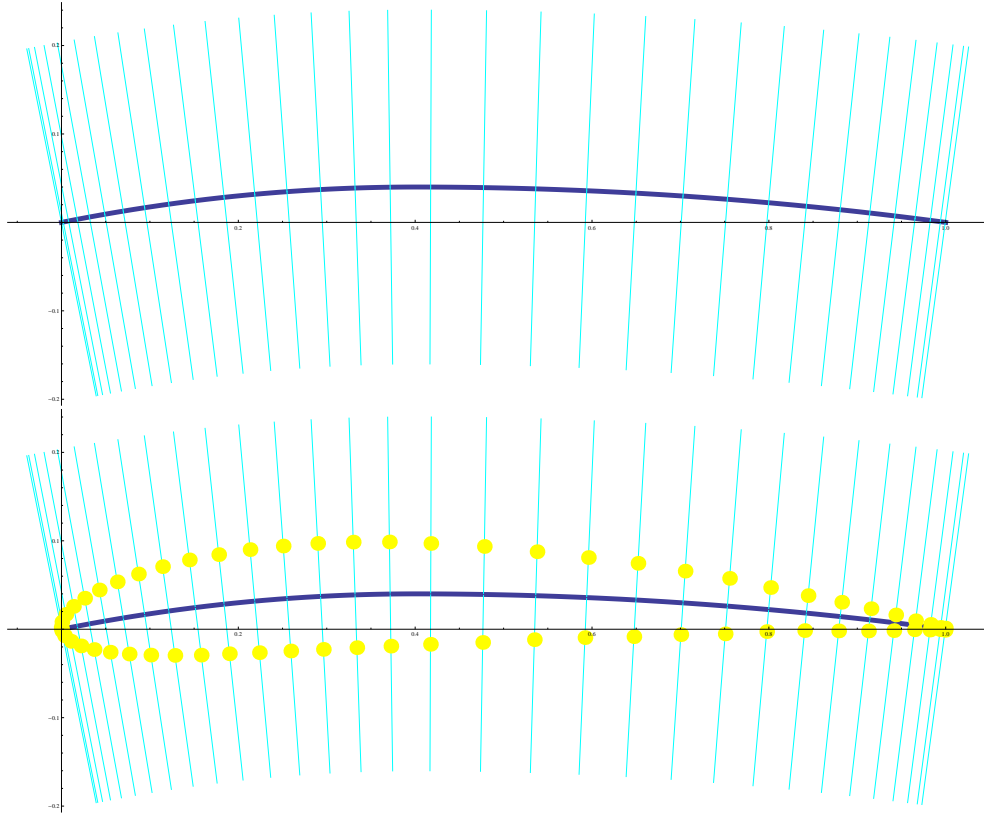


Figure 2.16: Top: Normals of the camber line. Bottom: Applying the thickness to several points of the camber line.

If we have a set of points of the final 2D profile, we can approximate these points with a B-spline curve of the chosen degree. The algorithm described in Algorithm 2 is adopted. Input to the algorithm are points $\{\mathbf{B}_i\}_{i=0}^m$, that we desire to approximate, initial control polygon $\{\mathbf{P}_i\}_{i=0}^n$ of B-spline curve that approximates given points and the knot vector \mathbf{U} of the final curve (thus we also choose the degree of final curve). The points of the initial control polygon are suitably chosen from points $\{\mathbf{B}_i\}_{i=0}^m$. In Fig. 2.17 (top) approximation points and the initial control polygon are shown. Then, for each point $\{\mathbf{B}_i\}_{i=0}^m$ we look for parameter value u_i of the closest point on the B-spline curve $\mathbf{c}(u)$ determined by the control polygon $\{\mathbf{P}_i\}_{i=0}^n$ and the knot vector \mathbf{U} . Finally, least squares method is used to find the translation points $\{\mathbf{P}_i\}_{i=0}^m$ to new positions and to minimize the least squares of the approximation. Algorithm is iterative, i.e., the resulting transformed polygon is used in the following iteration. After running the algorithm on several examples it has been shown that it is enough to proceed one or two iteration to obtain the error that is less than 10^{-2} - 10^{-3} .

At first the algorithm is used to the points on the pressure side and then on the suction side. The final B-spline curve is composed of these two results and the connecting point is the leading edge point, i.e. point $(0, 0)$. The final knot vector is obtained from the corresponding knot vectors of the each approximation curve. The output is one B-spline curve with the control polygon $\{\mathbf{R}_i\}_{i=0}^{2n-1}$ and knot vector V .

There is a small change in the Algorithm 2 to guarantee the C^1 continuity. The prescribed tangent vector in the leading edge has to be the same for suction and pressure side, thus also the last but one control point is maintained (not just the first and the last control points). In the blade profile case, the tangent vector is determined such that we apply algorithm for the suction side of the curve and we compute tangent vector from the result B-spline curve. This tangent vector is prescribed for the pressure side of the B-spline curve.

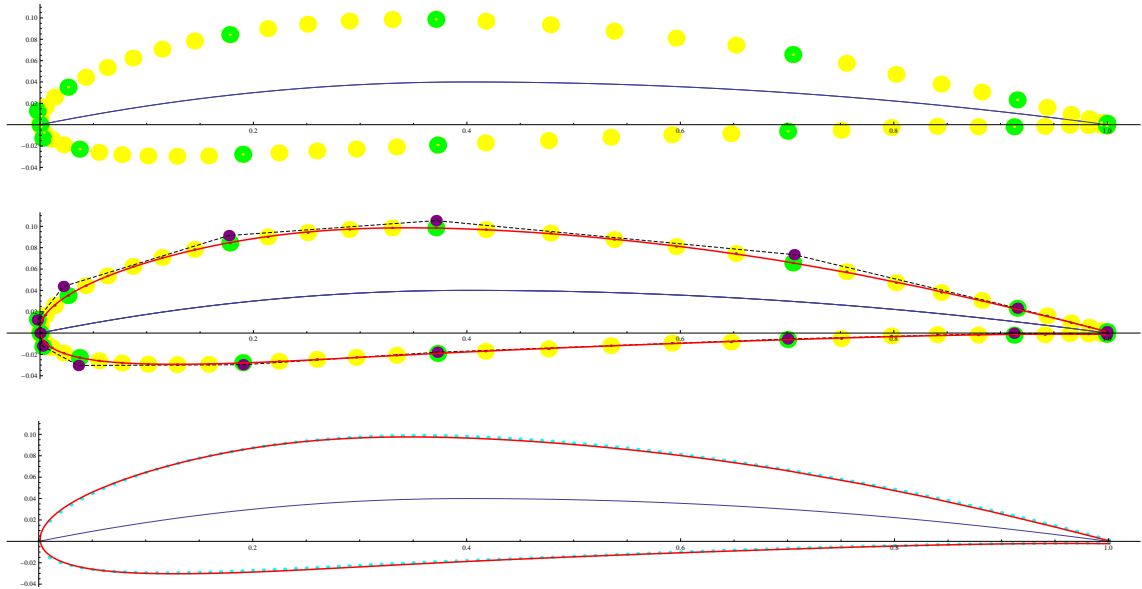


Figure 2.17: Top: Input to approximation - approximation points (yellow), the choice of the initial control polygon (green). Middle: Output of approximation after the continuity correction with new polygon (purple). Bottom: Comparison with the profile NACA 4412 (point of NACA profile are marked blue).

3. Correction of the continuity

To have curvature continuity G^2 in the leading edge point, it is necessary to change the neighbouring control points of the leading edge, that lies at the origin of the Cartesian coordinate system. Algorithm 3 describes the necessary correction. Input is control polygon, index of the control point of the leading edge and the radius of the osculating circle. The conditions are obtained from the equation (2.19) in the leading edge point.

In Fig. 2.17 (middle) the result of the approximation with the corrected continuity is shown. We chose the parameters such that the result corresponds to the profile NACA 4412. The camber line is represented as quadratic B-spline curve, the thickness function as cubic B-spline curve (see Sections 2.2.1 and 2.2.2). The final curve is cubic B-spline curve and the knot vector is

$$(0, 0, 0, 0, 1/10, 1/5, 3/10, 2/5, 1/2, 1/2, 1/2, 3/5, 7/10, 4/5, 9/10, 1, 1, 1, 1).$$

Approximation error corresponding to the Hausdorff distance is 0.00312274 for the suction side and 0.00313807 for the pressure side before G^2 correction and 0.00316664 for the suction side and 0.00303038 for the pressure side after G^2 correction. The error could be improved by applying more iterations (using the result as the input for approximation process). In Fig. 2.17 (bottom), the comparison with the NACA 4412 is shown.

2.2.4 3D profile of guide vanes/runner blades

In this section we focus on the modelling of 3D blade profiles computed from the 2D blade profiles (described in the previous paragraphs). The 2D profiles are transformed (scaling, rotation, circle inversion) and then mapped to a cylindrical surface or to a conical surface according to the type of the blade (runner blades or guide vanes respectively). The common number of the cylindrical surfaces is from three to seven for the runner blade and there is just one conical surface for the guide vane. The result of this

Algorithm 2 CurveApproximation2D(Points, InitialControlPolygon, KnotVector)

Input: Approximation points $\{\mathbf{B}_i\}_{i=0}^m$, initial control polygon $\{\mathbf{P}_i\}_{i=0}^n$ ($\mathbf{P}_0 = \mathbf{B}_0$, $\mathbf{P}_n = \mathbf{B}_m$), knot vector U

Output: Control polygon $\{\bar{\mathbf{P}}_i\}_{i=0}^n$,

- 1: $\mathbf{c}(t) \leftarrow$ parameterization of B-spline curve determined by $\{\mathbf{P}_i\}_{i=0}^n$ and U
- 2: For each point \mathbf{B}_i , $i = 1, \dots, m-1$, search for the closest point on $\mathbf{c}(t)$, represented by its parametric value, i.e.,

$$T_i = \min_{0 \leq t \leq 1} \|\mathbf{B}_i - \mathbf{c}(t)\|, \quad i = 1, \dots, m-1$$

- 3: Add the unknown translations to the control points (we maintain the first and the last control points), i.e.,

$$\hat{\mathbf{P}}_i = \mathbf{P}_i + (X_i, Y_i), \quad i = 1, \dots, n-2$$

- 4: Compute the parameterization of the corresponding B-spline curve $\hat{\mathbf{c}}(t)$
- 5: Assemble the objective function for the minimization

$$F = \sum_{i=1}^{m-1} \|\hat{\mathbf{c}}(T_i) - \mathbf{B}_i\|^2$$

- 6: Find the minimum of the objective function F by solving the linear system of equations

$$\{(\hat{X}_i, \hat{Y}_i)\} = \text{solve} \left(\frac{\partial F}{\partial X_i} = 0 \wedge \frac{\partial F}{\partial Y_i} = 0, i = 1, \dots, n-2 \right)$$

- 7: **return** $\bar{\mathbf{P}}_i = \mathbf{P}_i + (\hat{X}_i, \hat{Y}_i)$
-

section is the B-spline description of the 3D blade profiles as the preparation step for the final B-spline description of the blade.

2.2.4.1 Profiles of the runner blades of KT

The 2D blade profiles determining runner blade are mapped to cylindrical surfaces with the given radii. Without the loss of generality we assume that the axis of the all cylindrical surfaces is identical to the z -axis and the radius is r . 3D blade profile is determined by the following parameters:

- 2D blade profile with the unit length and with the control points $\{\mathbf{P}_i\}_{i=0}^n$,
- radius of the cylindrical surface r ,
- number of blades in the runner n ,
- rotation of the blade γ ,
- the centre of rotation (x_0, y_0) ,
- the length of the chord c of the 2D blade profile.

At first, we translate the planar blade profile (defined in Section 2.3.1) such that the centre of rotation coincides with the origin of the Cartesian coordinate origin. The transformation matrix is in the form

$$\mathbf{T} = \begin{pmatrix} 1 & 0 & -x_0 \\ 0 & 1 & -y_0 \\ 0 & 0 & 1 \end{pmatrix}.$$

Algorithm 3 G2ControlPolygon2D(ControlPolygon, Index, Curvature)

Input: Control polygon $\{\mathbf{P}_i\}_{i=0}^n$, index k of the control point corresponding to the multiple knot in the knot vector, curvature κ

Output: Control polygon $\{\tilde{\mathbf{P}}_i\}_{i=0}^n$,

- 1: Translation of the control points such that the new point $\bar{\mathbf{P}}_k$ lies in the origin

$$\bar{\mathbf{P}}_i = \begin{pmatrix} 1 & 0 & -P_{k,x} \\ 0 & 1 & -P_{k,y} \\ 0 & 0 & 1 \end{pmatrix} \cdot \begin{pmatrix} P_{i,x} \\ P_{i,y} \\ 1 \end{pmatrix}$$

- 2: $p \leftarrow$ degree of the B-spline curve
- 3: Determination of the tangent vector direction $\mathbf{t} = (t_x, t_y)$ in $\bar{\mathbf{P}}_k$

$$\mathbf{t} = \frac{\bar{\mathbf{P}}_k - \bar{\mathbf{P}}_{k-1}}{\|\bar{\mathbf{P}}_k - \bar{\mathbf{P}}_{k-1}\|}$$

- 4: To guarantee G^2 continuity, substitute the B-spline parameterization with control points $\{\bar{\mathbf{P}}_i\}_{i=0}^n$ in (2.19) and obtain the correction of the control point coordinates that are neighbours to $\bar{\mathbf{P}}_k$

$$\bar{\mathbf{P}}_{k-1} = -\mathbf{t} \frac{\sqrt{p-1}}{2p} \sqrt{\frac{|\bar{P}_{k-2,y}t_x - \bar{P}_{k-2,x}t_y|}{\kappa}}, \quad \bar{\mathbf{P}}_{k+1} = \mathbf{t} \frac{\sqrt{p-1}}{2p} \sqrt{\frac{|\bar{P}_{k+2,y}t_x - \bar{P}_{k+2,x}t_y|}{\kappa}}$$

- 5: Translation of the points to the original position

$$\tilde{\mathbf{P}}_i = \begin{pmatrix} 1 & 0 & P_{k,x} \\ 0 & 1 & P_{k,y} \\ 0 & 0 & 1 \end{pmatrix} \cdot \begin{pmatrix} \bar{P}_{i,x} \\ \bar{P}_{i,y} \\ 1 \end{pmatrix}$$

Then, the scaling is applied such that the result has the chord length c . As we start with the profile with the length 1, we apply simple dilatation

$$\mathbf{S} = \begin{pmatrix} c & 0 & 0 \\ 0 & c & 0 \\ 0 & 0 & 1 \end{pmatrix}.$$

Subsequently, we rotate the profile with γ around the origin, the rotation matrix is

$$\mathbf{R} = \begin{pmatrix} \cos \gamma & -\sin \gamma & 0 \\ \sin \gamma & \cos \gamma & 0 \\ 0 & 0 & 1 \end{pmatrix}.$$

Control points (in homogeneous coordinates) of dilatated and rotated profiles are computed as

$$\bar{\mathbf{P}}_i = \mathbf{R} \cdot \mathbf{S} \cdot \mathbf{T} \cdot \mathbf{P}_i^\top, \quad i = 0, \dots, n,$$

where input points \mathbf{P}_i , $i = 0, \dots, n$ are again in homogeneous coordinates (the third coordinate 1 is appended to planar coordinates). The example of several transformed profiles is in Fig. 2.18 (left).

The mapping of the blade to the cylindrical surface with radius r and z -axis can be realized with the transformation to the cylindrical coordinates. Let's identify the plane where we constructed the blade profile with the tangent plane to the cylindrical surface in point $(r, 0, 0)$ along its generatrix, each point in this plane has coordinates $\mathbf{X}_0 = (r, y, z)$. The corresponding coordinates on the cylindrical surface are

$$\mathbf{X} = \left(r \sin \frac{y}{r}, r \cos \frac{y}{r}, z \right). \quad (2.21)$$

Algorithm 4 G2ControlPolygon3D(ControlPolygon, Index, Curvature, Plane)

Input: Control polygon $\{\mathbf{P}_i\}_{i=0}^n$, index k of the control point corresponding to the multiple knot in the knot vector, curvature κ , orthonormal vectors $\mathbf{e}_1, \mathbf{e}_2$

Output: Control polygon $\{\tilde{\mathbf{P}}_i\}$,

- 1: Translation of the control points that the new point $\bar{\mathbf{P}}_k$ lies in the origin

$$\bar{\mathbf{P}}_i = \begin{pmatrix} 1 & 0 & 0 & -P_{k,x} \\ 0 & 1 & 0 & -P_{k,y} \\ 0 & 0 & 1 & -P_{k,z} \\ 0 & 0 & 0 & 1 \end{pmatrix} \cdot \begin{pmatrix} P_{i,x} \\ P_{i,y} \\ P_{i,z} \\ 1 \end{pmatrix}$$

- 2: $p \leftarrow$ degree of the B-spline curve

- 3: Project the points $\bar{\mathbf{P}}_{k-2}, \bar{\mathbf{P}}_{k-1}, \bar{\mathbf{P}}_{k+1}, \bar{\mathbf{P}}_{k+2}$ to the plane defined by point $\bar{\mathbf{P}}_k$ and vectors $\mathbf{e}_1, \mathbf{e}_2$, i.e.

$$\bar{\mathbf{P}}_j = (\bar{\mathbf{P}}_j - \bar{\mathbf{P}}_k) \cdot \mathbf{e}_1 \mathbf{e}_1 + (\bar{\mathbf{P}}_j - \bar{\mathbf{P}}_k) \cdot \mathbf{e}_2 \mathbf{e}_2 + \bar{\mathbf{P}}_k, \quad j = k-2, k-1, k+1, k+2$$

- 4: Determination of the tangent vector direction $\bar{\mathbf{P}}_k$ in the form $\mathbf{t} = \frac{\bar{\mathbf{P}}_k - \bar{\mathbf{P}}_{k-1}}{\|\bar{\mathbf{P}}_k - \bar{\mathbf{P}}_{k-1}\|}$

- 5: To guarantee G^2 continuity, substitute the B-spline parameterization with control points $\{\bar{\mathbf{P}}_i\}_{i=0}^n$ in (2.19) and obtain the correction of the control point coordinates that are neighbours to $\bar{\mathbf{P}}_k$

$$\bar{\mathbf{P}}_{k-1} = -\mathbf{t} \frac{\sqrt{p-1}}{2p} \frac{\sqrt[4]{\mathbf{t} \cdot \mathbf{M}_{k-2} \cdot \mathbf{t}}}{\sqrt{\kappa}}, \quad \bar{\mathbf{P}}_{k+1} = -\mathbf{t} \frac{\sqrt{p-1}}{2p} \frac{\sqrt[4]{\mathbf{t} \cdot \mathbf{M}_{k+2} \cdot \mathbf{t}}}{\sqrt{\kappa}}$$

where

$$\mathbf{M}_q = \begin{pmatrix} 0 & 0 & 0 & 0 \\ -2\bar{P}_{q,x}\bar{P}_{q,y} & \bar{P}_{q,x}^2 - \bar{P}_{q,y}^2 & 0 & 0 \\ -2\bar{P}_{q,x}\bar{P}_{q,z} & -2\bar{P}_{q,y}\bar{P}_{q,z} & \bar{P}_{q,x}^2 - \bar{P}_{q,z}^2 & 0 \\ 0 & 0 & 0 & \bar{P}_{q,y}^2 + \bar{P}_{q,z}^2 \end{pmatrix}$$

- 6: Translation of the control polygon to the original position

$$\tilde{\mathbf{P}}_i = \begin{pmatrix} 1 & 0 & 0 & P_{k,x} \\ 0 & 1 & 0 & P_{k,y} \\ 0 & 0 & 1 & P_{k,z} \\ 0 & 0 & 0 & 1 \end{pmatrix} \cdot \begin{pmatrix} \bar{P}_{i,x} \\ \bar{P}_{i,y} \\ \bar{P}_{i,z} \\ 1 \end{pmatrix}$$

Now, we take the components of 2D blade profile B-spline parameterization and substitute them for y and z coordinates in (2.21) and we obtain parametric expression on the cylindrical surface. However, the obtained parameterization (after the substitution) is not polynomial or rational and it can not be directly described as the B-spline/NURBS curve. Thus, it is necessary to employ approximation of that curve.

We apply Algorithm 5 to approximate the curve on the cylinder by a B-spline curve and then Algorithm 4 to improve the continuity for the approximation B-spline curve to G^2 at the leading point. Firstly, points of the 3D profile located on the cylinder are found. These points are going to be approximated. Initial control polygon, that is input in Algorithm 5, is obtained by mapping the control polygon of B-spline curve on the cylindrical surface. The next step is correction to maintain G^2 continuity of the final curve with the help of Algorithm 4. Plane ϱ , where the control points are arranged (see Algorithm 4), is chosen as tangent plane to the cylindrical surface in the leading edge point. Moreover, its two orthonormal directions are represented by the direction of camber line and the corresponding orthogonal vector in ϱ . The direction of camber line is computed as the rotation of the vector collinear to the plane xy placed in the leading edge in the plane ϱ around the normal to the cylindrical surface and the angle of rotation is $\beta_1 + \gamma$, where β_1 is attack angle and γ is output angle. After improvement of control polygon

Algorithm 5 CurveApproximation3D(Points, InitialControlPolygon, Knot vector)

Input: Approximate points $\{\mathbf{B}_i\}_{i=0}^m$, initial control polygon $\{\mathbf{P}_i\}_{i=0}^n$ ($\mathbf{P}_0 = \mathbf{B}_0$, $\mathbf{P}_n = \mathbf{B}_m$), knot vector U

Output: Control polygon $\{\bar{\mathbf{P}}_i\}_{i=0}^n$,

- 1: $\mathbf{c}(t) \leftarrow$ parameterization of B-spline curve determined by $\{\mathbf{P}_i\}_{i=0}^n$ and U
- 2: For each point $\mathbf{B}_i, i = 1, \dots, m-1$, search for the closest point on $\mathbf{c}(t)$, represented by its parametric value, i.e.,

$$T_i = \min_{0 \leq t \leq 1} \|\mathbf{B}_i - \mathbf{c}(t)\|, \quad i = 1, \dots, m-1$$

- 3: Add the unknown translation to the control points (we maintain the first and the last control points)

$$\hat{\mathbf{P}}_i = \mathbf{P}_i + (X_i, Y_i, Z_i), \quad i = 1, \dots, n-2$$

- 4: Compute parameterization of the corresponding B-spline curve $\hat{\mathbf{c}}(t)$
- 5: Assemble the objective function F for the minimization

$$F = \sum_{i=1}^{m-1} \|\hat{\mathbf{c}}(T_i) - \mathbf{B}_i\|^2$$

- 6: Find the minimum of the objective function by solving the linear system of equations

$$\{(\hat{X}_i, \hat{Y}_i, \hat{Z}_i)\} = \text{solve} \left(\frac{\partial F}{\partial X_i} = 0 \wedge \frac{\partial F}{\partial Y_i} = 0, \frac{\partial F}{\partial Z_i} = 0, i = 1, \dots, n-2 \right)$$

- 7: **return** $\bar{\mathbf{P}}_i = \mathbf{P}_i + (\hat{X}_i, \hat{Y}_i, \hat{Z}_i)$
-

we use Algorithm 5, separately to suction side and pressure side. Then we combine the two results to one final B-spline curve. Because the points \mathbf{P}_{k-2} and \mathbf{P}_{k+2} are changed (k is index of the control point corresponding to the leading edge), we again apply Algorithm 4 for G^2 continuity. There is also possibility to repeat this process to decrease the error of approximation. In practical examples it has been shown that two or three iteration are enough as the error is less than 10^{-2} - 10^{-3} . The result B-spline parameterization of profile on the cylindrical surface is G^2 continuous (see Fig. 2.18 (right)).

2.2.4.2 Guide vanes profile of KT

For the guide vanes of KT we also start with the construction of a planar blade profile. This profile is mapped to a conical surface which could be that the profile is mapped to the tangent plane of conical surface. This simplified variant could be used for optimization cycle when the blade is computed in every step of optimization. In the following the both approaches are presented.

Without loss of generality we assume that the conical surface has the axis coincident with z -axis, its base is in the plane xy with centre at the origin, radius r and vertex of the cone \mathbf{V} is on z -axis and has coordinates $\mathbf{V} = (0, 0, v)$. Blade profile is in the plane σ , which is a tangent plane of the conical surface in its generatrix that goes through $(r, 0, 0)$. During the modelling of blade we work with the local coordinate system, origin is $(r, 0, 0)$, local x -axis is collinear to global y -axis and local y -axis corresponds to the generatrix that goes through $(r, 0, 0)$ in global coordinate system.

First of all we apply several transformations to the 2D blade profile in the plane (see Fig. 2.19). The profile is scaled such that the resulting chord length is c and rotated around the origin about the angle ξ . Then we translate the blade such that the trailing edge is on the y -axis. Before the blade profile is mapped on the conical surface it has to be mapped to a circular mesh with the help of conformal transformation. The reason is to preserve angles also after mapping on the conical surface. Circular mesh has the following parameters: input radius r_i , output radius r_o and the width of circular mesh

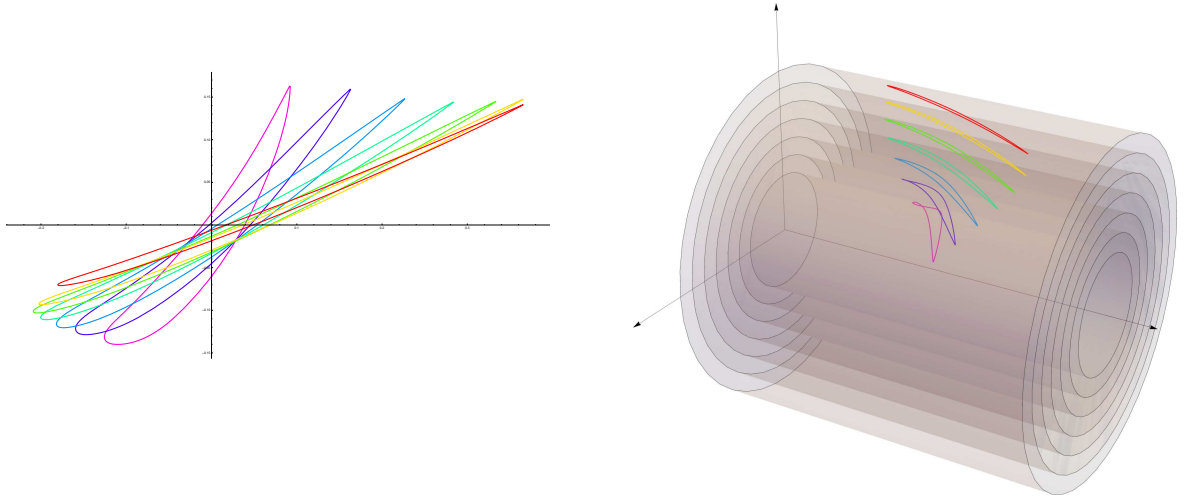


Figure 2.18: Left: Transformed blade profiles. Right: Mapping to the cylinders.

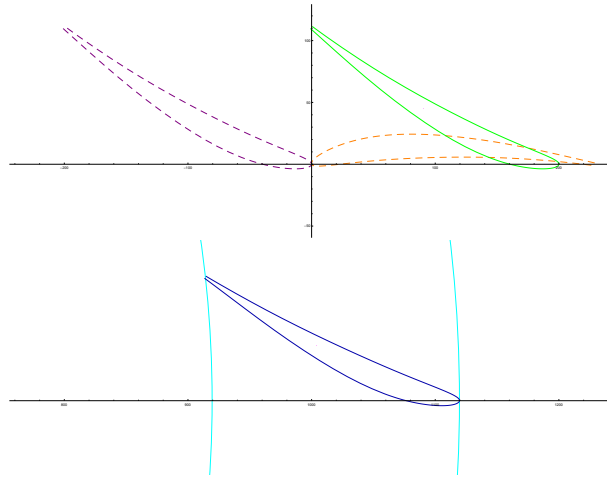


Figure 2.19: Top: Transformation of 2D profile for guide vanes – scaling (orange), rotation (purple) and translation (green); Bottom: Profile in circular mesh.

$b = r_i - r_o$. The new coordinates are

$$\begin{aligned}\hat{x} &= r_o e^{Kx}, \\ \hat{y} &= Ky,\end{aligned}$$

where $K = \frac{\ln \frac{r_i}{r_o}}{b}$.

In the following paragraphs we assume that this circular mesh is lying in the plane tangent to the conical surface (if not it can be done by simple transformations - translation and rotation depending on the position of the cone).

The next step (not the necessary one) is to map the transformed profile to the conical surface. Let \mathbf{X}_0 be the point in plane σ (see Fig. 2.20 (left)) and we want to find the corresponding point on the conical surface. Firstly, we find \mathbf{B}_0 in plane σ that has the same distance from \mathbf{V}_0 as point \mathbf{X}_0 and lies on y -axis, i.e.,

$$\mathbf{B}_0 = \left(0, \sqrt{r^2 + v^2} - d\right),$$

where $d = \text{dist}(\mathbf{X}_0, \mathbf{V}_0)$ is Euclidean distance of two points. Hence, we can derive coordinates of \mathbf{B} in

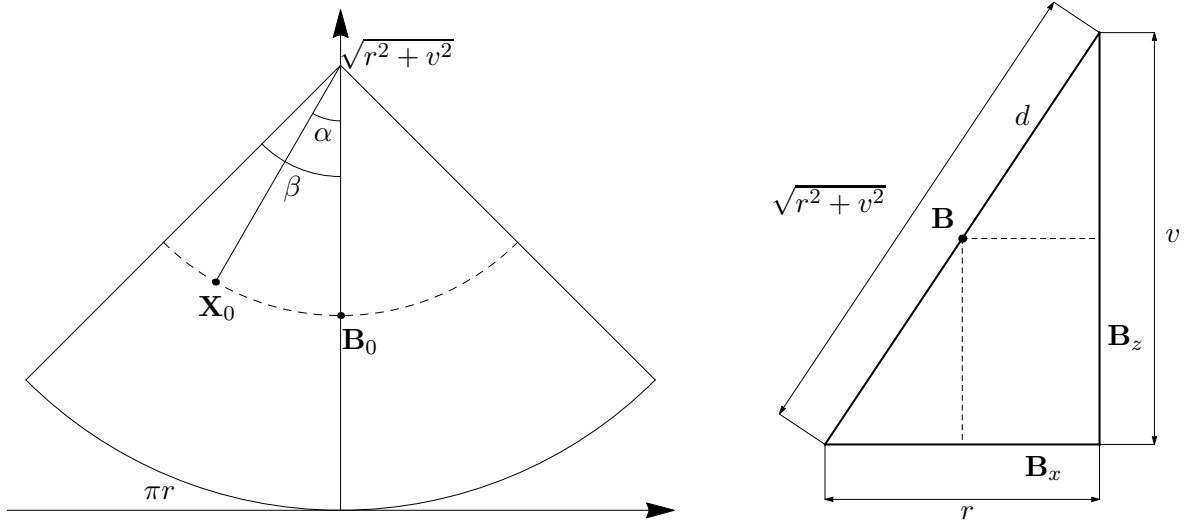


Figure 2.20: Illustrative figures for deriving the formulas of mapping to the cone.

global coordinates system. From the triangle resemblance (see Fig. 2.20 (right)) it follows

$$\mathbf{B} = (B_x, B_y, B_z) = \left(\frac{d}{\sqrt{r^2 + v^2}} r, 0, \frac{\sqrt{r^2 + v^2} - d}{\sqrt{r^2 + v^2}} v \right).$$

The last thing is determination of angle φ that is used to rotate \mathbf{B} around z -axis, to obtain \mathbf{X} . As it holds

$$\frac{\varphi}{\pi} = \frac{\alpha}{\beta},$$

where

$$\alpha = \arccos \frac{\overrightarrow{\mathbf{V}_0 \mathbf{X}_0} \cdot (0, -1)^\top}{\|\overrightarrow{\mathbf{V}_0 \mathbf{X}_0}\|} \quad \text{and} \quad \beta = \frac{\pi r}{\sqrt{r^2 + v^2}},$$

we deduce

$$\varphi = \frac{\alpha}{\beta} \pi.$$

Then, coordinates of point \mathbf{X} on the conical surface, corresponding to \mathbf{X}_0 in plane σ , are

$$\mathbf{X} = (B_x \cos \varphi, B_x \sin \varphi, B_z).$$

With this method we are capable to map blade profile to the corresponding cone. We just substitute the components of blade profile parameterization for \mathbf{X}_0 and then we obtain parametric expression on the conical surface (see Fig. 2.21). Of course, neither polynomial, nor rational parameterization is obtained and it is necessary to employ approximation of that curve. Thus, we also apply the process of approximation analogous to the one described in Section 2.2.4.1. The only change is in the plane ϱ that we choose as tangent to the conical surface in the leading edge. To sum up, the guide vane is characterized with one profile that is subsequently mapped to the adjacent cones or tangent planes. The final non-trimmed blade is defined by two profiles and it is linear in the direction of the blade axis (see Section 2.2.5.3). The profiles and the blade before trimming are shown in Fig. 2.22.

2.2.5 Construction of the final blade from 3D profiles

This part is devoted to the description of the final blade that is created from 3D profile(s). The resulting surface represents the runner blade. First of all the construction of trailing edge is presented and then the construction of the control net is described followed by process of trimming.

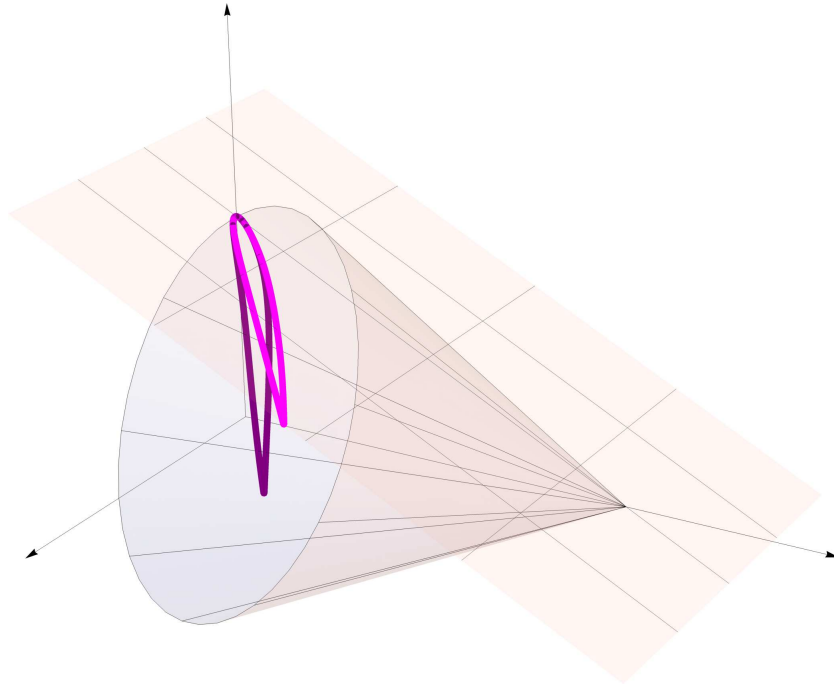


Figure 2.21: Planar profile (pink) mapped to the cone.

2.2.5.1 The trailing edge of runner blade

The trailing edge is given by points $\mathbf{Q}_i, i = 0, \dots, l - 1$, where l is the number of cylinders, which are the trailing edge points of the 3D blade profiles on circular surfaces described in Section 2.2.4.1. The goal is to obtain cubic B-spline curve that interpolates given data. Thus, we search control polygon and knot vector of the result curve. The first step is to construct spline curve $\mathbf{q}(t)$ that interpolates given points. The spline curve is parametrized by centripetal parameterization and the boundary conditions are vanishing second derivatives. The parameters t_i identify points \mathbf{Q}_i on $\mathbf{q}(t)$

$$\mathbf{q}(t_i) = \mathbf{Q}_i.$$

Then, we transform interpolation cubic spline curve to B-spline form. Let us denote the tangent vector for each point \mathbf{Q}_i as $\mathbf{t}_{\mathbf{Q}_i} = \mathbf{q}'(t_i)$. The control points are

$$\mathbf{P}_i = \mathbf{q}(t_i), \quad i = 0, 3, 6, \dots, 3l - 3,$$

and

$$\mathbf{P}_{i+1} = \mathbf{P}_i + \frac{1}{3}\mathbf{t}_{\mathbf{Q}_i}, \quad \mathbf{P}_{i+2} = \mathbf{P}_{i+3} - \frac{1}{3}\mathbf{t}_{\mathbf{Q}_{i+1}}, \quad i = 0, 3, 6, \dots, 3l - 3.$$

The corresponding knot vector is based on \mathbf{Q}_i , where each trailing edge point adds one triple knot in the knot vector $(0, 0, 0, 0, 1, 1, 1, 1)$. The specific knots could be obtained by chordal or centripetal parameterization.

The resulting B-spline curve is used for the following construction of the final blade. The trailing edge is shown in Fig. 2.23.

2.2.5.2 Construction of the final runner blade

The set-up for the final construction of the blade surface consists of profiles on cylindrical surfaces and the B-spline description of the trailing edge of the blade. If we know the desired setting we can describe the final control net of the blade.

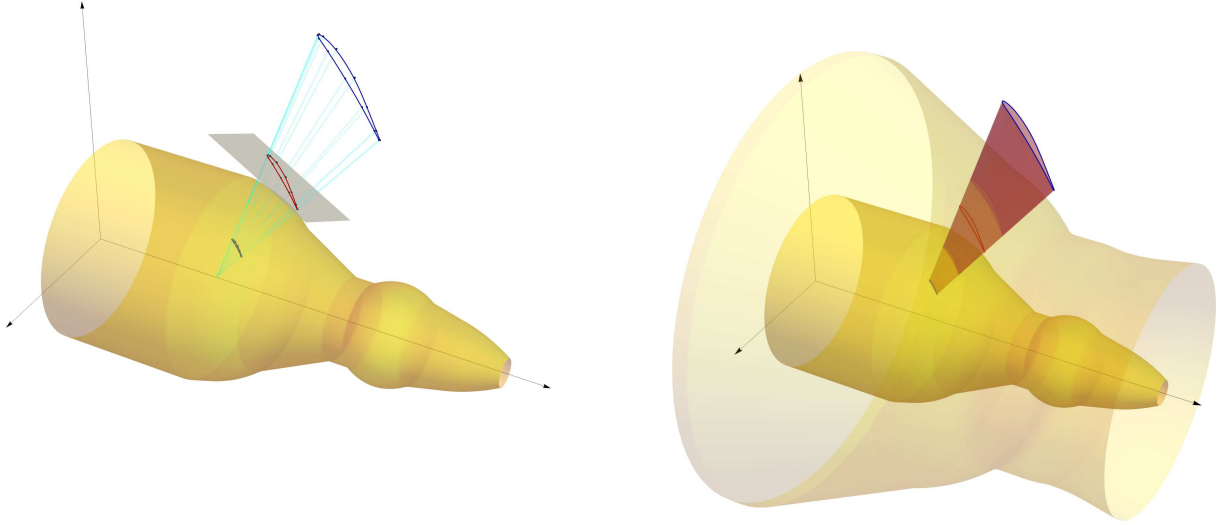


Figure 2.22: Left: Profiles of the guide vane. Right: Guide vane before trimming.

The resulting B-spline surface has degrees $(N, 3)$, where N is the degree of the B-spline curves representing 3D profiles. Thus, the first knot vector of the final surface is defined by the B-spline representation of 3D blade profiles, the second knot vector corresponds to the number of profiles – each profile adds one triple knot in the base knot vector $(0, 0, 0, 0, 1, 1, 1, 1)$, the particular values of knots are determined by chordal or centripetal parameterization. The control net has $m \times n$ control points $\{\mathbf{P}_{i,j}\}_{i,j=0}^{m-1,n-1}$, where n is the number of control points for one profile on the cylindrical surface and $m = 3(l - 1)$ and l is the number of these profiles.

The initialization of the control net starts with adding already known curves – the control points of trailing edges to the first and the last columns and the control points of the 3D profiles into the rows such that two free rows are between two spatial profiles.

The final surface should be at least C^1 continuous across the profiles (which are G^2 continuous), thus the control points fulfill the conditions

$$\mathbf{P}_{i+4,j} = 2\mathbf{P}_{i+3,j} - \mathbf{P}_{i+2,j}, \quad i = 0, 3, \dots, 3l - 3, \quad j = 0, \dots, n - 1, \quad (2.22)$$

that are added to the control net.

The next step is to compute the control points of the leading edge with the minimization of the second differences. The leading edge goes through the leading points of 3D blade profiles. The leading edge of the resulting blade is C^1 cubic B-spline curve and the objective function is in the form

$$F = \sum_{i=0}^{m-2} (\mathbf{P}_{i,k} - 2\mathbf{P}_{i+1,k} + \mathbf{P}_{i+2,k})^2,$$

where k is the index of the column corresponding to the leading edge and the variables are unknown control points in the k -th column. The linear system is obtained after computing the derivative of F with respect to all unknowns. The solution of this system are the control points of the leading edge.

The next step is to ensure G^2 continuity of the control polygons “adjacent” to control polygons of 3D profiles (but still ensuring C^1 continuity across the profiles). It means we apply Algorithm 4 on the points $\mathbf{P}_{i+2,j}$, $\mathbf{P}_{i+4,j}$, $i = 0, 3, \dots, 3(l - 2)$, $j = k - 2, k - 1, k + 1, k + 2$. In the remaining rows (the second and the last but one rows), it holds

$$\mathbf{P}_{i,k+1} = (1 + a_i)\mathbf{P}_{i,k} - a_i\mathbf{P}_{i,k-1}, \quad i = 1, m - 1,$$

where real coefficients a_i are included as variables in the final minimization. We calculate the control points in the $(k - 1)$ -th and $(k + 1)$ -th columns by minimizing the second differences. The objective

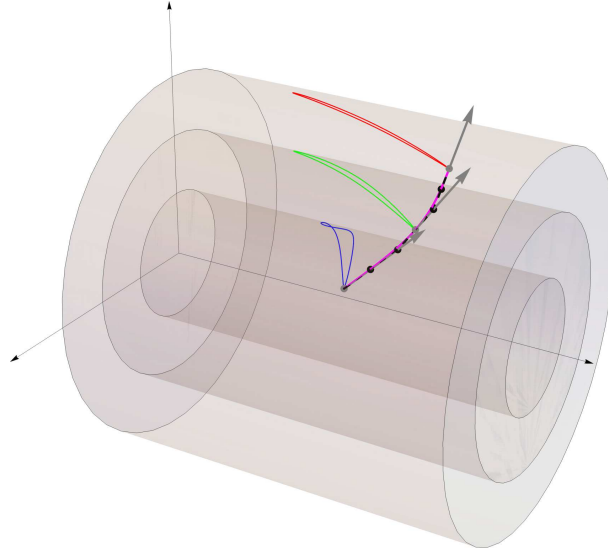


Figure 2.23: The input data for the trailing edge are grey points. The trailing edge is pink and the result control polygon is dashed black.

functions are

$$F_1 = \sum_{i=0}^{m-2} (\mathbf{P}_{i,k-1} - 2\mathbf{P}_{i+1,k-1} + \mathbf{P}_{i+2,k-1})^2,$$

$$F_2 = \sum_{i=0}^{m-2} (\mathbf{P}_{i,k+1} - 2\mathbf{P}_{i+1,k+1} + \mathbf{P}_{i+2,k+1})^2.$$

We obtain two linear systems of equations and the unknowns are the control points of $(k-1)$ -th and $(k+1)$ -th columns.

There are still unknown points in the control net that are computed with the global minimization of third differences. This minimization is applied on all rows and columns. The objective function is

$$G = \sum_{j=1}^{n-1} \sum_{i=0}^{m-3} (\mathbf{P}_{i+3,j} - 3\mathbf{P}_{i+2,j} + 3\mathbf{P}_{i+1,j} - \mathbf{P}_{i,j})^2 + \sum_{i=1}^{m-1} \sum_{j=0}^{n-3} (\mathbf{P}_{i,j+3} - 3\mathbf{P}_{i,j+2} + 3\mathbf{P}_{i,j+1} - \mathbf{P}_{i,j})^2.$$

G is differentiated with respect to all unknowns and the linear system of equation is obtained.

The last step is to correct the second and the last but one rows around the leading edge. These polygons are just G^1 continuous (it follows from the previous rules) and we correct them to be G^2 continuous around the leading edge. We apply Algorithm 4 that change points $\mathbf{P}_{i,k-1}$, $\mathbf{P}_{i,k+1}$, $i = 1, m-1$ with the help of points $\mathbf{P}_{i,k-2}$, $\mathbf{P}_{i,k}$, $\mathbf{P}_{i,k+2}$, $i = 1, m-1$ and the given curvatures that are obtained as linear interpolation of the first two (or the last two) profile curves. The illustrative figure of control net is shown in Fig. 2.24.

2.2.5.3 Trimming by spheres

The guide vanes can be rotated around their axis to regulate the flow and there are not allowed any spaces between the guide vanes and the turbine housing. Thus, the guide vanes are trimmed by the spheres. These spheres correspond to the description of turbine housing where the guide vanes are situated.

The result of the trimming process should be a curve that is the intersection of the blade and the sphere. Let $\mathbf{b}(u, v)$ be the parameterization of the blade and $\mathbf{S} = (S_x, S_y, S_z)^\top$ be the centre of sphere

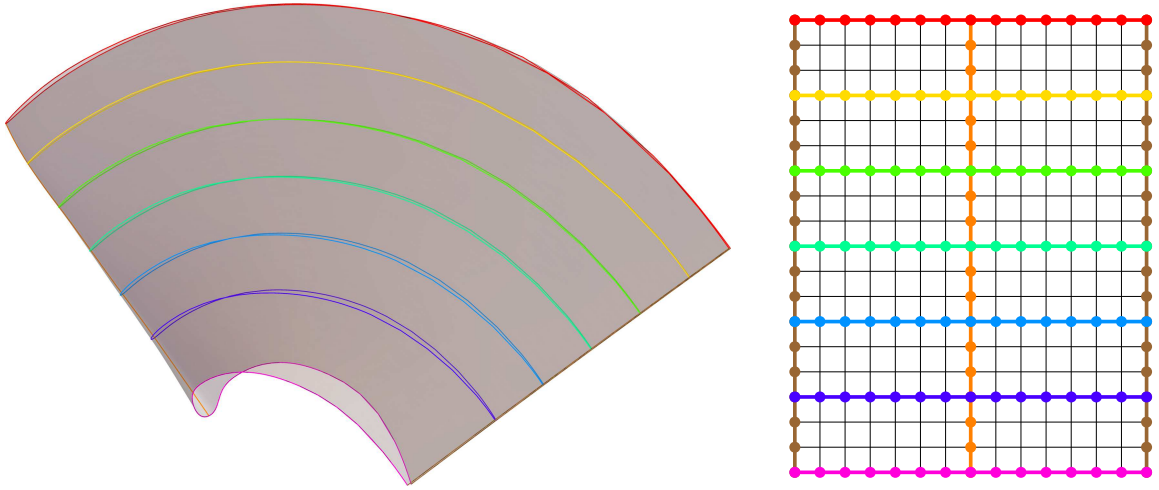


Figure 2.24: Left: KT blade with important curves. Right: Illustrative figure of control net.

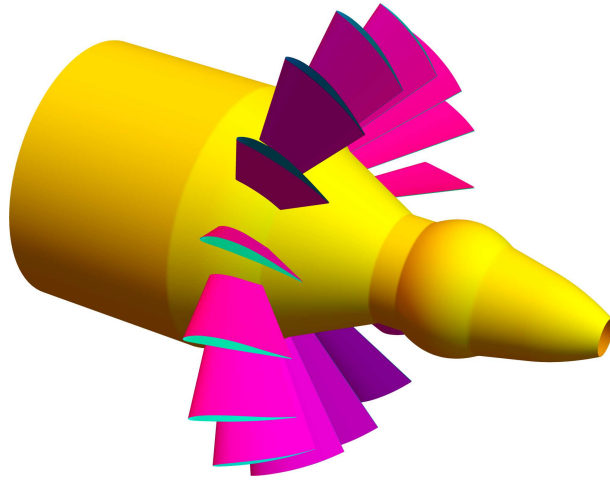


Figure 2.25: Guide vanes after trimming.

with radius r . The sphere is described by implicit equation

$$(x - S_x)^2 + (y - S_y)^2 + (z - S_z)^2 = r^2. \quad (2.23)$$

The components of blade parameterization are substituted to (2.23) and we obtain implicitly given curve $c(u, v) = 0$ in the parametric space of $\mathbf{b}(u, v)$ and its points are parameters of intersection curve of blade with the sphere. It is not necessary to solve the cases with no intersection or with the partial intersection. By sampling $c(u, v) = 0$ in the parametric domain and substituting the points to the parameterization of $\mathbf{b}(u, v)$, we obtain intersection points that define the curve common to the sphere and the blade. The next step is approximation of these points by a B-spline curve with Algorithm 5 that has same properties (degree, knot vector) as the original boundary curve of $\mathbf{b}(u, v)$. The result control polygon is corrected such that the final curve is G^2 around the leading edge (see Algorithm 4). The input to the trimming process is shown in Fig. 2.22 (right) and the final blade is shown in Fig. 2.25.

2.2.5.4 Trimming by general surface

Similar process of trimming as for the guide vane is applied to the runner blade. The only change is that the trimming surface is general surface of revolution. There are two possibilities:

1. the inner trimming surface is precise description of turbine housing and the outer trimming surface is sphere (see Fig. 2.26 (left column))
2. the inner trimming surface is approximation of the inner turbine housing and the outer trimming surface is cylinder (see Fig. 2.26 (right column))

The second case is analogical to the case of trimming by spheres (cf. Section 2.2.5.3) because the approximation surface of inner turbine housing is not divided into several parts and consists only of one spline surface. Fig. 2.26 (top, right) shows the implicitly given curve in parametric space of the blade before trimming. The boundary of the trimmed blade is shown in Fig. 2.26 (middle, right) and the blades after trimming with turbine housing are shown in Fig. 2.26 (bottom, right).

For the first case, the inner part of housing used for trimming includes several types of surfaces that can be described implicitly: cylinder, sphere, torus and cone. This type of trimming generates the volume with five patches (see Section 3.3) and it is more complicated thus it is used mainly for analyzing the flow through turbine not for the optimization process. Let's describe the second process in more detail. Firstly, we do exactly the same process as for the sphere (described in Section 2.2.5.3) for each surface that characterize the turbine housing (i.e. for cylinder, sphere, torus and cone). Now, the only difference is that the resulting trimming curve in parameter space of untrimmed surface is composed of several parts and could be C^0 continuous (Fig. 2.26 (top, left)). The boundary of the blade is shown in Fig. 2.26 (middle, left) and the blades after trimming with turbine housing are shown in Fig. 2.26 (bottom, left).

2.3 Blades of Francis turbine

The procedure of modelling of FT blades is similar to the modelling of KT blades. There are three types of blades: stay vanes, guide vanes and runner blades in FT. The stay vanes and guide vanes has the same shape and they are prismatic in the direction of the blades axis. The development of the B-spline surface for runner blade is more complicated.

2.3.1 Stay vanes and guide vanes of FT

The stay vanes are situated in the spiral case and the guide vanes are placed before the runner. Both of them serve to streamline the flow of water. From the geometric point of view the planar profile of stay/guide vane is same as for KT guide vanes (described in previous Section 2.2). It means that we start with description of camber line that is followed by definition of the function of thickness (for more information see Sections 2.2.1 and 2.2.2). There are similar parameters included in the final parameterization and the final blade is G^2 continuous.

2.3.1.1 2D profile

See Sections 2.2.1, 2.2.2 and 2.2.3 for creating 2D profile of KT blades since the process for FT does not change.

2.3.1.2 Construction of the final blade

For finding B-spline description of stay/guide vanes it is necessary to know only 2D blade profile and one additional parameter

- h_d ... height of the blade,

that is same for the stay vane and guide vane and corresponds to the distance between disks of spiral (see section 3.2.1). 2D profile in the plane yz is also computed in the plane $x = h_d$ and the control net is determined. The final blade is linear in the direction of the blade axis. Fig. 2.27 (left) shows the guide vane where the parameters are: $v = 0.00625909$, $d = 0.506391$, $\beta_1 = -0.00585567$, $\beta_2 = -0.0242671$, $v_t = 0.0738626$, $d_t = 0.386106$, $\gamma = -0.00585567$, $k_t = 0.00554457$.

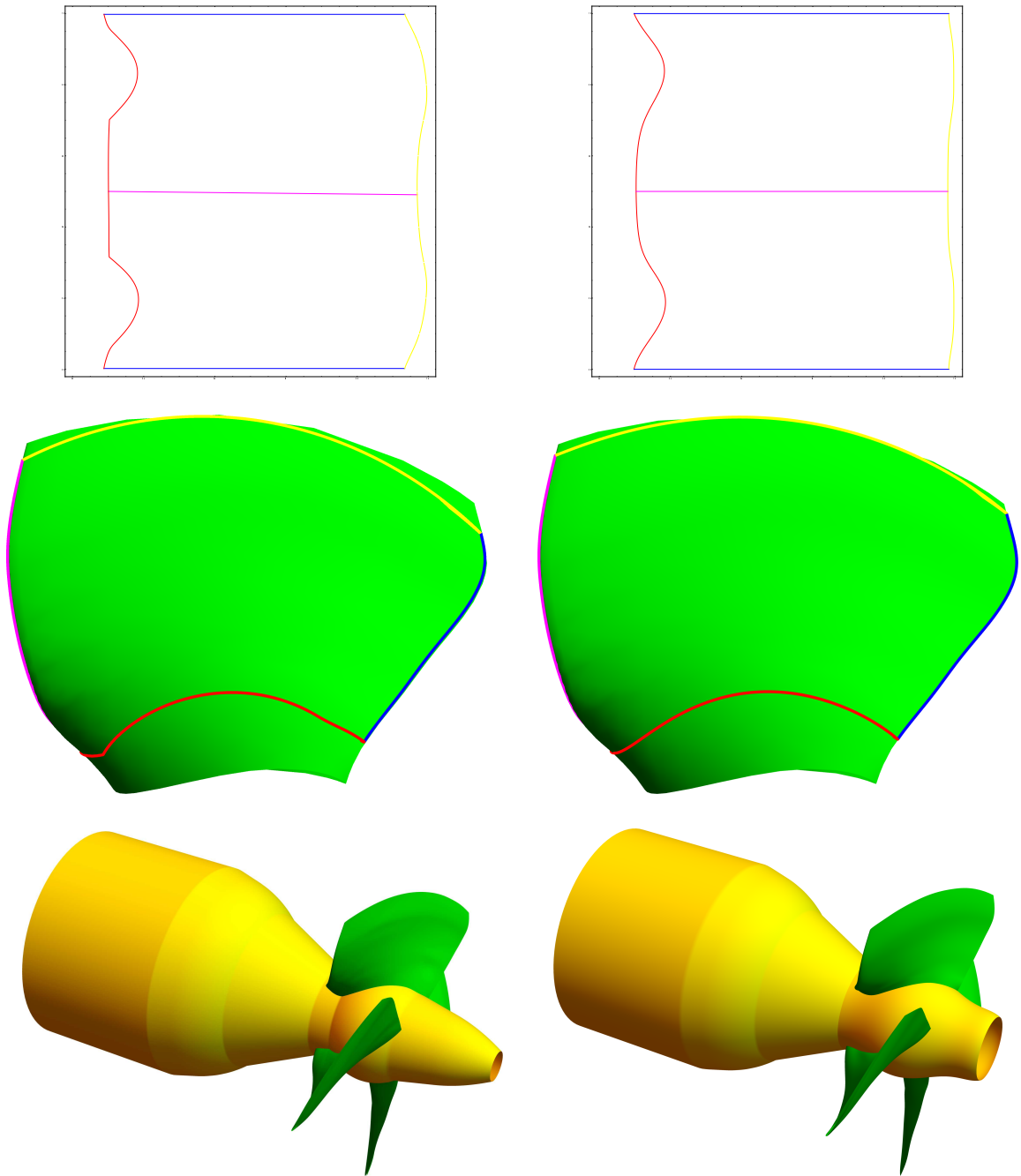


Figure 2.26: Trimming process of runner blade, trimming by inner housing (red), trimming by outer housing (yellow), leading edge (pink) and trailing edge (blue). Left: Runner blades of KT trimmed with the exact turbine housing, parametric space (top), blade before trimming (right), blade after trimming together with turbine housing (bottom). Right: Runner blades of KT trimmed with the approximate turbine housing, parametric space (top), blade before trimming (right), blade after trimming together with turbine housing (bottom).

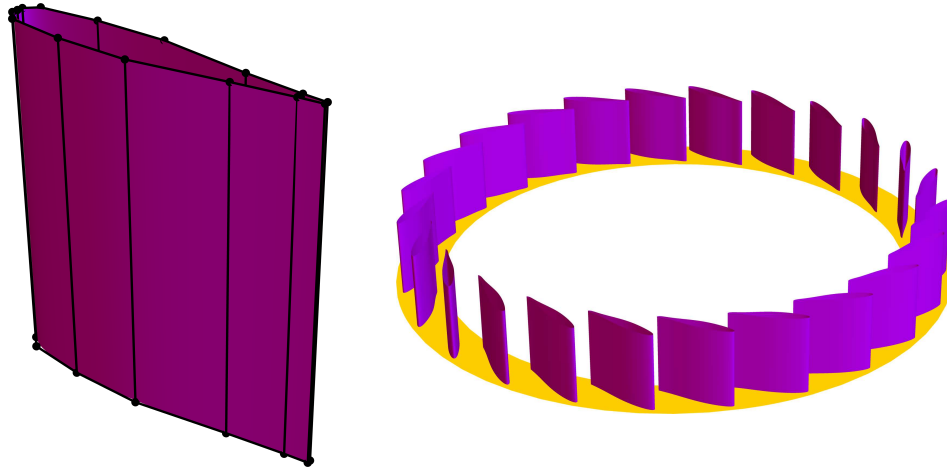


Figure 2.27: Left: B-spline surface and the control net of the guide vane FT. Right: The guide vanes of FT.

2.3.2 Runner blades of FT

The following process is divided into several steps. Preprocessing consists of composing trailing and leading edge from given parameters, computing the parametric sections of the runner from its B-spline volume parameterization (3D profiles are approximated on these sections) and the last step is to define intersections of the trailing/leading edge with these parametric sections. We map these intersections to a general plane that is determined by a normal vector defined by trailing/leading edge points and point on the x -axis. 2D blade profiles are created in this plane and they have the same parameters as for stay vanes/guide vanes. Moreover, we transform 2D profiles such that mapped intersections correspond with the leading/trailing edge points. 2D blade profiles are mapped to the parametric sections and 3D blade profiles are obtained. The last part of the process is devoted to the computation of B-spline surface representing blade.

2.3.2.1 Preprocessing

There are several components that should be defined before determining blade profiles of the runner blade.

1. Trailing edge and the leading edge

The trailing edge has the following parameters – two points and two vectors

- \mathbf{A}_o ... starting point of trailing edge,
- \mathbf{B}_o ... ending point of trailing edge,
- $t_{\mathbf{A}_o}$... starting tangent vector,
- $t_{\mathbf{B}_o}$... ending tangent vector.

The trailing edge is represented as cubic B-spline curve. From the numerous experiments, the suitable choice seems to be B-spline curve with three segments (this number of parts was discovered after experiments with data from the Francis turbine blade provided by MAVEL a.s.). If no other shape restrictions or requirements are given, the remaining control points are computed with minimization of second differences. Similarly, the leading edge has four parameters ($\mathbf{A}_l, \mathbf{B}_l, t_{\mathbf{A}_l}, t_{\mathbf{B}_l}$) and the B-spline representation is also cubic with three parts and the rest of degrees of freedoms are determined by minimization of second differences, if no other shape requirements are given. Fig. 2.28 shows the trailing and the leading edge.

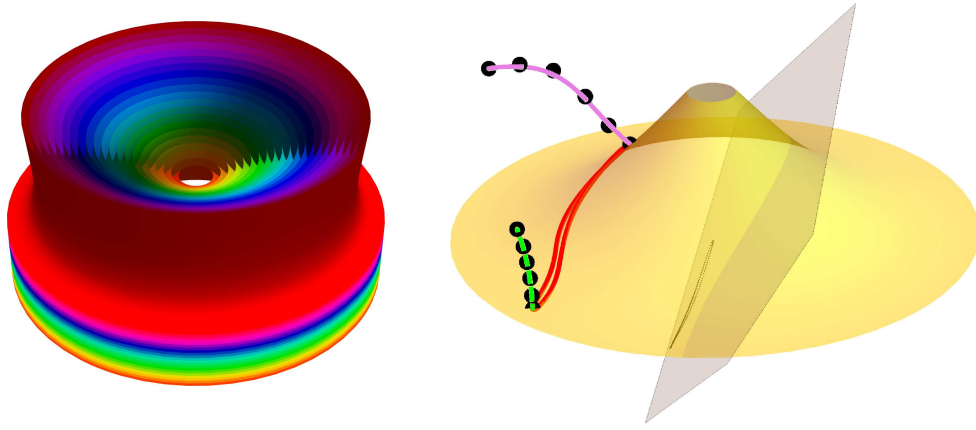


Figure 2.28: Left: Sections of the runner (the hub is orange and the turbine housing is red). Right: 2D profile mapped to the hub, trailing edge (pink) and leading edge (green) together with the control points.

2. The plane for 2D blade profiles

The special plane that serves as the plane where 2D blade profiles are constructed is determined from the previous parameters of leading/trailing edge. The plane is given as

$$p(u, v) : \mathbf{X} = (A_{hx}, 0, 0) + u \vec{s} + v(1, 1, 0), \quad (2.24)$$

where A_{hx} is the x coordinate of the hub (see Section 3.2.4) and the direction vector \vec{s} depends on the parameters of leading and trailing edge. The vector \vec{s} is

$$\vec{s} = \frac{(\mathbf{A}_n - \mathbf{B}_n) + (\mathbf{A}_o - \mathbf{B}_o)}{2}.$$

Fig. 2.28 shows the plane for construction of 2D profiles.

3. Parametric sections

The sections of runner that are used for mapping 2D profiles are determined from B-spline volume parameterization of the runner. This parameterization is defined the inner and outer surfaces of runner. The linear transition is between the outer and inner part of runner described as B-spline surfaces, i.e. the last knot vector of B-spline volume representation $\mathbf{B}(u, v, w)$ is

$$W = (0, 0, 1, 1).$$

The sections are obtained for parameters $w = w_i$, where $i = 0, \dots, m - 1$ and m is number of profiles. Fig. 2.28 shows different sections of runner.

4. Intersections of parametric sections and edges

The next preprocessing step is to find intersections of the leading and trailing edges with parametric sections. The intersections are found by solving the system of nonlinear equations (e.g. by using Newton method)

$$\mathbf{r}(u, v) = \mathbf{e}(t),$$

where $\mathbf{r}(u, v)$ is the parameterization of the section and $\mathbf{e}(t)$ parameterization of trailing/leading edge.

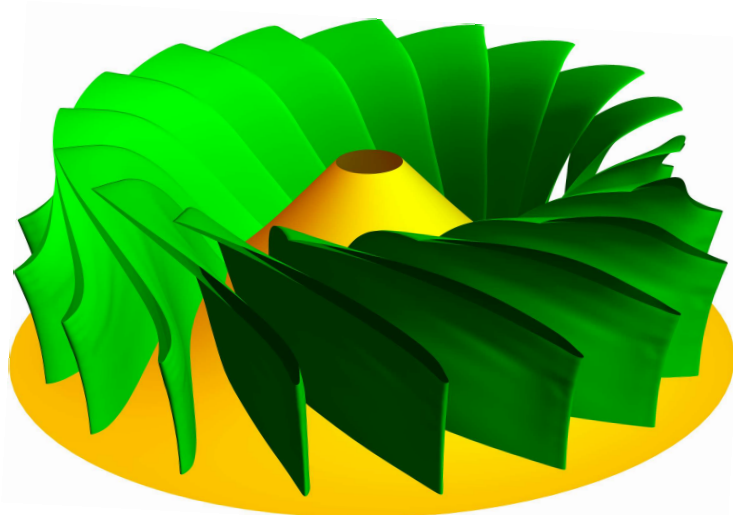


Figure 2.29: The runner blades of FT.

2.3.2.2 2D profile

The planar blade profile is computed for parameters not different from the ones in Section 2.3.1. The main difference is in the plane where they are constructed (stay/guide vanes are made in the yz -plane). The specific plane is defined in (2.24) and the blade profile is constructed as the one described in the Sections 2.2.1, 2.2.2 and 2.2.3.

2.3.2.3 3D profile

First of all, 2D blade profile is sampled and then mapped to the parametric volume sections presented in Section 2.3.2.1 with the help of orthogonal projection where projection direction is given as normal vector of the plane (2.24). The next step is to use Algorithm 5 to approximate these mapped points by a B-spline curve (this process is divided into two parts – suction and pressure side). This process is applied to each 2D blade profile constructed in the special plane (2.24). The described steps determine 3D blade profiles that are necessary for the construction of the final B-spline surface shown in the next paragraph.

2.3.2.4 Construction of the final blade

The final blade of FT is constructed in the same way as KT blades (see section 2.2.5.2). It means that the resulting B-spline surface contains $m \times n$ control points, where n is the number of control points determining one 3D blade profile in the runner section and $m = 3(l - 1)$, where l is the number of these profiles. The construction of the control net starts with adding the already known curves to the net: 3D blade profiles (rows of the net), trailing edges (the first and the last columns) and leading edge ($\frac{n+1}{2}$ column). After adding continuity conditions the remaining control points are computed with the help of minimization of third differences (see Section 2.2.5.2 for more details). The final B-spline surface is C^1 continuous across the profiles, profile curves are G^2 continuous and degrees are $(N, 3)$, where N is the degree of profile curves on the runner blade sections. The knot vectors also depend on the knot vector of the profile curves and the number of profile curves because one profile curve adds triple knot to the base knot vector $(0, 0, 0, 0, 1, 1, 1, 1)$. On the contrary to KT blade, the FT blade does not have to be trimmed because the FT runner blades are stationary and do not rotate around their axes. The runner of FT with blades is shown in Fig. 2.29.

It is the glory of geometry that from so few principles, fetched from without, is able to accomplish so much.

Isaac Newton

3

B-spline volume parameterizations

This chapter contains mainly the description of methods and approaches used for finding the volume parameterizations of Kaplan and Francis turbines. These methods provide so-called parametric geometric models, i.e., for given shape parameters the corresponding B-spline model respecting these shape parameters is constructed. Such parametric geometric models allow to describe a wide range of different shapes just by one model. The volume B-spline models are necessary for analysis of the flow through the turbine utilizing IGA. The process of analysis is followed by optimization of water turbine blades to improve the desired properties of water turbines (efficiency, reduction of cavitation etc.). This chapter is organized as follows. We mention more general methods for determining B-spline volumes in the first part of this chapter. The second section is devoted to parts of water turbines and their parameterizations as boundaries for B-spline volumes. In the last section, the results for B-spline volumes of KT and FT are presented as the main part of this chapter.

3.1 Methods for determining B-spline/NURBS volumes

In this section, we present two methods required for the description B-spline/NURBS volumes arising in the context of water turbines. The first one is a method of determining approximate B-spline volume of revolution, which is obtained by rotation of surface around the given axis. The second method is more general and the input are six surfaces forming boundary of the resulting volume. For increasing the speed of the follow-up computations based on isogeometric analysis, we parametrized all surfaces and volumes just by polynomial B-spline functions. Thus, we apply polynomial approximation wherever it was required.

3.1.1 Polynomial approximation of a circle/circular arc

If it is possible to accept small-enough error in the description of a circle/circular arc, the standard rational parameterization can be replaced by polynomial approximation. There are several approaches but the method presented in [30] is adopted in the following. The polynomial approximation of circular arc starts with searching control points of a Bézier curve. We know that the first and the last control points are the first and last points of a circular arc which we approximate and the rest of the control points lie on the tangents of the circular arc. Thus, we would like to find the distance of the second and the third control point from the boundary ones (see Fig 3.1). The distance is obtained as

$$K = 4 \frac{\tan(\frac{\alpha}{4})}{3}, \quad (3.1)$$

where $\alpha \leq \frac{\pi}{2}$ is a central angle of circular arc (details of the computation are in [30]). The control points of the unit circle with the centre at the origin approximated with polynomial functions are

$$\mathbf{P} = \{(0, 1), (K, 1), (1, K), (1, 0), (1, -K), (K, -1), (0, -1), (-K, -1), (-1, -K), (-1, 0), (-1, K), (-K, 1), (0, 1)\}, \quad (3.2)$$

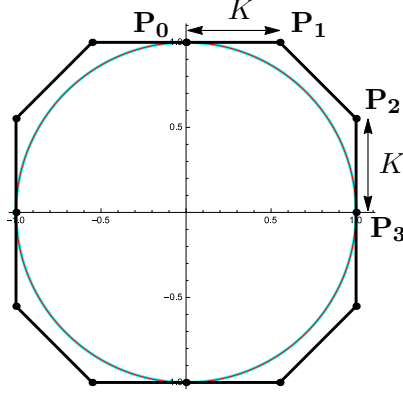


Figure 3.1: The control points of the approximation of the unit circle with the centre at the origin.

where all weights are equal to one. To approximate the whole circle at least four circular arcs are needed (then $\alpha = \frac{\pi}{2}$). The corresponding knot vector is

$$U = (0, 0, 0, 0, 1/4, 1/4, 1/4, 1/2, 1/2, 1/2, 3/4, 3/4, 3/4, 1, 1, 1, 1).$$

For example the approximation error for the circular arc with central angle $\frac{\pi}{2}$ is 2×10^{-6} .

3.1.2 Approximate B-spline volume of revolution

Let us consider two B-spline curves $\mathbf{c}(t)$ and $\mathbf{c}'(t)$ such that

$$\begin{aligned} \mathbf{c}(t) &= \sum_{k=0}^l \mathbf{P}_k N_{k,r}(t) = \sum_{k=0}^l (x_k, y_k, z_k) N_{k,r}(t), \\ \mathbf{c}'(t) &= \sum_{k=0}^l \mathbf{P}'_k N_{k,r}(t) = \sum_{k=0}^l (x'_k, y'_k, z'_k) N_{k,r}(t), \end{aligned}$$

$N_{k,r}(t)$, $k = 0, \dots, l$ are B-spline basis functions for the knot vector $W = (w_0, \dots, w_{l+r+1})$.

Let us assume that x -axis is the rotation axis. Then, each of the curves $\mathbf{c}(t)$, $\mathbf{c}'(t)$ defines an approximate B-spline surface of revolution $\mathbf{s}(v, w)$, $\mathbf{s}'(v, w)$, respectively, such that

$$\begin{aligned} \mathbf{s}(v, w) &= \sum_{j=0}^{12} \sum_{k=0}^l \mathbf{P}_{j,k} N_{j,3}(v) N_{k,r}(w), \\ \mathbf{s}'(v, w) &= \sum_{j=0}^{12} \sum_{k=0}^l \mathbf{P}'_{j,k} N_{j,3}(v) N_{k,r}(w), \end{aligned} \quad (3.3)$$

where

$$\begin{aligned} \{\mathbf{P}_{j,k}\}_{j=0, k=0}^{12,l} &= \{d_k \mathbf{R}_j + (x_k, 0, 0)\}_{j=0, k=0}^{12,l}, \\ \{\mathbf{P}'_{j,k}\}_{j=0, k=0}^{12,l} &= \{d'_k \mathbf{R}_j + (x'_k, 0, 0)\}_{j=0, k=0}^{12,l}, \end{aligned}$$

and $d_k = \sqrt{y_k^2 + z_k^2}$, $d'_k = \sqrt{y'_k{}^2 + z'_k{}^2}$ and

$$\begin{aligned} \{\mathbf{R}_j\}_{j=0}^{12} &= \{(0, 0, 1), (0, K, 1), (0, 1, K), (0, 1, 0), (0, 1, -K), (0, K, -1), (0, 0, -1), \\ &\quad (0, -K, -1), (0, -1, -K), (0, -1, 0), (0, -1, K), (0, -K, 1), (0, 0, 1)\}, \end{aligned}$$

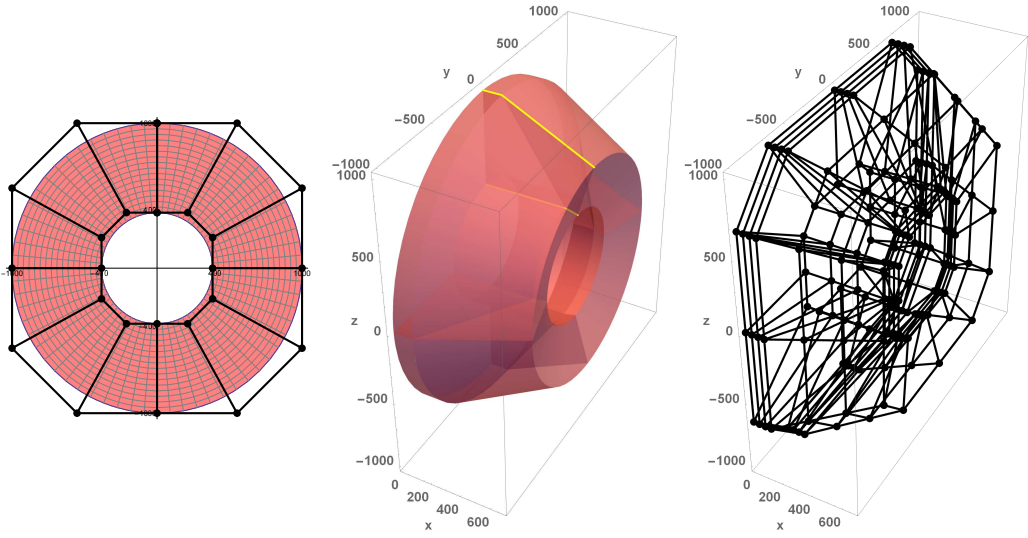


Figure 3.2: Left: B-spline annulus with $r_1 = 400$, $r_2 = 1000$ and the centre in the origin with the control net. Middle: Approximate B-spline volume of revolution of degree $(3, 3, 2)$ with its generatrix (yellow). Right: Control net of approximate B-spline volume.

where K is defined in (3.1). Further, $N_{j,3}(v)$, $j = 0, \dots, 12$ are B-spline basis functions for the knot vector

$$V = (0, 0, 0, 0, 1/4, 1/4, 1/4, 1/2, 1/2, 1/2, 3/4, 3/4, 3/4, 1, 1, 1, 1).$$

Joining the control nets $\{\mathbf{P}_{j,k}\}_{j=0,k=0}^{12,l}$ and $\{\mathbf{P}'_{j,k}\}_{j=0,k=0}^{12,l}$ to one control net

$$\{\mathbf{Q}_{i,j,k}\}_{i=0,j=0,k=0}^{1,12,l},$$

where

$$\begin{aligned} \{\mathbf{Q}_{0,j,k}\}_{j=0,k=0}^{12,l} &= \{\mathbf{P}_{j,k}\}_{j=0,k=0}^{12,l}, \\ \{\mathbf{Q}_{1,j,k}\}_{j=0,k=0}^{12,l} &= \{\mathbf{P}'_{j,k}\}_{j=0,k=0}^{12,l}, \end{aligned}$$

determines approximate B-spline volume of revolution, which is defined as

$$\mathbf{v}(u, v, w) = \sum_{i=0}^1 \sum_{j=0}^{12} \sum_{k=0}^l \mathbf{Q}_{i,j,k} N_{i,1}(u) N_{j,3}(v) N_{k,r}(w),$$

where $N_{i,1}(u)$ are B-spline basis functions for the knot vector $U = (0, 0, 1, 1)$. The example of approximate B-spline volume of revolution is in Fig. 3.2.

3.1.3 Revision of algorithms for construction of planar and volume domains for given boundary

The method for finding B-spline or NURBS volume parameterization for given boundary in water turbines is described in the following Section 3.1.4. Some steps of this method include different algorithms for obtaining the parameterization for given boundary curves or boundary surfaces. This section is devoted to brief revision of the used algorithms (precise definitions of algorithms and their analysis are in [24, 34, 40, 15, 91]).

3.1.3.1 2D methods

Let $\mathbf{b}_1(u)$, $\mathbf{b}_2(v)$, $\mathbf{b}_3(u)$ and $\mathbf{b}_4(v)$ be four boundary B-spline curves, $u \in [0, 1]$, $v \in [0, 1]$, fulfilling the conditions

$$\mathbf{b}_1(1) = \mathbf{b}_2(0), \quad \mathbf{b}_2(1) = \mathbf{b}_3(1), \quad \mathbf{b}_3(0) = \mathbf{b}_4(1), \quad \mathbf{b}_4(0) = \mathbf{b}_1(0). \quad (3.4)$$

Assume that each boundary B-spline curve \mathbf{b}_l is determined by the control points \mathbf{B}_k^l , where $k = 0, \dots, n$, for $l = 1, 3$ and $k = 0, \dots, m$, for $l = 2, 4$, the non-periodic knot vector \mathbf{U}_l and the degree p_l . We want to find a control net for planar B-spline surface describing domain $\mathbf{s}(u, v)$ given by four boundary curves \mathbf{b}_l . We assume without loss of generality that the domain of the parametric surface is the unit square, i.e., $0 \leq u, v \leq 1$. If the curves $\mathbf{b}_1(u)$ and $\mathbf{b}_3(u)$ do not have same degrees or knot vectors we use the algorithms for degree elevation or knot insertion (see [69]) to obtain the same knot vectors or degrees (analogously for the pair $\mathbf{b}_2(v)$ and $\mathbf{b}_4(v)$). See Fig. 3.3 (top, left) for the initial setting.

There are several methods for finding the parameterization, i.e., methods how to find the control points $\mathbf{P}_{i,j}$, where $i = 0, \dots, n$ and $j = 0, \dots, m$. For all mentioned methods it holds

$$\mathbf{P}_{i,0} = \mathbf{B}_k^1, \quad \mathbf{P}_{0,j} = \mathbf{B}_k^4, \quad \mathbf{P}_{i,m} = \mathbf{B}_k^3, \quad \mathbf{P}_{n,j} = \mathbf{B}_k^2.$$

The methods are:

- Discrete Coons patch

This method comes from the bilinear blended Coons patch and it can be easily modified to discrete version for control points

$$\begin{aligned} \mathbf{P}_{i,j} = & \left(1 - \frac{i}{n}\right) \mathbf{P}_{0,j} + \frac{i}{n} \mathbf{P}_{n,j} + \left(1 - \frac{j}{m}\right) \mathbf{P}_{i,0} + \frac{j}{m} \mathbf{P}_{i,m} - \\ & - \begin{bmatrix} 1 - \frac{i}{n} & \frac{i}{n} \end{bmatrix} \begin{bmatrix} \mathbf{P}_{0,0} & \mathbf{P}_{0,m} \\ \mathbf{P}_{n,0} & \mathbf{P}_{n,m} \end{bmatrix} \begin{bmatrix} 1 - \frac{j}{m} \\ \frac{j}{m} \end{bmatrix}. \end{aligned}$$

The process of computing the control net is very computationally inexpensive, on the other hand the resulting parameterization is sometimes not injective and postprocess needs to be accomplished to obtain valid (bijective) parameterization. See Fig. 3.3 (top, right) that shows the discrete Coons patch application.

- Spring model

The spring model possesses similar qualities as discrete Coons patch. This method uses “elastic strings” to construct edges in the control net, i.e.,

$$4\mathbf{P}_{i,j} = \mathbf{P}_{i+1,j} + \mathbf{P}_{i-1,j} + \mathbf{P}_{i,j+1} + \mathbf{P}_{i,j-1}. \quad (3.5)$$

This leads to solving simple system of linear algebraic equations. Other options of this model are obtained by adding different constants to different edges. The result of this method is shown in Fig. 3.3 (middle, left).

- Mean Value coordinates

This method uses initial control net $\hat{\mathbf{P}}_{i,j}$ (can be computed either by discrete Coons patch or by spring model) and its boundary points $\hat{\mathbf{P}}_k$, $k = 0, \dots, 2m + 2n - 1$ (counter clockwise arranged) where arbitrary point \mathbf{P} could be defined as an affine combination of the boundary control points

$$\mathbf{P} = \sum_{k=0}^{2m+2n-1} \lambda_k(\mathbf{P}) \hat{\mathbf{P}}_k, \quad \text{where} \quad \lambda_k(\mathbf{P}) = \frac{w_k(\mathbf{P})}{\sum_{k=0}^{2m+2n-1} w_k(\mathbf{P})}$$

Functionals	Q_l	Q_u	Q_o	Q_s	Q_a
Methods					
SPR	0.850981	3.44547	0.0175097	0.0139665	0.163767
DCP	0.890113	5.77134	0.0261811	0.0276505	0.169803
GM (0.1, 0.1)	0.837359	2.71164	0.0157024	0.0120443	0.15917
MN	0.855965	2.91335	0.0180346	0.0130495	0.163879
NL (0.1, 0.1, 0.3, 0.2, 0.1)	0.839481	2.92738	0.0133441	0.00921776	0.159155

Table 3.1: Functionals for the planar parameterization: SPR – spring method, DC – discrete Coons patch, GM – method with geometric measure with corresponding weights (w_l, w_u) , MN – mean value method and NL – non-linear case with weights $(w_l, w_u, w_o, w_s, w_a)$. Initial parameterization for MN and NL methods is GM (0.1, 0.1). The result parameterizations are shown in Fig. 3.3.

and weights are defined by

$$w_k(\mathbf{P}) = \frac{2}{\|\widehat{\mathbf{p}}_k\|} \left(\frac{|\widehat{\mathbf{p}}_{k-1}, \widehat{\mathbf{p}}_k|}{\|\widehat{\mathbf{p}}_{k-1}\| \|\widehat{\mathbf{p}}_k\| + \langle \widehat{\mathbf{p}}_{k-1}, \widehat{\mathbf{p}}_k \rangle} + \frac{|\widehat{\mathbf{p}}_k, \widehat{\mathbf{p}}_{k+1}|}{\|\widehat{\mathbf{p}}_k\| \|\widehat{\mathbf{p}}_{k+1}\| + \langle \widehat{\mathbf{p}}_k, \widehat{\mathbf{p}}_{k+1} \rangle} \right),$$

where $\widehat{\mathbf{p}}_k$ is vector defined by points $\widehat{\mathbf{P}}_k$ and \mathbf{P} , $\langle \cdot, \cdot \rangle$ is inner product and $|\cdot, \cdot|$ is determinant.

The new control net is then obtained as

$$\mathbf{P}_{i,j} = \sum_{k=0}^{2m+2n-1} \lambda_k(\widehat{\mathbf{P}}_{i,j}) \mathbf{P}_k,$$

i.e, we use weights of initial control net to compute new one. See Fig. 3.3 (bottom, left).

- Method with geometric measures

This method focus on the properties of the parameterization and the linear direct method is used. The optimization problem is solved and objective function is

$$\min_{\mathbf{P}_{i,j}^*} [w_l Q_l(\mathbf{P}_{i,j}) + w_u Q_u(\mathbf{P}_{i,j})] \quad (3.6)$$

where $\mathbf{P}_{i,j}^*$ are unknown inner points and $\mathbf{P}_{i,j}$ is the whole control net including boundaries. Parametric length functional $Q_l(\mathbf{P}_{i,j})$ is defined as

$$Q_l(\mathbf{P}_{i,j}) = \int_{\Omega} \|\mathbf{s}_u\|^2 + \|\mathbf{s}_v\|^2 \text{dudv} \quad (3.7)$$

and uniformity functional $Q_u(\mathbf{P}_{i,j})$ is defined as

$$Q_u(\mathbf{P}_{i,j}) = \int_{\Omega} \|\mathbf{s}_{uu}\|^2 + 2\|\mathbf{s}_{uv}\|^2 + \|\mathbf{s}_{vv}\|^2 \text{dudv}. \quad (3.8)$$

The choice of weights w_l and w_u is more discussed in [15]. Fig. 3.3 (middle, right) shows the result of this approach with geometric measures.

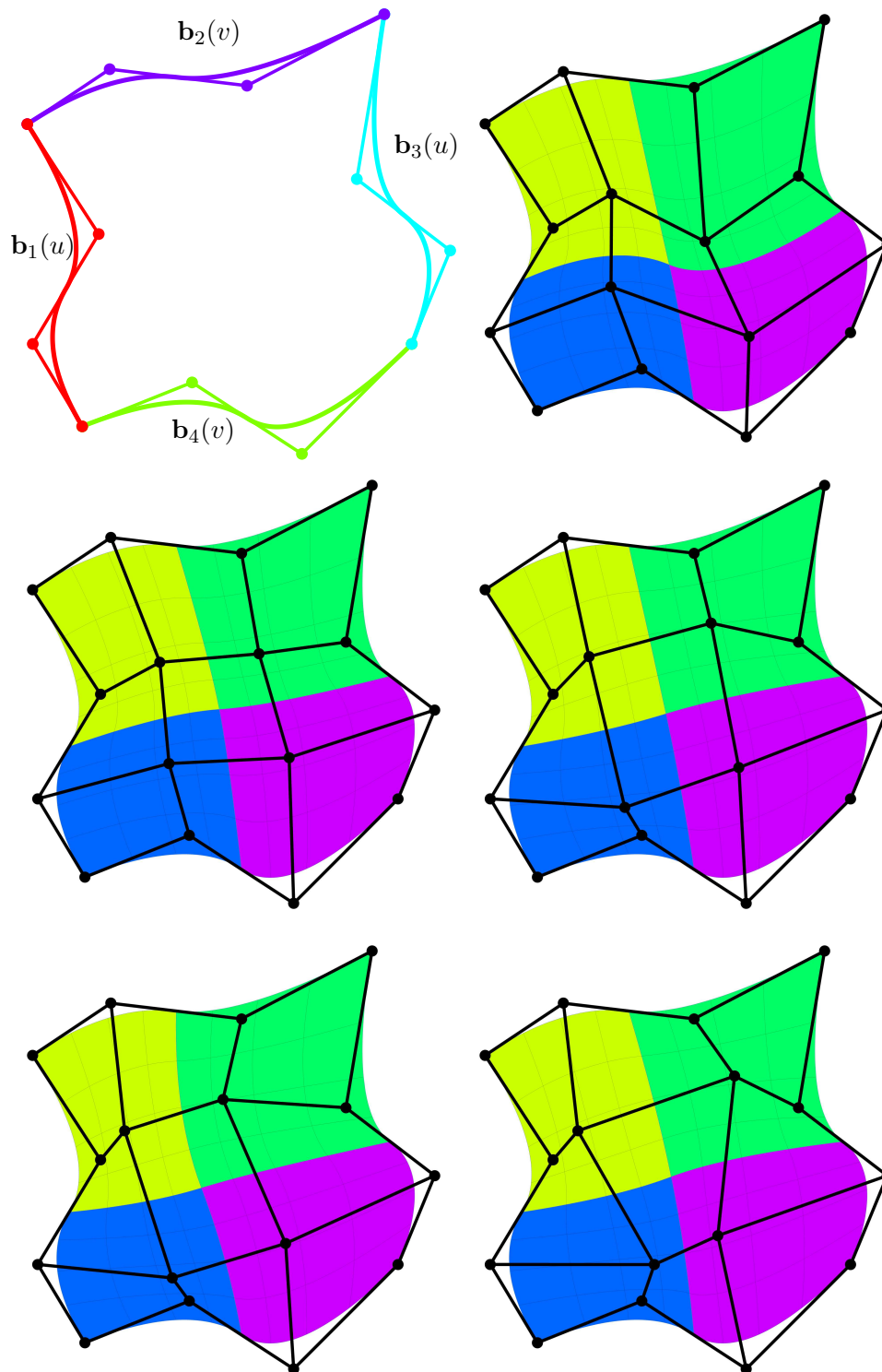


Figure 3.3: Planar parameterization methods. Top: Given boundary curves (left) and discrete Coons patch (right) with control net. Middle: Spring model with control net (left) and geometric measures case (right) with control net for weights are $w_l = w_u = 0.1$. Bottom: Mean value coordinate method (right) with control net and non-linear case (left) with control net for weights $w_l = w_u = w_a = 0.1$, $w_o = 0.3$, $w_s = 0.2$. Initialization parameterization for the previous two methods is geometric measure case with the weights $w_l = w_u = 0.1$.

Functionals	Q_l	Q_u	Q_o	Q_s	Q_a
Methods					
SPR	3.12749	7.4222	0.102625	0.0110431	1.0442
DCP	3.20202	12.267	0.157006	0.0199801	1.03363
GM (0.1, 0.1)	3.11473	6.38167	0.0932294	0.00958371	1.03419
NL (0.1, 0.1, 0.3, 0.2, 0.1)	3.11411	6.38422	0.0921767	0.00948747	1.03357

Table 3.2: Functionals for the volume parameterization: SPR – spring method, DC – discrete Coons patch, GM – method with geometric measure with corresponding weights (w_l, w_u) and NL – non-linear case with weights (w_l, w_u, w_o, w_s, w_a), where initial parameterization for NL method is GM (0.1, 0.1). The result parameterizations are shown in Fig. 3.5.

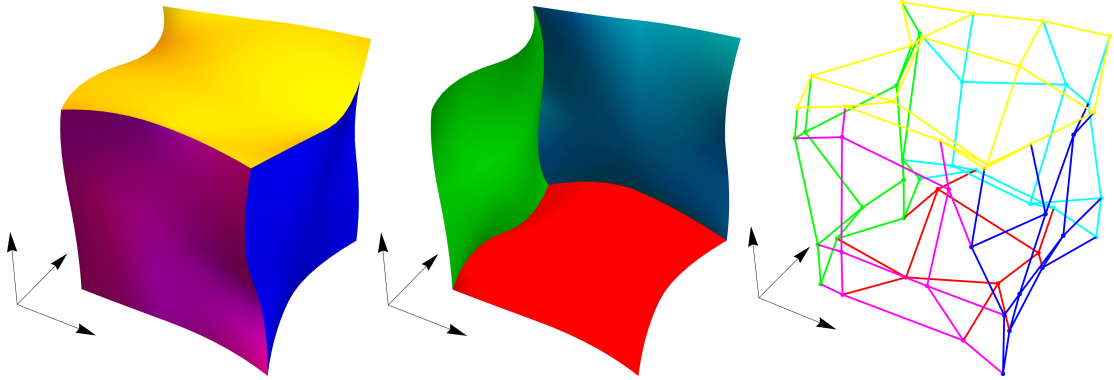


Figure 3.4: Given boundary surfaces for volume parameterization, visible three surfaces (left) and non-visible three surfaces (middle) with control nets (right).

- Non-linear case

Now, the more complex objective function than (3.6) is used and another functionals are added. More precisely, the objective function for minimization is now in the form

$$\min_{\mathbf{P}_{i,j}^*} [w_l Q_l(\mathbf{P}_{i,j}) + w_u Q_u(\mathbf{P}_{i,j}) + w_o Q_o(\mathbf{P}_{i,j}) + w_s Q_s(\mathbf{P}_{i,j}) + w_a Q_a(\mathbf{P}_{i,j})]$$

where $Q_l(\mathbf{P}_{i,j})$ and $Q_u(\mathbf{P}_{i,j})$ were defined in (3.7) and (3.8). The orthogonality functional is in the form

$$Q_o(\mathbf{P}_{i,j}) = \int_{\Omega} (\mathbf{s}_u \cdot \mathbf{s}_v)^2 \text{dudv}, \quad (3.9)$$

skewness functional is determined as

$$Q_s(\mathbf{P}_{i,j}) = \int_{\Omega} \left(\frac{(\mathbf{s}_u \cdot \mathbf{s}_v)^2}{(\mathbf{s}_u \cdot \mathbf{s}_u)(\mathbf{s}_v \cdot \mathbf{s}_v)} \right)^2 \text{dudv} \quad (3.10)$$

and the area functional is

$$Q_a(\mathbf{P}_{i,j}) = \int_{\Omega} |\mathbf{s}_u, \mathbf{s}_v|^2 \text{dudv}, \quad (3.11)$$

The previous method with geometric measures is used for initialization. Application of this non-linear method is shown in Fig. 3.3 (bottom, right).

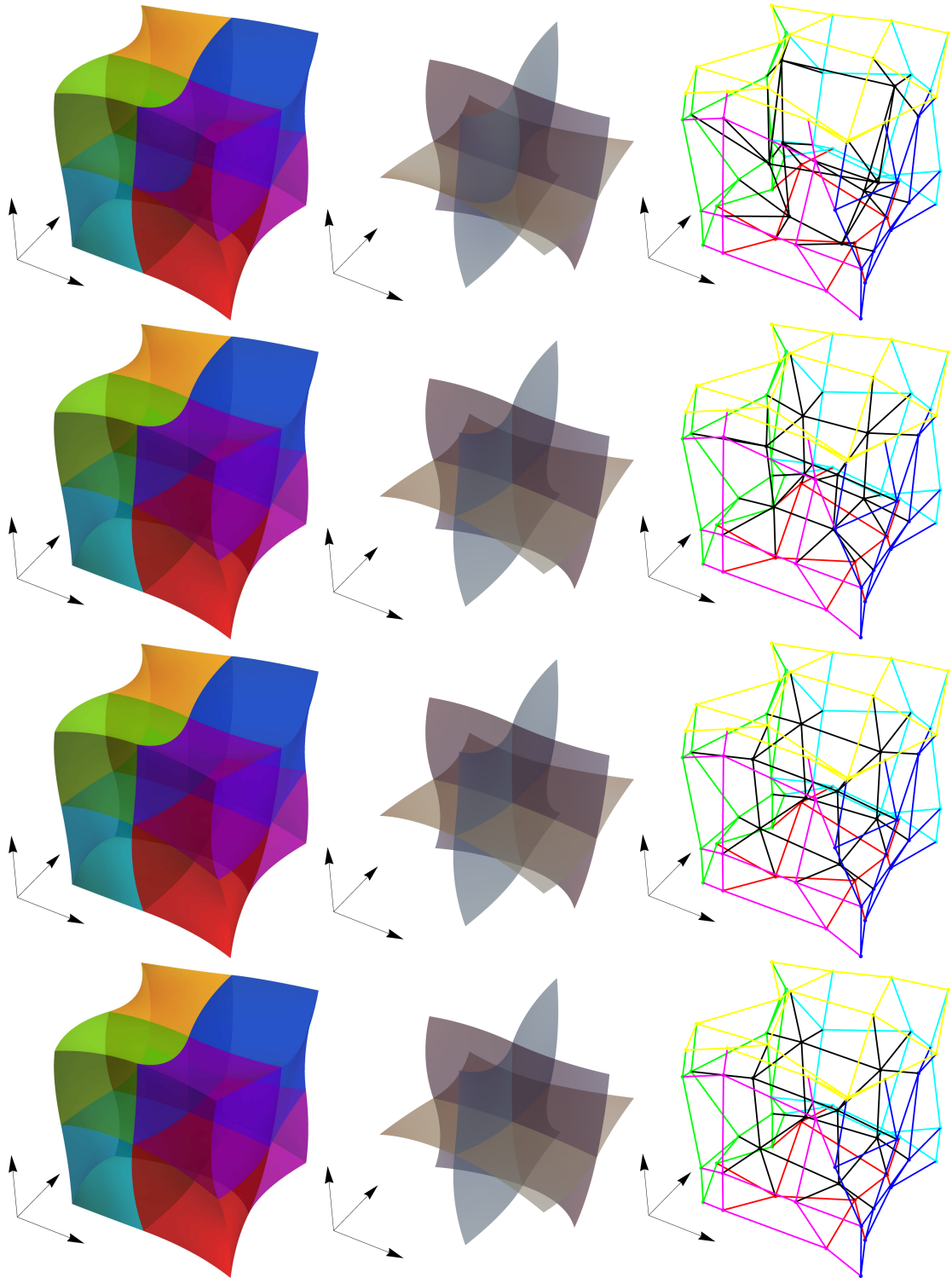


Figure 3.5: Volume parameterization methods. Left: Resulting parameterizations. Middle: Inner parametric surfaces. Right: Control nets. Top: Discrete Coons patch. Second row: Spring model. Third row: Geometric measures case with weights $w_l = w_u = 0.1$. Bottom: Non-linear method with weights $w_l = w_u = w_a = 0.1$, $w_o = 0.3$, $w_s = 0.2$, initial parameterization is geometric measure case with the weights $w_l = w_u = 0.1$.

Table 3.1 shows the comparison of values of functionals defined in (3.7), (3.8), (3.9), (3.10) and (3.11) for different approaches that are shown in Fig. 3.3.

3.1.3.2 3D methods

The similar problem can be solved in 3D to find volume parameterizations. Now, let $\mathbf{b}_a(u, v)$ be six boundary B-spline surfaces, $u \in [0, 1]$, $v \in [0, 1]$. Assume that each boundary surface \mathbf{b}_a is determined by the control points $\mathbf{B}_{r,s}^a$, the non-periodic knot vectors \mathbf{U}_a , \mathbf{V}_a and the degrees p_a , q_a . We want to find a control net for B-spline volume describing domain $\mathbf{v}(u, v, w)$ given by six boundary surfaces \mathbf{b}_a . We assume without loss of generality that the parametric domain is the unit cube, i.e., $0 \leq u, v, w \leq 1$. Then, we assume that the boundary surfaces fulfill compatibility conditions analogous to the planar case (3.4). If it is necessary (to change the boundary surfaces degrees or knot vectors when the corresponding pairs of boundaries differ) we use the algorithms for degree elevation or knot insertion (cf. [69]). See Fig. 3.4 for the initial setting.

Our goal is to find the control points $\mathbf{P}_{i,j,k}$ for $\mathbf{v}(u, v, w)$. The methods described in the following paragraphs are generalized approaches of 2D methods:

- Discrete Coons patch

Let $\mathbf{P}_{0,j,k}$, $\mathbf{P}_{n,j,k}$, $\mathbf{P}_{i,0,k}$, $\mathbf{P}_{i,m,k}$, $\mathbf{P}_{i,j,0}$, $\mathbf{P}_{i,j,l}$ be the control nets of boundary surfaces corresponding to control nets $\mathbf{B}_{r,s}^a$, $a = 0, \dots, 5$. Then, the control points of the control net are

$$\begin{aligned} \mathbf{P}_{i,j,k} = & \left(1 - \frac{i}{n}\right) \mathbf{P}_{0,j,k} + \frac{i}{n} \mathbf{P}_{n,j,k} + \left(1 - \frac{j}{m}\right) \mathbf{P}_{i,0,k} + \frac{j}{m} \mathbf{P}_{i,m,k} + \left(1 - \frac{k}{l}\right) \mathbf{P}_{i,j,0} + \\ & + \frac{k}{l} \mathbf{P}_{i,j,l} - \begin{bmatrix} 1 - \frac{i}{n} & \frac{i}{n} \end{bmatrix} \begin{bmatrix} \mathbf{P}_{0,0,k} & \mathbf{P}_{0,m,k} \\ \mathbf{P}_{n,0,k} & \mathbf{P}_{n,m,k} \end{bmatrix} \begin{bmatrix} 1 - \frac{j}{m} \\ \frac{j}{m} \end{bmatrix} - \\ & - \begin{bmatrix} 1 - \frac{j}{m} & \frac{j}{m} \end{bmatrix} \begin{bmatrix} \mathbf{P}_{i,0,0} & \mathbf{P}_{i,0,l} \\ \mathbf{P}_{i,m,0} & \mathbf{P}_{i,m,l} \end{bmatrix} \begin{bmatrix} 1 - \frac{k}{l} \\ \frac{k}{l} \end{bmatrix} - \\ & - \begin{bmatrix} 1 - \frac{k}{l} & \frac{k}{l} \end{bmatrix} \begin{bmatrix} \mathbf{P}_{0,j,0} & \mathbf{P}_{n,j,0} \\ \mathbf{P}_{0,j,l} & \mathbf{P}_{n,j,l} \end{bmatrix} \begin{bmatrix} 1 - \frac{i}{n} \\ \frac{i}{n} \end{bmatrix} + \\ & + \frac{k}{l} \left(\begin{bmatrix} 1 - \frac{i}{n} & \frac{i}{n} \end{bmatrix} \begin{bmatrix} \mathbf{P}_{0,0,l} & \mathbf{P}_{0,m,l} \\ \mathbf{P}_{n,0,l} & \mathbf{P}_{n,m,l} \end{bmatrix} \begin{bmatrix} 1 - \frac{j}{m} \\ \frac{j}{m} \end{bmatrix} \right) + \\ & + \left(1 - \frac{k}{l}\right) \left(\begin{bmatrix} 1 - \frac{i}{n} & \frac{i}{n} \end{bmatrix} \begin{bmatrix} \mathbf{P}_{0,0,0} & \mathbf{P}_{0,m,0} \\ \mathbf{P}_{n,0,0} & \mathbf{P}_{n,m,0} \end{bmatrix} \begin{bmatrix} 1 - \frac{j}{m} \\ \frac{j}{m} \end{bmatrix} \right). \end{aligned}$$

See Fig. 3.5 (top) that shows resulting parameterization of discrete Coons Patch.

- 3D Spring model

This method is generalized spring model from (3.5). Now, it holds

$$6\mathbf{P}_{i,j,k} = \mathbf{P}_{i+1,j,k} + \mathbf{P}_{i-1,j,k} + \mathbf{P}_{i,j+1,k} + \mathbf{P}_{i,j-1,k} + \mathbf{P}_{i,j,k-1} + \mathbf{P}_{i,j,k+1}.$$

This again leads to solving linear system of algebraic equations for unknown control points. Fig. 3.5 (second row) shows application of the 3D spring model.

- Method with geometric measures

This approach includes minimization of objective function

$$\min_{\mathbf{P}_{i,j,k}^*} [w_l Q_l(\mathbf{P}_{i,j,k}) + w_u Q_u(\mathbf{P}_{i,j,k})],$$

where $\mathbf{P}_{i,j,k}^*$ are unknown inner points and $\mathbf{P}_{i,j,k}$ is the whole control net including boundaries. Parametric length functional $Q_l(\mathbf{P}_{i,j,k})$ is defined as

$$Q_l(\mathbf{P}_{i,j,k}) = \int_{\Omega} \|\mathbf{s}_u\|^2 + \|\mathbf{s}_v\|^2 + \|\mathbf{s}_w\|^2 \text{dudvdw} \quad (3.12)$$

and uniformity functional $Q_u(\mathbf{P}_{i,j,k})$ is defined as

$$Q_u(\mathbf{P}_{i,j,k}) = \int_{\Omega} \|\mathbf{s}_{uu}\|^2 + 2\|\mathbf{s}_{uv}\|^2 + 2\|\mathbf{s}_{uw}\|^2 + 2\|\mathbf{s}_{vw}\|^2 + \|\mathbf{s}_{vv}\|^2 + \|\mathbf{s}_{ww}\|^2 \text{dudvdw}. \quad (3.13)$$

The choice of weights w_l and w_u is more discussed in [15]. Fig. 3.5 (third row) shows the result parametrization for this approach with geometric measures.

- Non-linear case

Now, the objective function is extended by three functionals to

$$\min_{\mathbf{P}_{i,j,k}^*} [w_l Q_l(\mathbf{P}_{i,j,k}) + w_u Q_u(\mathbf{P}_{i,j,k}) + w_o Q_o(\mathbf{P}_{i,j,k}) + w_s Q_s(\mathbf{P}_{i,j,k}) + w_a Q_a(\mathbf{P}_{i,j,k})],$$

where $Q_l(\mathbf{P}_{i,j,k})$ and $Q_u(\mathbf{P}_{i,j,k})$ were defined in (3.12) and (3.13). The orthogonality functional is in the form

$$Q_o(\mathbf{P}_{i,j,k}) = \int_{\Omega} (\mathbf{s}_u \cdot \mathbf{s}_v)^2 + (\mathbf{s}_u \cdot \mathbf{s}_w)^2 + (\mathbf{s}_v \cdot \mathbf{s}_w)^2 \text{dudvdw}, \quad (3.14)$$

skewness functional is determined as

$$Q_s(\mathbf{P}_{i,j,k}) = \int_{\Omega} \left(\frac{(\mathbf{s}_u \cdot \mathbf{s}_v)^2}{(\mathbf{s}_u \cdot \mathbf{s}_u)(\mathbf{s}_v \cdot \mathbf{s}_v)} \right)^2 + \left(\frac{(\mathbf{s}_u \cdot \mathbf{s}_w)^2}{(\mathbf{s}_u \cdot \mathbf{s}_u)(\mathbf{s}_w \cdot \mathbf{s}_w)} \right)^2 + \left(\frac{(\mathbf{s}_v \cdot \mathbf{s}_w)^2}{(\mathbf{s}_v \cdot \mathbf{s}_v)(\mathbf{s}_w \cdot \mathbf{s}_w)} \right)^2 \text{dudvdw} \quad (3.15)$$

and the volume functional is

$$Q_a(\mathbf{P}_{i,j,k}) = \int_{\Omega} |\mathbf{s}_u, \mathbf{s}_v, \mathbf{s}_w|^2 \text{dudvdw}. \quad (3.16)$$

The previous method with geometric measures is used for initialization. Application of this non-linear method is shown in Fig. 3.5 (bottom).

Table 3.2 shows the comparison of above mentioned methods for the example shown in Fig. 3.5.

3.1.4 B-spline/NURBS volume for given boundary

The second type of volume which occurs in the volumetric parameterization of water turbines is defined by six general boundary surfaces. Two of them lie on the inner/outer housing of the turbine. We apply the following steps:

1. determine boundary curves of the patch (parts of the blades or boundaries of the neighbouring volumes),
2. determine surfaces for the given boundary curves
 - (a) for the surfaces with the boundary curves on the housing of turbine we apply
 - find the B-spline description of the boundary curves in the parametric space of the housing of turbine,

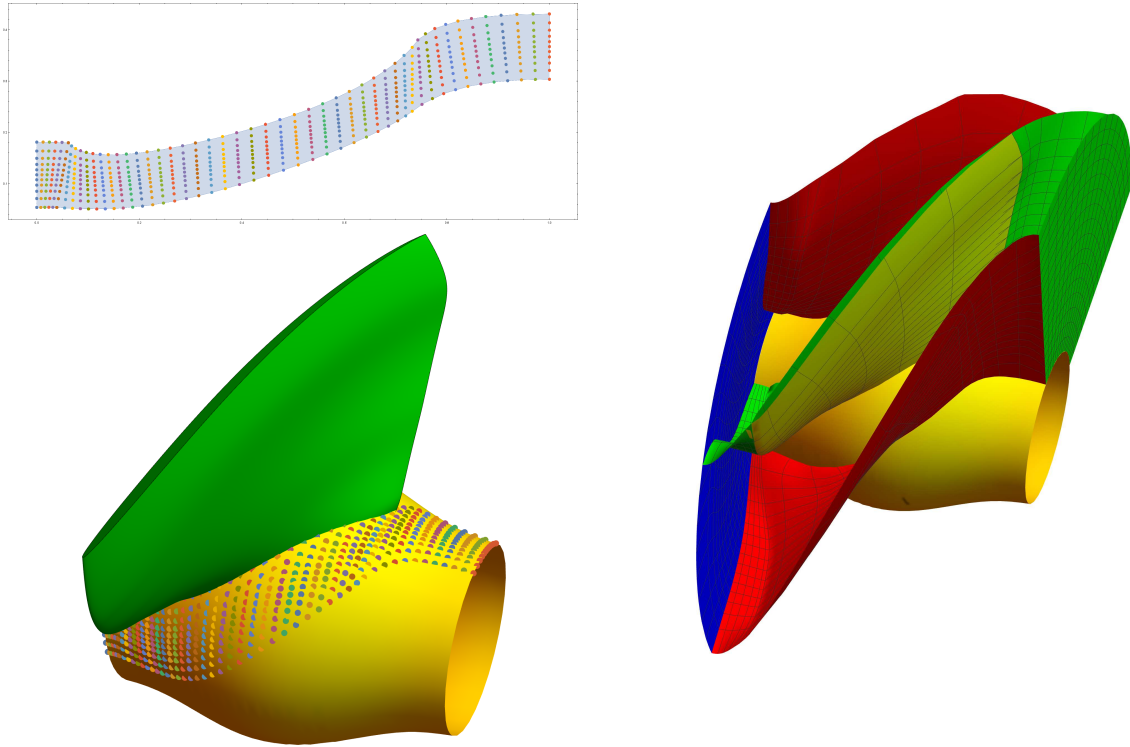


Figure 3.6: Left: Points on the turbine housing for parameters (bottom) from the sampled parametric space of turbine housing (top). Right: Boundary surfaces that are not parts of the turbine housing.

- determine the inner control points of the B-spline surface for the given boundary in the parametric space of the housing of turbine (for example, we can use discrete Coons patch in 2D or some other planar algorithms – see Section 3.1.3),
 - sample the surface in the parametric space and find the corresponding points that lie on the housing between the boundary curves,
 - approximate the surface on the housing,
- (b) in the case that all boundary curves do not lie on the housing, we apply discrete Coons patch algorithm or spring model described in Section 3.1.3,
3. for the final hexahedron we compute the inner control points with the discrete Coons patch algorithm in 3D described in Section 3.1.3.

Fig. 3.6 shows some steps of the process.

3.2 Parts of water turbines as the boundaries for NURBS volumes

Besides turbine blades (mentioned in the previous chapter) our intention is also to describe all other surfaces representing all other parts of turbine as B-spline/NURBS surfaces. Thus, we present also other parts of turbines: the spiral shaped pipe with stay vanes (entrance of vertical KT and FT), turbine housing for KT, part with guide vanes in FT, runner of FT and draft tube. All presented geometric models are polynomial because the approach described in Section 3.1.1 is used for surfaces of revolution or for parameterization of circle. Several parts of FT and KT described in this section are shown in Fig. 3.8 and 3.7.

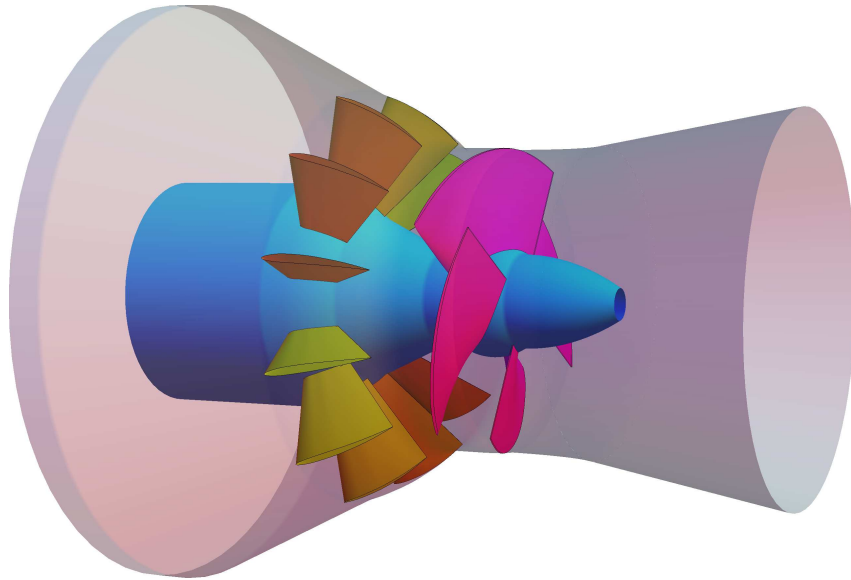


Figure 3.7: Kaplan turbine defined with B-spline parameterizations.

3.2.1 Spiral shaped pipe

The task of the spiral shaped pipe is to bring water into the part with guide vanes. The entrance pipe, which is formed of several sections defined by circular arcs with the ellipse at the end (in the whole spiral part these ellipses determine disks with the stay vanes). At the beginning of the entrance pipe the truncated cone is placed, and at the end there is a section connecting the first/last stay vane. The spiral shaped pipe has the following parameters:

- r_1 ... radius of the inlet circle of the truncated cone,
- d_1 ... the length of the truncated cone,
- n_s ... the number of segments in the spiral shaped pipe,
- r_s ... radius of the circular arc forming the section of the spiral shaped pipe,
- r_c ... distance between the centre of the section and the centre of the spiral that lies on the axis of the turbine,
- a_s ... angle of rotation of spiral section,
- r_{d1} ... inner distance of the disk from the axis of turbine,
- r_{d2} ... outer distance of the disk from the axis of turbine,
- h_d ... distance between the disks,
- w_d ... width of the disk.

Fig. 3.9 shows the parameters of the spiral section together with the control polygon. The knot vector corresponding to the direction of the flow of water depends on the number of sections. The surface is bicubic and the second knot vector is

$$U = (0, 0, 0, 0, 1/12, 1/12, 1/12, 2/12, 2/12, 2/12, 3/12, 3/12, 3/12, 4/12, 4/12, 4/12, 5/12, 5/12, 5/12, 6/12, 6/12, 6/12, 7/12, 7/12, 7/12, 8/12, 8/12, 8/12, 9/12, 9/12, 9/12, 10/12, 10/12, 10/12, 11/12, 11/12, 11/12, 1, 1, 1, 1)$$

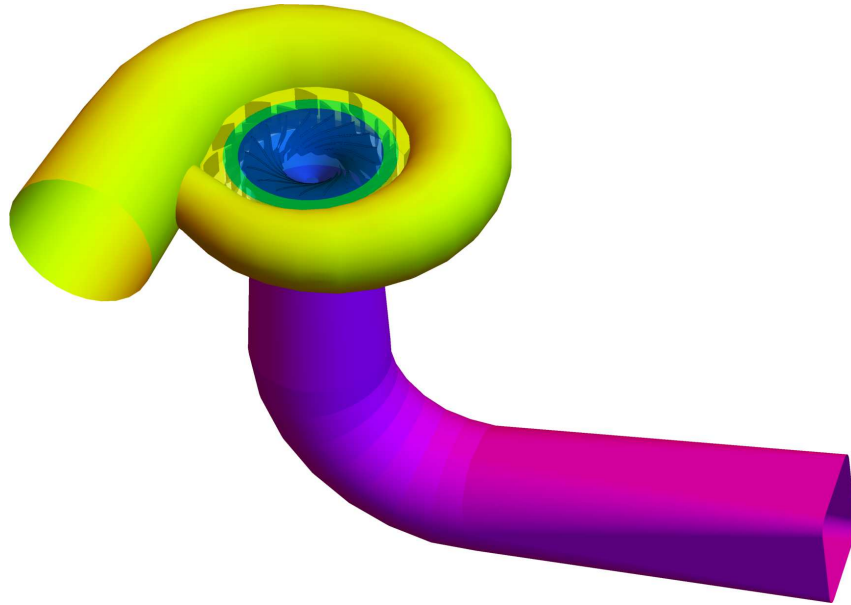


Figure 3.8: Right: Francis turbine defined with B-spline surfaces: the entrance pipe - spiral (yellow), part with guide vanes (green), runner (blue) a draft tube (purple).

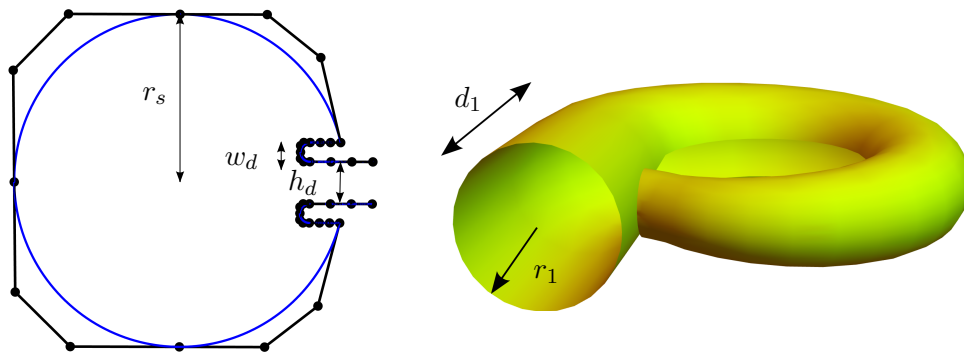


Figure 3.9: Left: The section of spiral pipe with parameters; Right: The beginning of the spiral case (without disks) with parameters.

The control points of the section and the example of specific parameters are in Appendix A. Stay vanes and their geometric representation are described in Section 2.3.1, we just remind that h_d is also the parameter for the height of the stay vane.

3.2.2 Part with guide vanes and runner in KT

In this section we describe inner and outer surfaces of blade canal of Kaplan turbine - part containing the guide vanes and the runner. The final surfaces are determined as approximate B-spline surfaces of revolution. Firstly, we model the generatrix of the revolution surface, which is consequently rotated around the axis of the turbine. Description of the turbine housing split into two parts - outer turbine case and inner turbine case. We start with the outer part and in each case we consider the turbine axis is identical with the z -axis.

Meridian of outer surface consists of lines and circular arcs, the curve is placed so that it lies in xz -plane. B-spline description of the generatrix is based on determination of control points that are dependent on the parameters, for example lengths of lines, angles and radii of circular arcs (see Fig. 3.10

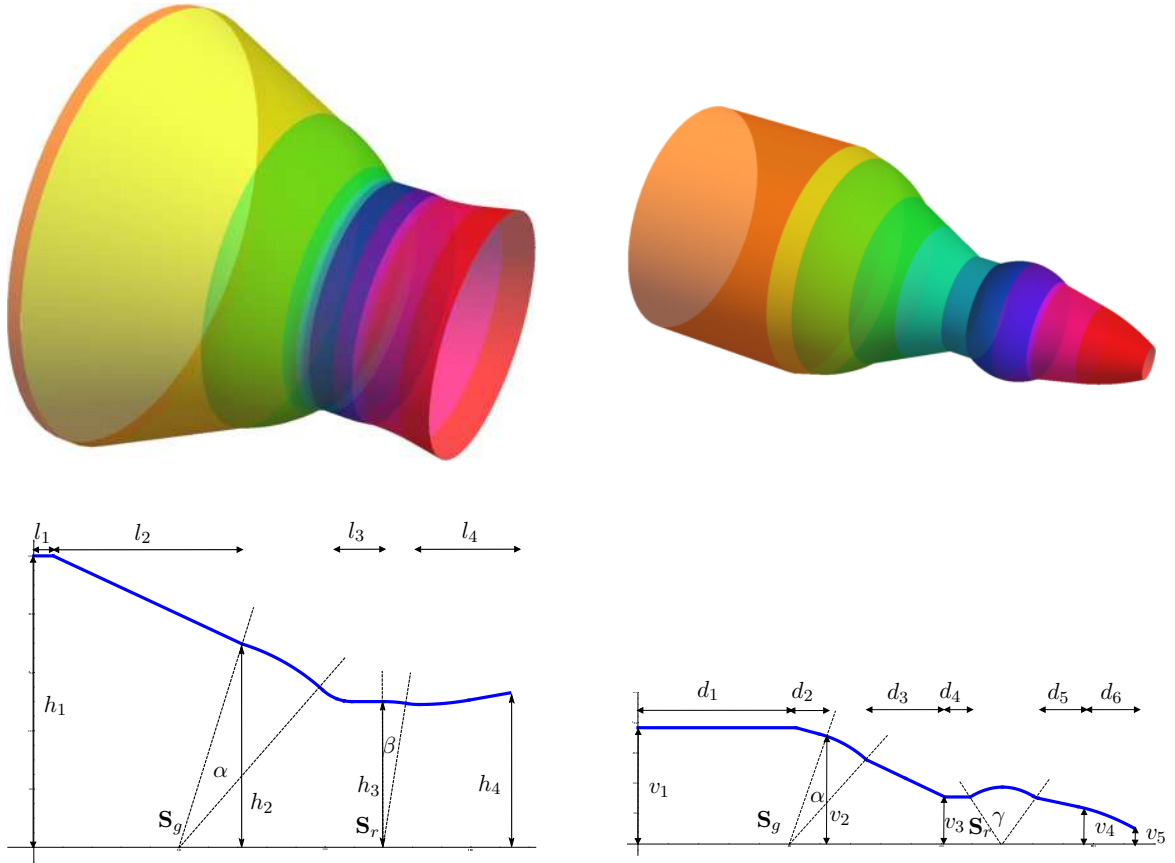


Figure 3.10: Top: Outer surface of a main section of turbine containing guide vanes and a runner (left) and inner surface of a main section of turbine containing guide vanes and a runner (right); Bottom: Generatrix with parameters of the outer surface (left) and of the inner surface (right).

(bottom, left)), and the knot vector

$$\begin{aligned}
 U = & (0, 0, 0, 0, 0.03791, 0.03791, 0.03791, 0.44541, 0.44541, 0.44541, \\
 & 0.62725, 0.62725, 0.62725, 0.65869, 0.65869, 0.65869, 0.6744, 0.6744, 0.6744, \\
 & 0.69027, 0.69027, 0.69027, 0.75117, 0.75117, 0.75117, 0.79769, 0.79769, 0.79769, \\
 & 0.82095, 0.82095, 0.82095, 0.91826, 0.91826, 0.91826, 1, 1, 1, 1) .
 \end{aligned}$$

The knot vector is determined by the chordal parameterization of generatrix. We do not present the specific coordinates of control points because they have complicated description. The next step is to form approximate surface of revolution. Thus, the second knot vector is

$$V = (0, 0, 0, 0, 1/4, 1/4, 1/4, 2/4, 2/4, 2/4, 3/4, 3/4, 3/4, 1, 1, 1, 1) .$$

This determines the outer turbine case uniquely for the given parameters, an example of the outer surface is shown in Fig. 3.10 (top, left).

The construction of inner surface is analogous to the outer turbine case. There are also lines and circular arcs, but the knot vector of generatrix (see Fig. 3.10 (bottom, right)) is different

$$\begin{aligned}
 U = & (0, 0, 0, 0, 0.30372, 0.30372, 0.30372, 0.35068, 0.35068, 0.35068, \\
 & 0.45344, 0.45344, 0.45344, 0.62045, 0.62045, 0.62045, 0.66963, 0.66963, 0.66963, \\
 & 0.73411, 0.73411, 0.73411, 0.75117, 0.75117, 0.75117, 0.79594, 0.79594, 0.79594, \\
 & 0.80648, 0.80648, 0.80648, 0.88463, 0.88463, 0.88463, 1, 1, 1, 1) .
 \end{aligned}$$

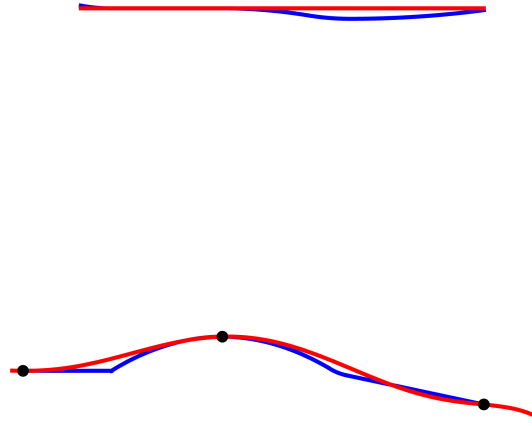


Figure 3.11: New generatrices (red) for the hub and turbine housing of KT.

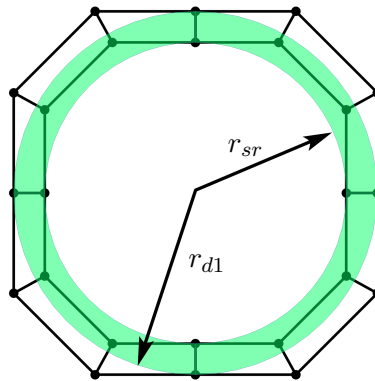


Figure 3.12: Part with guide vanes with parameters.

Generatrix lies in xz -plane and control points are dependent on the parameters (lengths of lines, angles and radii of circular arcs). The second knot vector is same as in the outer case because we use polynomial approximation of the circle again, i.e.

$$V = (0, 0, 0, 0, 1/4, 1/4, 1/4, 2/4, 2/4, 2/4, 3/4, 3/4, 3/4, 1, 1, 1, 1).$$

B-spline surface is shown in Fig. 3.10 (top, right).

For the optimization process, the simplified versions of inner and outer surfaces were constructed. The generatrix of inner surface is replaced by spline curve that interpolates important points. This leads to C^2 continuous generatrix, instead of C^0 continuous original version. The approximate the original generatrix of turbine housing by the line and the generatrix of outer surface is simplified to a line segment which leads to outer surface corresponding to approximate cylinder (see Fig. 3.11).

3.2.3 Part with guide vanes in FT

The following paragraphs include the description of the part with the guide vanes together with the parameters characterizing its shape. The guide vanes situated in this part of turbine are described in Section 2.3.1. The part with the guide vanes is composed of two anuli. The parameters are:

- h_d ... the height of the part with the guide vanes,
- r_{d1} ... radius of the outer circle,

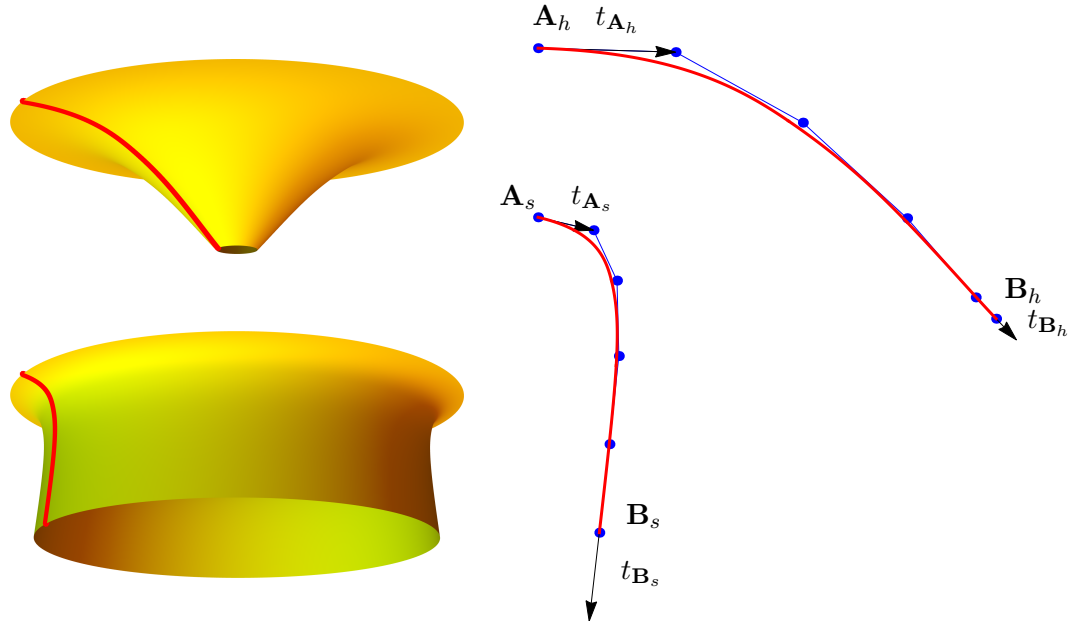


Figure 3.13: Top: Hub with the generatrix. Bottom: Shroud with the generatrix.

- r_{sr} ... radius of the inner circle,

and it holds that h_d is same as the distance between the disks in the spiral shaped piped and r_{d1} is also the distance of the disk from the axis of turbine (see Section 3.2.1), r_{sr} is the parameter of the runner (see more in Section 3.2.4). The parameters of the part with the guide vanes are shown in Fig. 3.12. The knot vectors are

$$\begin{aligned}
 U &= (0, 0, 0, 0, 1/4, 1/4, 1/4, 2/4, 2/4, 2/4, 3/4, 3/4, 3/4, 1, 1, 1, 1), \\
 V &= (0, 0, 1, 1).
 \end{aligned}$$

3.2.4 Hub and shroud of FT

This part is devoted to the FT runner that is situated between the guide vanes and the draft tube. The runner is constructed from two surfaces of revolution. For the B-spline description it is necessary to define the generatrices of the surfaces. The generatrix of the hub is cubic B-spline curve with three parts and the parameters are

- A_h ... starting point,
- B_h ... ending point,
- t_{A_h} ... starting tangent vector,
- t_{B_h} ... ending tangent vector.

analogically for the outer surface $A_s, B_s, t_{A_s}, t_{B_s}$. Because the prescribed parameters do not define all of the control points the remaining ones are computed by the minimalization of the second differences (see Section 2.2.5.2). Knot vectors are same for the both surfaces:

$$\begin{aligned}
 U &= (0, 0, 0, 0, 1/3, 2/3, 1, 1, 1, 1), \\
 V &= (0, 0, 0, 0, 1/4, 1/4, 1/4, 2/4, 2/4, 2/4, 3/4, 3/4, 3/4, 1, 1, 1, 1).
 \end{aligned}$$

Fig. 3.13 shows B-spline surfaces of hub (top) and shroud (bottom).

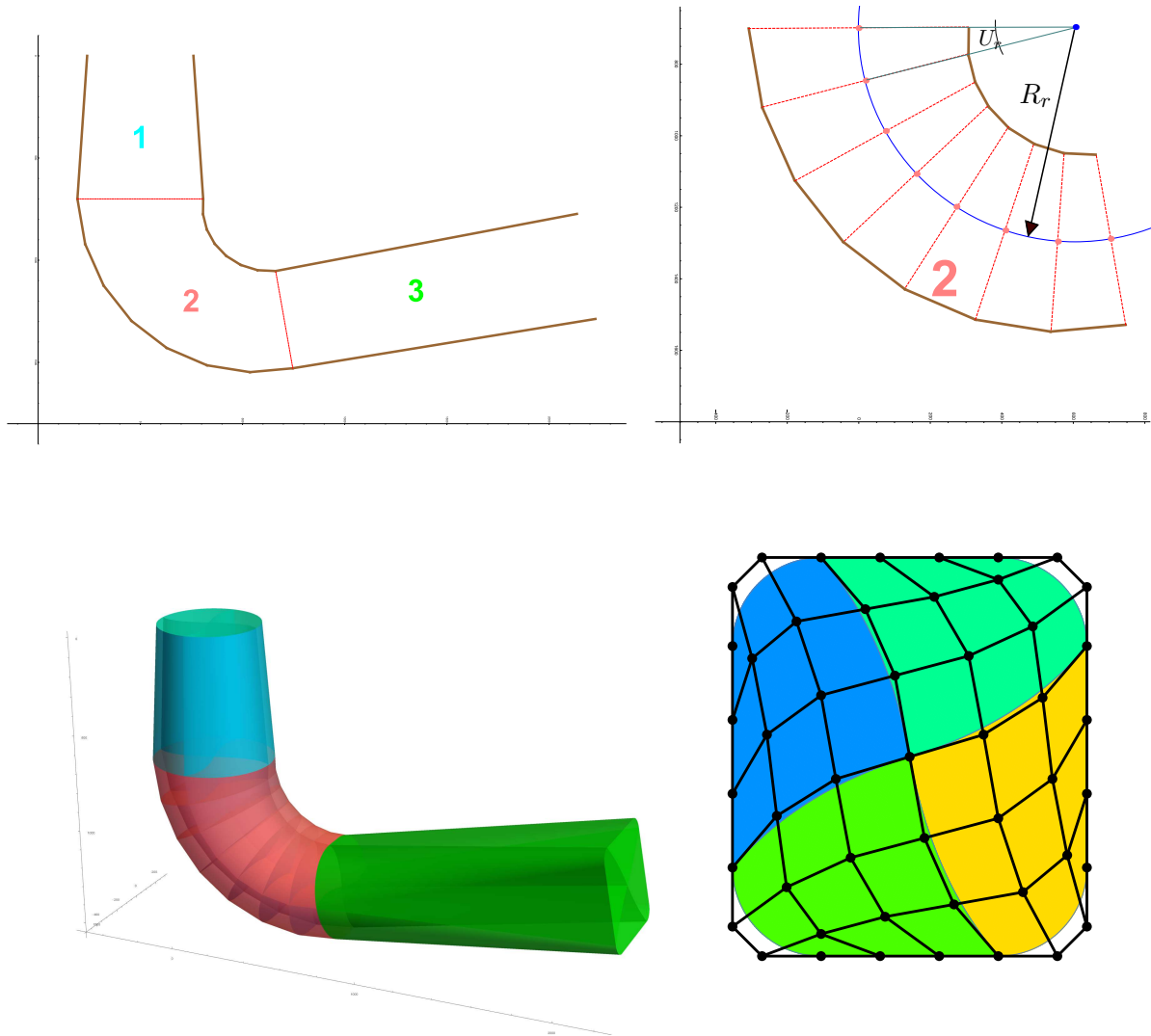


Figure 3.14: Top: Three parts of the draft tube: 1) cone part, 2) L-part a 3) diffuser (left); parameters of the elbow part (right). Bottom: NURBS volume of draft tube (left), see Appendix B for given parameters; parameterization of the draft tube section (right).

3.2.5 Draft tube

Draft tube is a device for water drainage after it leaves the runner, which means that it is located at the end of a water turbine behind the runner. It serves to two purposes:

- Decrease of kinetic energy – diffuser

The draft tube makes it possible to recover kinetic energy of water still remaining in the discharge from runner. The draft tube expands in the direction of water flow, which leads to the decrease of outlet water speed, i.e., the draft tube behaves as a diffuser.

- Expansion of potential energy

The hydraulic turbine does not have to be placed under the bottom water surface, if draft tube is included. Moreover, the pressure behind the runner is lowered because of the weight of water column in draft tube.

Further, it also creates consistent streamflow to the tailrace and, as follows from the above mentioned properties, it reduces exit loss. Due to mentioned purposes the draft tube is very important part of the water turbine.

The shape of the draft tube depends on the placement of the hydroelectric power station, it could be straight or elbow.

First of all, we describe different parts of a draft tube. We focus on the description of specific sections of a draft tube because these parts are just transitional surfaces between two consecutive sections. At the beginning of the draft tube (i.e., after the runner) the sections are circles, it means that at the beginning of a draft tube there are parts of cones. At the end, sections of draft tube are represented by rectangles with rounded corners. As the draft tube has to be simply manufactured, transitional surfaces between circle and rounded rectangle or two rectangles with rounded corners needs to be composed of developable surfaces. The geometric description of straight draft tube follows.

We start with forming the rounded rectangle section, because approximate B-spline description of circle section follows from the B-spline description of the rounded rectangle section. The given parameters of this section are:

- $v + 2r$... height of section,
- $s + 2r$... width of section,
- r ... radius,
- S ... centre of section .

The corresponding knot vector is

$$U = (0, 0, 0, 0, 1/8, 1/8, 1/8, 2/8, 2/8, 2/8, 3/8, 3/8, 3/8, 4/8, 4/8, 4/8, 5/8, 5/8, 5/8, 6/8, 6/8, 6/8, 7/8, 7/8, 7/8, 1, 1, 1, 1) .$$

The example of rounded rectangle section is shown in Fig. 3.14 (bottom right). For the circle section we need the same number of control points as in the rounded rectangle section and the same knot vector. It is necessary to obtain planes and cones in particular parts of the transitional surface between circle and rounded rectangle. This requires to use multiple control points (the control points lying on a circle are tripled). In Appendix B the control points of specific section of draft tube are shown.

Finally, we need to define the second knot vector to determine the B-spline surface of a draft tube. It depends on the number of sections and also on the position of sections. To obtain a good distribution of parametric lines, the second knot vector is obtained with the help of chordal parameterization.

In the case of elbow draft tube, it has 3 parts (see Fig. 3.14 (top left)), where the first and last parts are same as for the straight draft tube. The elbow part is composed of rounded rectangles that are rotated. Then, two parameters for each section in elbow part are added (see Fig. 3.14 (top right))

- R_r ... radius of rotation,
- U_r ... angle of rotation.

The next steps are analogous as for the straight version of draft tube, it means that transitional surfaces are computed between each two sections. See more approaches of draft tube geometric description in [55].

3.2.5.1 B-spline volume in draft tube

To create the volume parameterization of the draft tube we need to parametrize each section as a surface for given boundary. Each boundary curve that describes the section in draft tube is divided into four pieces and then the discrete Coons patch is applied to find the inner points (see Fig. 3.14 (bottom right)). Thus, the final volume is just linear transition between surfaces that describe sections in draft tube (see Fig. 3.14 (bottom left)).

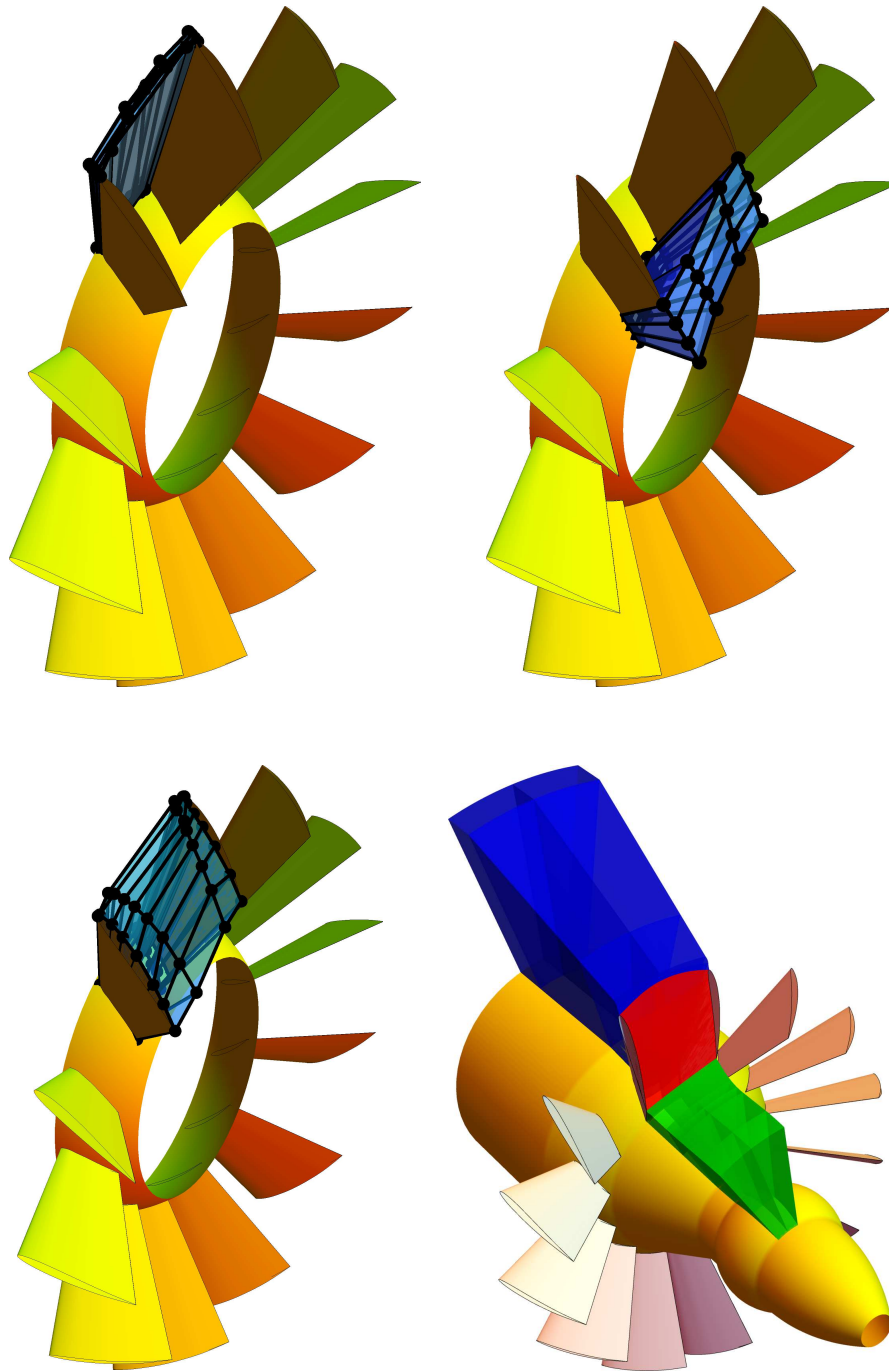


Figure 3.15: Top: The special part segment before guide vanes (left) and the part behind guide vanes. Bottom: The part between the guide vanes (right) and the whole 3-patch model (left).

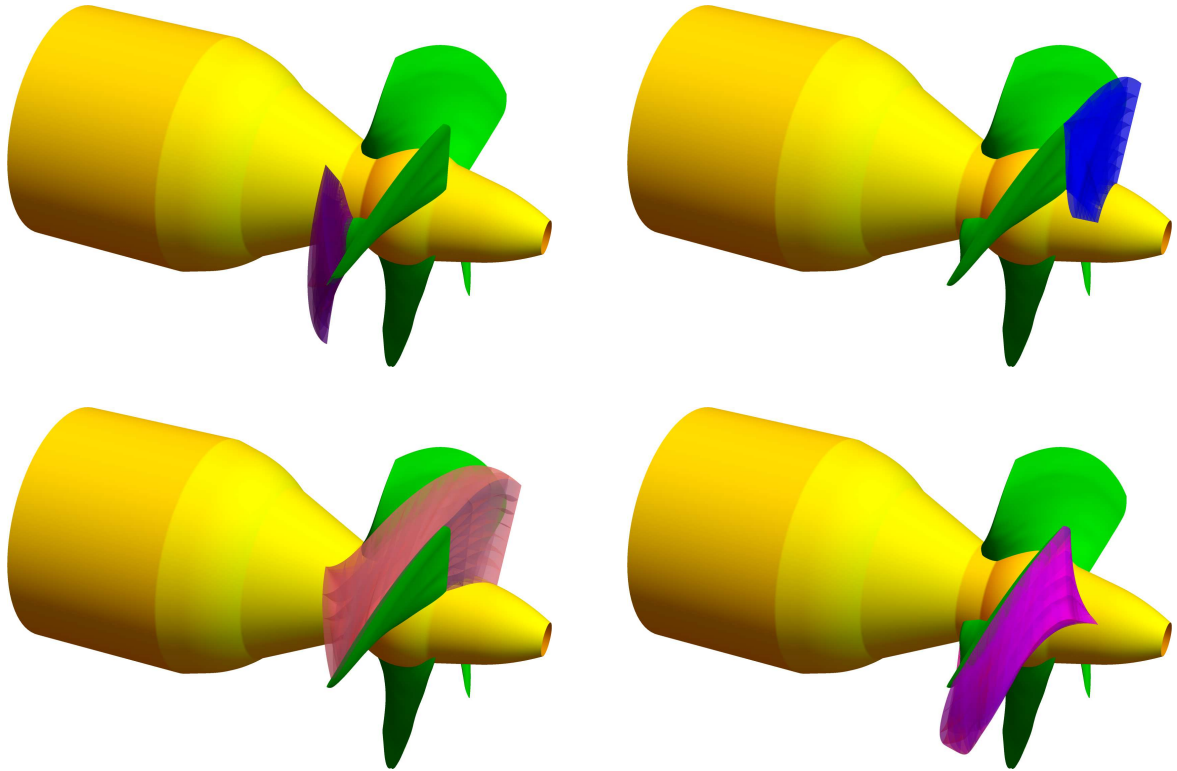


Figure 3.16: Top: Patch before the blade (left) and patch behind the blade (right). Bottom: Left patch (left) and right patch (right).

3.3 Volume parameterizations in KT

In this section we present segmentation of Kaplan turbine and we analyze each part in the terms of B-spline volume parameterization.

As it was mentioned in the introduction, KT was divided into several parts because it is not possible to describe the volumetric parameterization in one piece from the geometric point of view (the problem arises especially in parts where blades are situated). The first basic segmentation of KT is into two parts: blade canal and the draft tube. Volumetric parameterization of a draft tube has already been given in Section 3.2.5. Segmentation of a blade canal of a KT is divided into four parts: entrance volume, part with guide vanes, the section between blades and part with runner blades.

3.3.1 3-patch model with guide vanes

As the optimization process includes only runner blade, we use volume model of a blade canal with only guide vanes (without runner blades) to determine the input velocity field to the runner. Thus, the 3-patch model is constructed. It is divided into three parts - part before the guide vanes, part between the guide vanes and the part behind the guide vanes. We consider the zero thickness of the guide vanes to simplify the model.

3.3.1.1 Volume parameterizations before and behind the guide vanes

Both segments are parametrized as approximate B-spline volumes of revolution (described in section 3.1.2). But each of the volume also includes the part before the leading edges of guide vanes and part after the trailing edges of guide vanes. The approach described in Section 3.1.4 is used to construct this special parts (see Fig. 3.15 (top)).

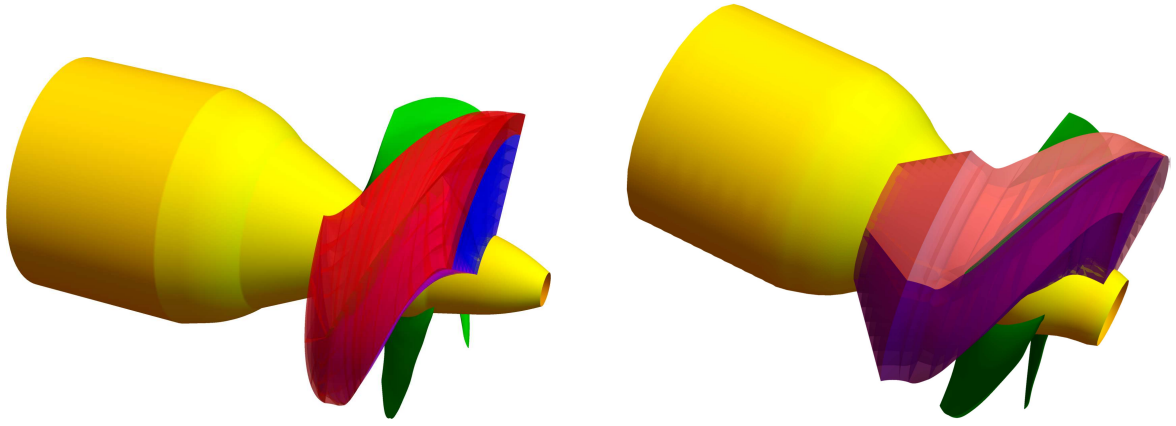


Figure 3.17: Left: 5-patches model of KT runner. Right: Simplified 2-patch model.

3.3.1.2 Volume between guide vanes

The last part is segment between the guide vanes. The method from Section 3.1.4 was applied and the volume is shown in Fig. 3.15.

3.3.2 Volume parameterizations surrounding the runner blade

3.3.2.1 5 patch model

First model of volume parameterization consists of 5 different volumes:

- patch before the blade (Fig. 3.16 (top, left)),
- left patch (Fig. 3.16 (bottom, left)),
- right patch (Fig. 3.16 (bottom, right)),
- patch behind the blade (Fig. 3.16 (top, right)),
- patch above the blade (red part in Fig. 3.17 (left)).

First four patches are computed as volumes for the given boundary (see Section 3.1.4). The last patch above the blade is approximate B-spline volume of revolution (cf. Section 3.1.2). The special boundary surface that is between two neighbouring blades is computed as average surface of suction side of one blade and pressure side of the other one. The whole multi-patch domain contain non-conformal interfaces due to the patch above the blade. In Fig. 3.17 (left) all 5 patches are shown.

3.3.2.2 2 patch model

The two patch model is just simplified version of the 5-patches model. The housing of turbine is slightly changed (see Section 3.2.2) and thus the patch above the blade does not exist. We also consider the zero thickness of the blade. The advantage of this model is that there is conformal coupling between patches. 2-patch model is shown in Fig. 3.17 (right).

The obtained patches determined by discrete Coons method (see Section 3.1.3.2) were improved by the non-linear method described also in Section 3.1.3.2. The reason that we use the Discrete coons patch as the initial net for the non-linear case and not the geometric measure type method or the spring model is that these methods do not provide usable control nets (with respect to the required property of positivity of Jacobian of the mapping from parametric to physical space) Numerous experiments has shown that the best choice of the initial net is the Discrete coons patch. Table 3.3 shows the values of the functionals

Methods		Functionals				
		Q_l	Q_u	Q_o	Q_s	Q_a
linear methods	SPR	1.51862	204.847	0.120681	0.248637	0.00784428
	DCP	1.70954	456.453	0.0877296	0.272752	0.00505827
	GM (0.1, 0)	1.11447	101.389	0.116958	0.316071	0.00763666
	GM (0, 0.1)	1.39603	54.945	0.0784048	0.273317	0.00461025
	GM (0.1, 0.1)	1.38397	54.951	0.0774842	0.270953	0.00460024
non-linear method	NL (0, 0.1, 0.1, 0, 0)	1.3974	54.955	0.0782107	0.272159	0.0046381
	NL (0, 0.1, 0.1, 0, 0.2)	1.39769	54.9543	0.0782092	0.272193	0.0046312
	NL (0, 0.1, 0.1, 0.1, 0.2)	1.39548	54.9589	0.074213	0.264629	0.00465491

Table 3.3: Functionals for the right patch: SPR – Spring method, DC – discrete Coons patch, GM – method with geometric measure with corresponding weights (w_l, w_u) and NL – non-linear case with weights $(w_l, w_u, w_o, w_s, w_a)$. All methods are described in Section 3.1.3.2.

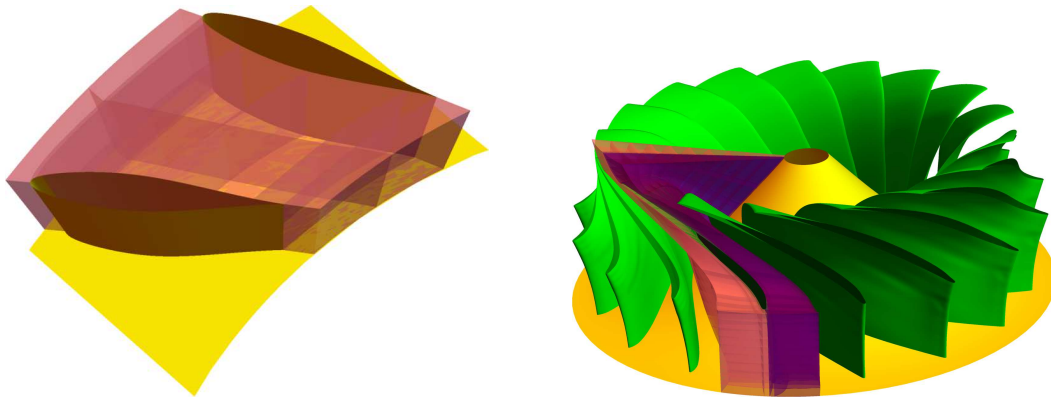


Figure 3.18: Left: The B-spline volume parameterization between FT guide vanes. Right: The B-spline volume parameterization around FT runner blade

described in Section 3.1.3.2 for the right patch and Table 3.4 shows the values of the functionals for the left patch.

From linear methods, the best result provides geometric measures method. Based on the choice of weights, much better results with respect to Q_l and Q_u than for discrete Coons patch or spring model can be obtained, and also other mentioned functionals are typically better. In this complicated case of finding volume parameterization of runner wheel, it is possible to observe from Table 3.3 that non-linear approach covering also functionals Q_o , Q_s and Q_a does not lead significantly better results. Focusing on the particular functional by increasing its weight, slightly better results for functional are obtained, but the difference is not significant. To sum up, it seems that reasonable approach for construction of control nets of volumetric parameterizations of runner wheel is geometric measures method which is fast (from the point of view of computation time) and gives good results.

More generally speaking, from the point of view of consequent computations based on isogeometric analysis, our main focus are functionals Q_u , Q_o and Q_a to obtain uniformly distributed and as much as orthogonal parameter lines and also equal-sized elements. This helps to obtain good results from consequent computations and to make the process of mesh refinement easy and reasonable. That is why the results for these functional are the most important ones and the non-linear method should be focused on these terms (by increasing their weights).

Methods		Functionals				
		Q_l	Q_u	Q_o	Q_s	Q_a
linear methods	SPR	1.47465	203.827	0.0911955	0.236379	0.00590249
	DCP	1.70742	427.362	0.0902625	0.282364	0.00456441
	GM (0.1, 0)	1.10451	99.157	0.118705	0.312064	0.00626679
	GM (0, 0.1)	1.40323	52.3234	0.0776653	0.252377	0.00420853
	GM (0.1, 0.1)	1.39031	52.3298	0.0766468	0.250889	0.00418781
non-linear method	NL (0, 0.1, 0.1, 0, 0)	1.40493	52.3343	0.0778659	0.251706	0.0042271
	NL (0, 0.1, 0.1, 0, 0.2)	1.40488	52.3342	0.0778757	0.251658	0.00422394
	NL (0, 0.1, 0.1, 0.1, 0.2)	1.40349	52.3349	0.0776486	0.249077	0.00422058

Table 3.4: Functionals for the left patch: SPR – spring method, DC – discrete Coons patch, GM – method with geometric measure with corresponding weights (w_l, w_u) and NL – non-linear case with weights $(w_l, w_u, w_o, w_s, w_a)$. All methods are described in Section 3.1.3.2.

3.4 Volume parameterizations in FT

B-spline volume parameterizations of the part with the guide vanes and around the FT runner blade are described in the following paragraphs. We omit the parameterization of the entrance spiral shaped pipe because it is not symmetric surface of revolution. Moreover, we know that water leaves the entrance pipe evenly at a constant angle. As the periodic conditions are used for the flow analysis it is sufficient to determine B-spline volumes for specific parts of the turbine (that depends on the number of the blades).

3.4.1 FT volume parameterization between guide vanes

The volume parameterization in the surroundings of the guide vanes is linear in the direction of the turbine axis, because guide vanes have prismatic shape. Moreover, the construction of the parameterization is based just on the planar net between guide vanes described with the help of discrete Coons patch. B-spline volume parameterization between guide vanes is shown in Fig. 3.18 (left).

3.4.2 FT volume parameterizations around runner blade

For the B-spline volume parameterization around the FT runner blade we apply the same procedure as described in the Section 3.3.2. The volume is composed of two patches: suction and pressure patch. For the simplification we use also the zero thickness at the trailing edge. In Fig. 3.18 (right) patches around the runner blade are shown.

If people do not believe that mathematics is simple, it is only because they do not realize how complicated life is.

John von Neumann

Conclusion

This thesis is focused on geometric modelling in industrial applications and we concentrate on models of water turbines (Pelton turbine, Kaplan turbine, Francis turbine). We use modern geometric approaches (B-spline/NURBS description) to describe water turbine hydraulic profiles. Such geometric models are then used to analyze the flow through the turbine and optimize the shape of water turbine parts via isogeometric analysis (IGA). The proposed geometric parameterizations of water turbines involve parameters to generalize the description of models. Therefore, we are able to make the process of shape optimization of turbines with the help of flow simulation for obtaining optimal flow inside the turbine to maximize the utility properties more efficient and more automatized. Currently, the results of flow simulations are usually obtained only for one particular model and the turbine models in CAD are subsequently manually modified with help of experience of designers to improve selected utility quantities (e.g. efficiency, cavitation). It can be seen that this is not a fully automatic process and results are often kept as secrets of companies.

In the second chapter we presented geometric models of a Pelton turbine bucket, Kaplan turbine and Francis turbine blades. In Chapter 2 we described a model of the Pelton turbine bucket that we divided into two parts – inner and outer surface. We needed to impose several given parameters and we found out that the most difficult part is to satisfy the given angle distributions along an outlet curve and a splitter which are boundary curves of a B-spline surface representing the inner surface of the bucket. We studied the existence of an exact solution of this problem, i.e., under which conditions on a given boundary curve and/or prescribed angle distribution a tangent ruled surface of a resulting B-spline surface can be found. It turned out that such conditions are very strict and an exact solution exists only in very special cases. Thus, we formulated an algorithm for finding an approximate solution of this problem, studied its approximation order and derived a bound on the approximation error. This part covers the main contribution and the main new results of the thesis. The second chapter was also devoted to geometric models of other water turbine blades. We presented methods for describing guide vanes and runner blade of Kaplan turbine as B-spline surfaces. Further, the methods for Francis turbine blades (stay vanes, guide vanes and runner blades) were also proposed to describe them in the context of B-spline objects. The main concept of the B-spline surface description of the blades was inspired by NACA airfoils and it is based on definition of important curves (camber line and thickness function).

In Chapter 3 we focused on B-spline volume parameterizations of computational domains from its boundary B-spline surfaces. Firstly, we described several methods used for the determination of B-spline volume parameterizations. The next part showed the description of the boundary surfaces in turbines, i.e., turbine housing entrance of the turbine, runner and draft tube. The main part of the last chapter was devoted to the B-spline volumes of Kaplan turbine parts and Francis turbine segments.

In the future we are going to concentrate on the following problems:

- Incorporation of methods which allow local and adaptive refinement of computational B-spline/NURBS meshes (which is not the case of standard B-spline/NURBS objects) also to the case of modelling water turbines. For example THB-splines can be used as modern approach allowing such local refinement.
- Propose methods for finding analysis-suitable volume B-spline/NURBS/THB parameterizations of spiral shaped pipes used for Francis and vertical Kaplan turbine for consequent flow simulation with IGA and shape optimization.

- Study of general approaches for finding volume B-spline/NURBS/THB parameterizations of object bounded by a set of B-spline/NURBS surfaces.
- Finish the model of Pelton turbine and analyze the flow through this type of turbine. Unfortunately, we need to study the problem of multiphase flow that is characterized as a flow in which more than one fluid is present (in Pelton turbine the bucket goes through two phases, the first with water and the second one is in the air).

Bibliography

- [1] P. Anděl, B. Bastl, K. Slabá: *Parameterizations of generalized NURBS volumes of revolution*. Engineering Mechanics, Vol. 19, pp. 293-306, 2012.
- [2] M. Aigner, C. Heinrich, B. Jüttler, E. Pilgerstorfer, B. Simeon, A.-V. Vuong : *Swept volume parameterization for isogeometric analysis*. In E. Hancock and R. Martin (eds.), The Mathematics of Surfaces (MoS XIII 2009), LNCS 5654, pp. 19-44, Springer, 2009.
- [3] B. Bastl, M. Brandner, J. Egermaier, K. Micháľková, E. Turnerová: *IgA-Based Solver for turbulence modelling on multipatch geometries*. Advances in Engineering Software, Vol. 113, pp. 7-18, 2017.
- [4] B. Bastl, M. Brandner, J. Egermaier, K. Micháľková, E. Turnerová: *Isogeometric analysis for turbulent flow*. Mathematics and Computers in Simulation, Vol. 145, pp. 3-17, 2018.
- [5] Y. Bazilevs, I. Akkerman: *Large eddy simulation of turbulent Taylor–Couette flow using isogeometric analysis and the residual-based variational multiscale method*. Journal of Computational Physics, Vol. 229, pp. 3402-3414, 2010.
- [6] Y. Bazilevs, L. Beirão de Veiga, J. A. Cottrell, T. J. R. Hughes, and G. Sangalli: *Isogeometric analysis: approximation, stability and error estimates for h-refined meshes*. Mathematical Models and Methods in Applied Sciences, Vol. 6, No. 7, pp. 1031-1090, 2006.
- [7] Y. Bazilevs, V. M. Calo, J. A. Cottrell, J. Evans, T. J. R. Hughes, S. Lipton, M. A. Scott, T. W. Sederberg: *Isogeometric analysis using T-splines*. Computer Methods in Applied Mechanics and Engineering, Vol. 199 (5-8), pp. 229-263, 2010.
- [8] Y. Bazilevs, T. Hughes: *Weak imposition of Dirichlet boundary conditions in fluid mechanics*. Computers & Fluids, Vol. 36, pp. 12-26, 2007.
- [9] Y. Bazilevs, T. Hughes: *NURBS-based isogeometric analysis for the computation of flows about rotating components*. Computational Mechanics, Vol. 43, pp. 143-150, 2008.
- [10] Y. Bazilevs, C. Michler, V. Calo, T. Hughes: *Weak Dirichlet boundary conditions for wall-bounded turbulent flows*. Computer Methods in Applied Mechanics and Engineering, Vol. 196, pp. 4853-4862, 2007.
- [11] P. Bézier: *Définition numérique des courbes et surfaces I*. Automatisme XI, pp. 625-632, 1966.
- [12] P. Bézier: *Définition numérique des courbes et surfaces II*. Automatisme XII, pp. 17-21, 1967.
- [13] C. de Boor: *On calculating with B-splines*. Journal of Approximation Theory, Vol. 6, pp. 50-62, 1972.
- [14] A. Bressan, G. Sangalli: *Isogeometric discretizations of the Stokes problem: stability analysis by the macroelement technique*. IMA Journal of Numerical Analysis, Vol. 33, pp. 629-651, 2012.
- [15] F. Buchegger, B. Jüttler: *Planar multi-patch domain parameterization via patch adjacency*. Computer-Aided Design, Vol. 82, pp. 2-12, 2017.

- [16] A. Buffa, C. de Falco, G. Sangalli: *Isogeometric analysis: stable elements for the 2D Stokes equation*. International Journal for Numerical Methods in Fluids, Vol. 65, pp. 1407-1422, 2011.
- [17] A. Buffa, G. Sangalli, R. Vázquez: *Isogeometric analysis in electromagnetics: B-splines approximation*. Computer Methods in Applied Mechanics and Engineering, Vol. 199 (17-20), pp. 1143-1152, 2010.
- [18] B. J. Cantwell: *The NACA airfoil series*. Course materials.
http://web.stanford.edu/~cantwell/AA200_Course_Material/The NACA airfoil series.pdf
- [19] P. de Casteljaou: *Courbes et surfaces à pôles*. Technical Report A, Citroën, Paris, 1963.
- [20] J.-M. Chapallaz, P. Eichenberger, G. Fisher: *Manual on pumps used as turbines*. A publication of Deutsches Zentrum für Entwicklungstechnologien - GATE, ISBN 3528020695, 1992.
- [21] M. Chen, A. E. Kaufman, R. Yagel: *Volume Graphics*. Springer Science & Business Media, ISBN - 13: 978-1-85233-192-4, 2012.
- [22] E. Cohen, T. Martin, R. M. Kirby, T. Lyche, R. F. Riesenfeld: *Analysis-aware modeling: Understanding quality considerations in modeling for isogeometric analysis*. Computer Methods in Applied Mechanics and Engineering, Vol. 199 (5-8), pp. 334-356, 2010.
- [23] J.A. Cottrell, A. Reali, Y. Bazilevs, T. J. R. Hughes: *Isogeometric analysis of structural vibrations*. Computer Methods in Applied Mechanics and Engineering, Vol. 195 (41-43), pp. 5257-5296, 2006.
- [24] S. Coons: *Surfaces for computer aided design*. Tech. Rep. MIT, Available as AD 663 504 from the National Technical Information Service, Springfield, VA 22161, 1964.
- [25] *Conserve Energy Future*, www.conserve-energy-future.com
- [26] H. Curry: *Review*. Mathematical Tables and Other Aids to Computation, Vol. 2, pp. 167-169, 211-213, 1947.
- [27] Z. Deng, T. J. Carlson, G. R. Ploskey, M. C. Richmond, D. D. Dauble: *Evaluation of blade-strike models for estimating the biological performance of Kaplan turbines*. Ecological Modelling, Vol. 208, pp. 165-176, 2007.
- [28] Z. Deng, J. Lu, M. J. Myjak, J. J. Martinez, C. Tian, S. J. Morris, T. J. Carlson, D. Zhou, H. Hou: *Design and Implementation of a new Autonomous Sensor Fish to Support Advanced Hydropower Development*. Review of Scientific Instruments, Vol. 85 (11), 2014.
- [29] M. Dörfel, B. Jüttler, B. Simeon: *Adaptive isogeometric analysis by local h-refinement with T-splines*. Computer Methods in Applied Mechanics and Engineering, Vol. 199 (5-8), pp. 264-275, 2010.
- [30] T. Dokken, M. Dæhlen, T. Lyche, K. Mørken: *Good approximation of circles by curvature-continuous Bézier curves*. Computer-Aided Design, Vol. 7, pp. 33-41, 1990.
- [31] T. Dokken, T. Lyche, K. F. Pettersen: *Polynomial splines over locally refined box-partitions*. Computer Aided Geometric Design, Vol. 30, pp. 331-356, 2013.
- [32] Electric Power Research Institute: *Fish Passage Through Turbines: Applicability of Conventional Hydropower Data to Hydrokinetic Technologies*. Palo Alto, California, 1024638, 2011.
- [33] *Eternoo machinery*, www.eternoohydro.com
- [34] G. Farin, D. Hansford: *Discrete Coons patches*. Computer Aided Geometric Design, Vol. 16, pp. 691-700, 1999.

- [35] R. T. Farouki: *Pythagorean-Hodograph Curves: Algebra and Geometry Inseparable*. ISBN 978-3-540-73398-0, Springer, Berlin, 2008.
- [36] D. R. Forsey, R. H. Bartels: *Hierarchical B-spline refinement*. Computer Graphics, Vol. 22 (4), pp. 205-212, 1988.
- [37] C. Giannelli, B. Jüttler, S. K. Kleiss, A. Mantzaflaris, B. Simeon, J. Špěh: *THB-splines: An effective mathematical technology for adaptive refinement in geometric design and isogeometric analysis*. Computer Methods in Applied Mechanics and Engineering, Vol. 299, pp. 337-365, 2016.
- [38] C. Giannelli, B. Jüttler, H. Speleers: *THB-splines: The truncated basis for hierarchical splines*. Computer Aided Geometric Design, Vol. 29 (7), pp. 485-498, 2012.
- [39] G+Smo (Geometry + Simulation Modules), www.gs.jku.at/gismo
- [40] J. Gravesen, A. Evgrafov, A. R. Gersborg, N. D. Manh, P. N. Nielsen: *Isogeometric analysis and shape optimisation*. In: Proceedings of 23rd Nordic Seminar on Computational Mechanics, (A. Erikson and G. Tibert eds.), pp. 14-17, Stockholm, 2010.
- [41] J. Gravesen, A. Evgrafov, D. M. Nguyen, P. Nørtoft: *Planar parametrization in isogeometric analysis*. International Conference on Mathematical Methods for Curves and Surfaces, Springer Berlin Heidelberg, pp. 189-212, 2012.
- [42] J. Hoschek, R. Müller: *Turbine blade design by lofted B-spline surfaces*. Journal of Computational and Applied Mathematics, Vol. 119, pp. 235-248, 2000.
- [43] T. J. R. Hughes, J. A. Cottrell, Y. Bazilevs: *Isogeometric analysis: CAD, finite elements, NURBS, exact geometry and mesh refinement*. Computer Methods in Applied Mechanics and Engineering, Vol. 194, pp. 4135-4195, 2005.
- [44] *Hydropower*, www.wikipedia.com
- [45] International Energy Agency: *Medium-Term Renewable Energy Market Report 2015*. ISBN PRINT 978-92-64-24361-3 PDF 978-92-64-24367-5, 2015.
- [46] *International Energy Agency*, www.iea.org
- [47] *International hydropower association*, www.hydropower.org
- [48] E. N. Jacobs, K. E. Ward, R. M. Pinkerton: *The characteristics of 78 related airfoil sections from tests in variable-density wind tunnel*. NACA Report No. 460, 1933.
- [49] K.A. Johannessen, T. Kvamsdal, T. Dokken: *Isogeometric analysis using LR B-splines*. Computer Methods in Applied Mechanics and Engineering, Vol. 269, pp. 471-514, 2014.
- [50] H. Keck, M. Sick: *Thirty years of numerical flow simulation in hydraulic turbomachines*. Acta Mechanica, Vol. 201, pp. 211-229, 2008.
- [51] H. Lin, S. Jin, Q. Hu, Z. Liu: *Constructing B-spline solids from tetrahedral meshes for isogeometric analysis*. Computer Aided Geometric Design, Vol. 35-36, pp. 109-120, 2015.
- [52] X. Liu, Y. Luo, B. W. Karney, W. Wang: *A selected literature review of efficiency improvements in hydraulic turbines*. Renewable and Sustainable Energy Reviews, Vol. 51, pp. 18-28, 2015.
- [53] T. Martin, E. Cohen, R. M. Kirby: *Volumetric parameterization and trivariate B-spline fitting using harmonic functions*. Computer Aided Geometric Design, Vol. 26, pp. 648-664, Elsevier, 2009.
- [54] *Mavel*, www.mavel.com

- [55] K. Michálková, B. Bastl: *A note on geometric modelling of water turbine parts*. Proceedings of the 33th Conference on Geometry and Graphics. Ostrava : VŠB-TU, pp. 169-180, 2013.
- [56] K. Michálková, B. Bastl: *Imposing angle boundary conditions on B-spline/NURBS surfaces*. Computer-Aided Design, Vol. 62, pp. 1-9, 2015.
- [57] P. L. Miller, J. H. Oliver, D. P. Miller, D. L. Tweedt: *BladeCAD: An Interactive Geometric Design Tool for Turbomachinery Blades*. NASA Technical Memorandum 107262, 1996.
- [58] J. Moran: *An Introduction to Theoretical and Computational Aerodynamics*. ISBN 0-486-42879-6, 1984.
- [59] S. Morganti, F. Auricchio, D.J. Benson, F.I. Gambarin, S. Hartmann, T.J.R. Hughes, A. Reali: *Patient-specific isogeometric structural analysis of aortic valve closure*. Computer Methods in Applied Mechanics and Engineering, Vol. 284, pp. 508-520, 2015.
- [60] A. Muis, P. Sutikno, A. Soewono, F. Hartono: *Design optimization of axial hydraulic turbine for very low head application*. Energy Procedia, Vol. 68, pp. 263-273, 2015.
- [61] D. M. Nguyen, A. Evgrafov, J. Gravesen: *Isogeometric shape optimization for electromagnetic scattering problems*. Progress In Electromagnetics Research B, Vol. 45, pp. 117-146, 2012.
- [62] V. P. Nguyen, C. Anitescu, S. P. A. Bordas, T. Rabczuk: *Isogeometric analysis: An overview and computer implementation aspects*. Mathematics and Computers in Simulations 117, pp. 89-116, 2015.
- [63] P. N. Nielsen, A. R. Gersborg, J. Gravesen, N. L. Pedersen: *Discretizations in isogeometric analysis of Navier–Stokes flow*. Computer Methods in Applied Mechanics and Engineering, Vol. 200, pp. 3242-3253, 2011.
- [64] H. Nilsson: *Some Experiences on the Accuracy and Parallel Performance of OpenFOAM for CFD in Water Turbines*. PARA 2006, LNCS 4699, pp. 168-176, 2007.
- [65] P. Nørtoft, J. Gravesen: *Isogeometric shape optimization in fluid mechanics*. Structural and Multi-disciplinary Optimization, Vol. 48, pp. 905-925, 2013.
- [66] M. Pauley, D. M. Nguyen, D. Mayer, J. Špeh, O. Weeger, B. Jüttler: *The isogeometric segmentation pipeline*. Isogeometric Analysis and Applications 2014, Springer International Publishing, pp. 51-72, 2015.
- [67] *Pelton turbine*, www.turbinesinfo.com
- [68] F. Perez-Arribas, I. Trejo-Vargas: *Computer-aided design of horizontal axis turbine blades*. Renewable Energy, Vol. 44, pp. 252-260, 2012.
- [69] L. Piegl, W. Tiller: *The NURBS book*. Monographs in visual communication, ISBN 3-540-61545-8, Springer, 1997.
- [70] A. Ratnani: *Pegasus, Isogeometric Analysis Simulations in Python*. INRIA Report, 2012.
- [71] R. Riesenfeld, R. Haimes, E. Cohen: *Initiating a CAD renaissance: Multidisciplinary analysis driven design Framework for a new generation of advanced computational design, engineering and manufacturing environments*. Computer Methods in Applied Mechanics and Engineering, Vol. 284, pp. 1054-1072, 2015.
- [72] D. Robb: *Hydro's fish-friendly turbines*. Renewable Energy Focus, Vol. 12 (2), pp. 16-17, 2011.

- [73] M. Rossgatterer, B. Jüttler, M. Kapl, G. D. Vecchia: *Medial design of blades for hydroelectric turbines and ship propellers*. Computational Methods , Vol. 36, pp. 434-444, 2012.
- [74] T. W. Sederberg, D. L. Cardon, G. T. Finnigan, N. S. North, J. Zheng, T. Lyche: *T-spline simplification and local refinement*. ACM Transactions on Graphics, Vol. 23, pp. 276-283, 2004.
- [75] I. J. Schoenberg: *Contributions to the problem of approximation of equidistant data by analytic functions*. Quarterly of Applied Mathematics, Vol. 4, pp. 45-99, 1946.
- [76] S. Štěch: *Inicializační návrh turbíny*. Výzkumná zpráva, Mavel, 2013.
- [77] P. M. V. Subbarao: *Design & analysis of Pelton wheel turbine*. <http://web.iitd.ac.in/~pmvs/mel346/pelton-design-tue.ppt>
- [78] A. B. Tepole, M. Gart, A. K. Gosain, E. Kuhl: *Characterization of living skin using multi-view stereo and isogeometric analysis*. Acta Biomaterialia, Vol. 10 (11), pp. 4822-4831, 2014.
- [79] C. H. Thai, H. Nguyen-Xuan, N. Nguyen-Thanh, T.-H. Le, T. Nguyen-Thoi, T. Rabczuk: *Static, free vibration, and buckling analysis of laminated composite Reissner–Mindlin plates using NURBS-based isogeometric approach*. International Journal for Numerical Methods in Engineering, Vol. 91 (6), pp. 571-603, 2012.
- [80] The American Society of Mechanical Engineers Hydro Power Technical Committee: *The Guide to Hydropower Mechanical Design*. United States: H. P. Books, ISBN 0-9651765-0-9, 1996.
- [81] R. Vásquez: *A new design for the implementation of isogeometric analysis in Octave and Matlab: GeoPDEs 3.0*. Computers & Mathematics with Applications, Vol. 72 (3), pp. 523-554, 2016.
- [82] K. Versprille: *Computer aided design applications of the rational B-spline approximation form*. Ph.D. Thesis. Syracuse University, 1975.
- [83] A.-V. Vuong, C. Giannelli, B. Jüttler, B. Simeon: *A hierarchical approach to adaptive local refinement in isogeometric analysis*. Computer Methods in Applied Mechanics and Engineering, Vol. 200 (49-52), pp. 3554-3567, 2011.
- [84] W. Wang, Y. Zhang, L. Liu, T. J. R. Hughes: *Trivariate solid T-spline construction from boundary triangulations with arbitrary genus topology*. Computer-Aided Design, Vol. 45 (2), pp. 351-360, 2013.
- [85] X. Wang, X. Qian: *An optimization approach for constructing trivariate B-spline solids*. Computer-Aided Design, Vol. 46, pp. 179-191, 2014.
- [86] S. Waters, G. A. Aggidis: *Over 2000 years in review: Revival of the Archimedes Screw from Pump to Turbine*. Renewable and Sustainable Energy Reviews, Vol. 51, pp. 497-505, 2015.
- [87] *Water wheel*, www.wikipedia.com
- [88] *Water turbine*, www.wikipedia.com
- [89] J. Wu, K. Shimmei, K. Tani, K. Niikura, J. Sato : *CFD-Based Design Optimization for Hydro Turbines*. Journal of Fluids Engineering, Vol. 129, pp. 159-168, 2007.
- [90] G. Xu, B. Mourrain, R. Duvigneau, A. Galligo: *Parameterization of computational domain in isogeometric analysis: Methods and comparison*. Computer Methods in Applied Mechanics and Engineering, Vol. 200, pp. 2021-2031, 2011.
- [91] G. Xu, B. Mourrain, R. Duvigneau, A. Galligo: *Optimal analysis-aware parameterization of computational domain in 3D isogeometric analysis*. Computer-Aided Design 45, pp. 812-821, 2013.

- [92] G. Xu, B. Mourrain, R. Duvigneau, A. Galligo: *Analysis-suitable volume parameterization of multi-block computational domain in isogeometric applications*. Computer-Aided Design 45, pp. 395-404, 2013.
- [93] G. Xu, B. Mourrain, X. Wu, L. Chen, K. Hui: *Efficient construction of multi-block volumetric spline parameterization by discrete mask method*. Journal of Computational and Applied Mathematics, Vol. 290, pp. 589-597, 2015.
- [94] Y. Zhang, Y. Bazilevs, S. Goswami, C.L. Bajaj, T.J.R. Hughes: *Patient-specific vascular NURBS modeling for isogeometric analysis of blood flow*. Computer Methods in Applied Mechanics and Engineering, Vol. 196, pp. 2943-2959, 2007.
- [95] A. Židonis, D. S. Benzon, G. A. Aggidis: *Development of hydro impulse turbines and new opportunities*. Renewable and Sustainable Energy Reviews, Vol. 51, pp. 1624-1635, 2015.

List of publications

Publications in journals with impact factors

B. Bastl, K. Slabá, M. Byrtus: *Planar C^1 Hermite interpolation with uniform and non-uniform TC-biarcs*. Computer Aided Geometric Design, Vol. 30 (1), pp. 58-77, 2013.

B. Bastl, M. Bizzarri, M. Krajnc, M. Lávička, K. Slabá, Z. Šír, V. Vitrih, E. Žagar: *C^1 Hermite interpolation with spatial Pythagorean-hodograph cubic biarcs*. Journal of Computational and Applied Mathematics, Vol. 257, pp. 65-78, 2014.

B. Bastl, M. Bizzarri, B. Kovač, M. Krajnc, M. Lávička, K. Micháلكová, K. Ferjančič, Z. Šír, E. Žagar: *C^2 Hermite interpolation by Pythagorean-hodograph quintic triarcs*. Computer Aided Geometric Design, Vol. 31 (7-8), pp. 412-426, 2014.

K. Micháلكová, B. Bastl: *Imposing angle boundary conditions on B-spline/NURBS surfaces*. Computer-Aided Design, Vol. 62, pp. 1-9, 2015.

K. Micháلكová, B. Bastl: *Tetrahedral subdivision scheme for spatial G^1 curves*. Journal of computational and applied mathematics, Vol. 281, pp. 196-206, 2015.

B. Bastl, M. Brandner, J. Egermaier, K. Micháلكová, E. Turnerová: *IgA-Based Solver for turbulence modelling on multipatch geometries*. Advances in Engineering Software, Vol. 113, pp. 7-18, 2017.

B. Bastl, M. Brandner, J. Egermaier, K. Micháلكová, E. Turnerová: *Isogeometric analysis for turbulent flow*. Mathematics and Computers in Simulation, Vol. 145, pp. 3-17, 2018.

Publications in journals without impact factors

P. Anděl, B. Bastl, K. Slabá: *Parameterizations of generalized NURBS volumes of revolution*. Engineering Mechanics, Vol. 19, pp. 293-306, 2012.

Conference papers

K. Slabá: *Modifikace nelineárního schématu zachovávajícího kružnice*. Proceedings of the 31st conference on geometry and graphics, Malá Morávka, 2011.

K. Slabá, B. Bastl: *Circle – preserving subdivision scheme based on Apollonius' circle*. Aplimat - Journal of Applied Mathematics, 2012.

K. Michálková, B. Bastl: *A note on geometric modelling of water turbine parts*. Proceedings of the 33th Conference on Geometry and Graphics. Ostrava: VŠB-TU, pp. 169-180, 2013.

B. Bastl, K. Michálková: *Solving Navier-Stokes equations with isogeometric analysis*. Proceedings of the 33th Conference on Geometry and Graphics. Ostrava: VŠB-TU, pp. 27-36, 2013.

B. Bastl, M. Brandner, K. Michálková: *Isogeometric collocation method for Navier-Stokes equations*. Proceedings of the 34th Conference on Geometry and Graphics, pp. 77-87, 2014.

K. Michálková, B. Bastl: *B-spline/NURBS volume parameterizations of Kaplan turbine*. In Proceedings of the Slovak-czech conference on geometry and graphics. In Proceedings of the Slovak-czech conference on geometry and graphics. Bratislava: Slovenská technická univerzita v Bratislavě, pp. 171-176, 2015.

B. Bastl, M. Brandner, J. Egermaier, K. Michálková, E. Turnerová: *Numerical modelling of turbulent flows*. In Proceedings of Seminář Numerické Analýzy, Institute of Computer Science AS CR, Praha, pp. 9-12, 2015.

B. Bastl, M. Brandner, J. Egermaier, K. Michálková, E. Turnerová: *Isogeometric Analysis for Fluid Flow Problems*. In: Chleboun, J., Příkryl, P., Segeth, K., Šístek, T. (eds.): Programs and Algorithms of Numerical Mathematics. Proceedings of Seminar. Dolní Maxov, June 8-13, 2014. Institute of Mathematics AS CR, Prague, pp. 23-31, 2015.

Other publications

B. Bastl, K. Michálková: *Implementace řešiče Navier-Stokesových rovnic založeného na isogeometrické analýze*. Výzkumná zpráva č. NTIS-VP5a-003/2013, Plzeň, 2013.

B. Bastl, K. Michálková: *Parametrický model lopatky Peltonovy turbíny*. Výzkumná zpráva č. NTIS-VP5a-004/2013, Plzeň, 2013.

K. Michálková, B. Bastl, M. Lávička, F. Ježek, S. Štěch, Z. Sysel: *Parametrický geometrický model Kaplanovy turbíny*. Výzkumná zpráva č. NTIS-VP5a-001/2013, Plzeň, 2013.

B. Bastl, M. Brandner, J. Egermaier, K. Michálková, E. Turnerová: *Modely nestlačitelného proudění a jejich numerické řešení*. Výzkumná zpráva č. NTIS-VP5a-002/2013, Plzeň, 2013.

K. Michálková, B. Bastl: *Objemová parametrizace hydraulického profilu Kaplanovy turbíny*. Výzkumná zpráva č. NTIS-VP5a-001/2014, Plzeň, 2014.

B. Bastl, M. Brandner, J. Egermaier, K. Michálková, E. Turnerová: *Turbulentní modely pro nestlačitelné proudění*. Výzkumná zpráva č. NTIS-VP5a-002/2014, Plzeň, 2014.

B. Bastl, M. Brandner, K. Michálková, E. Turnerová: *Implementace řešiče Navier-Stokesových rovnic založeného na isogeometrické analýze*. Výzkumná zpráva č. NTIS-VP5a-003/2014, Plzeň, 2014.

B. Bastl, K. Michálková: *Parametrický geometrický model Francisovy turbíny*. Výzkumná zpráva č. NTIS-VP5a-001/2015, Plzeň, 2015.

B. Bastl, M. Brandner, J. Egermaier, K. Michálková, E. Turnerová: *Metody tvarové optimalizace*. Výzkumná zpráva č. NTIS-VP5a-002/2015, Plzeň, 2015.

Appendix A

Control points of spiral shaped pipe

Let us assume section in xy -plane, that is subsequently transformed, parameters are described in the part 3.2.1

$$\mathbf{P}^a = \left\{ \begin{aligned} & \left(-\frac{h_d}{2}, -r_{d1}, 0 \right), \left(-\frac{h_d}{2}, -\frac{2r_{d1}}{3} - \frac{1r_{d2}}{3}, 0 \right), \left(-\frac{h_d}{2}, -\frac{r_{d1}}{3} - \frac{2r_{d2}}{3}, 0 \right), \\ & \left(-\frac{h_d}{2}, -r_{d2}, 0 \right), \left(-\frac{h_d}{2}, -r_{d2} - \frac{Kw_d}{2}, 0 \right), \left(-\frac{h_d}{2} + \frac{Kw_d}{2} - \frac{w_d}{2}, -r_{d2} - \frac{w_d}{2}, 0 \right) \\ & \left(-\frac{h_d}{2} - \frac{w_d}{2}, -r_{d2} - \frac{w_d}{2}, 0 \right), \left(-\frac{h_d}{2} - \frac{Kw_d}{2} - \frac{w_d}{2}, -r_{d2} - \frac{w_d}{2}, 0 \right), \\ & \left(-\frac{h_d}{2} - w_d, -r_{d2} - \frac{Kw_d}{2}, 0 \right), \left(-\frac{h_d}{2} - w_d, -r_{d2}, 0 \right), \\ & \left(-\frac{h_d}{2} - w_d, -\frac{1}{3} \left(\sqrt{r_s^2 - \left(\frac{h_d}{2} + w_d \right)^2} - r_c \right) - \frac{2r_{d2}}{3}, 0 \right), \\ & \left(-\frac{h_d}{2} - w_d, -\frac{r_{d2}}{3} - \frac{2}{3} \left(r_c - \sqrt{r_s^2 - \left(\frac{h_d}{2} + w_d \right)^2} \right), 0 \right), \\ & \left(-\frac{h_d}{2} - w_d, \sqrt{r_s^2 - \left(\frac{h_d}{2} + w_d \right)^2} - r_c, 0 \right), \\ & \left(\frac{1}{2} (-h_d - 2w_d) - Lr_s \sqrt{1 - \frac{\left(\frac{h_d}{2} + w_d \right)^2}{r_s^2}}, -r_c + \frac{1}{2} L (-h_d - 2w_d) + r_s \sqrt{1 - \frac{\left(\frac{h_d}{2} + w_d \right)^2}{r_s^2}}, 0 \right), \\ & (-r_s, Lr_s - r_c, 0), (-r_s, -r_c, 0), (-r_s, -r_c - Kr_s, 0), \\ & (-Kr_s, -r_c - r_s, 0), (0, -r_c - r_s, 0) \end{aligned} \right\},$$

where $K = 4 \frac{\tan(\frac{\pi}{8})}{3}$ and $L = 4 \frac{\tan(\frac{\pi}{2} - \arcsin(\frac{h_d + w_d}{r_s}))}{3}$. The rest of the points for $i = 0, \dots, 17$ are

$$\mathbf{P}_i^b = \begin{pmatrix} -1 & 0 & 0 \\ 0 & 1 & 0 \\ 0 & 0 & 1 \end{pmatrix} \cdot \mathbf{P}_{18-i}^a.$$

The points for the section are

$$\mathbf{P}_j = \mathbf{R} \cdot (\mathbf{P}_j^c)^\top$$

where $j = 0, \dots, 36$, $\mathbf{P}^c = \mathbf{P}^a \cup \mathbf{P}^b$ and \mathbf{R} is the rotation matrix that rotates point around x -axis through angle a_s .

The example set of parameters for the specific spiral shaped pipe

Consider the following parameters (nomenclature is mention in Section 3.2.1):

- The entrance cone

- $r_1 = 138.33$,

- $d_1 = 424.03$,

- Disks

- $r_{d1} = 234.7$,

- $r_{d2} = 284.2$,

- $h_d = 33.5$,

- $w_d = 15$,

- The sections of the spiral $n_s = 23$

section	a_s	r_c	r_s
1	0	388.05	131.74
2	15	385.05	128.76
3	30	381.93	125.74
4	45	378.75	122.66
5	60	375.53	119.55
6	75	372.24	116.38
7	90	368.88	113.16
8	105	365.46	109.87
9	120	361.94	106.51
10	135	358.34	103.09
11	150	354.65	99.574
12	165	350.82	95.961
13	180	346.88	92.246
14	195	342.78	88.411
15	210	338.51	84.436
16	225	334.03	80.302
17	240	329.29	75.978
18	255	324.26	71.437
19	270	318.85	66.631
20	285	312.93	61.493
21	300	306.34	55.956
22	315	298.78	49.911
23	316.43	298.78	49.911

Appendix B

Control points of the rounded rectangle in the draft tube

The section that lies in xz -plane and the centre is $(0, 0, 0)$ has the control points (parameters are described in Section 3.2.5)

$$\mathbf{P} = \{(s/2 + r, 0, -v/2, 1), (s/2 + r, 0, -v/2 - Kr, 1), (s/2 + Kr, 0, -v/2 - r, 1), (s/2, 0, -v/2 - r, 1), (s/4, 0, -v/2 - r, 1), (-s/4, 0, -v/2 - r, 1), (-s/2, 0, -v/2 - r, 1), (-s/2 - Kr, 0, -v/2 - r, 1), (-s/2 - r, 0, -v/2 - Kr, 1), (-s/2 - r, 0, -v/2, 1), (-s/2 - r, 0, -v/4, 1), (-s/2 - r, 0, v/4, 1), (-s/2 - 2r, 0, v/2, 1), (-s/2 - r, 0, +v/2 + Kr, 1), (-s/2 - Kr, 0, v/2 + r, 1), (-s/2, 0, v/2 + r, 1), (-s/4, 0, v/2 + r, 1), (s/4, 0, v/2 + r, 1), (s/2, 0, v/2 + r, 1), (s/2 + Kr, 0, v/2 + r, 1), (s/2 + r, 0, v/2 + Kr, 1), (s/2 + r, 0, v/2, 1), (s/2 + r, 0, v/4, 1), (s/2 + r, 0, -v/4, 1), (s/2 + r, 0, -v/2, 1)\},$$

where the last coordinate is the weight and $K = 4 \frac{\tan \frac{\pi}{8}}{3}$.

Parameters for the elbow draft tube

The specific parameters for draft tube shown in Fig. 3.14:

- Cone
 - $r_{e1} = 260$ (input radius),
 - $r_{e2} = 307.71$ (output radius),
 - $d_e = 700$ (length),
- Diffuser
 - $d = 1500$ (length)
 - $s = 456.99$
 - $v = 456.99$
 - $r = 32.5$
- Radius of the rotation
 - $R_r = 600$,

section	U_r	s	v	r
1	14.286	312.18	297.39	148.69
2	28.571	316.93	287.36	143.68
3	42.857	321.98	277.61	138.81
4	57.143	327.31	268.16	134.08
5	71.429	332.94	259	129.5
6	85.714	338.85	250.12	125.06
7	100	345.05	241.54	120.77